

Absolute Triangulation Algorithms for Space Exploration

Sébastien Henry* and John A. Christian†
Georgia Institute of Technology, Atlanta, GA 30332

Images are an important source of information for spacecraft navigation and for three-dimensional reconstruction of observed space objects. Both of these applications take the form of a triangulation problem when the camera has a known attitude and the measurements extracted from the image are line of sight (LOS) directions. This work provides a comprehensive review of the history and theoretical foundations of triangulation. A variety of classical triangulation algorithms are reviewed, including a number of suboptimal linear methods (many LOS measurements) and the optimal method of Hartley and Sturm (only two LOS measurements). Two new optimal non-iterative triangulation algorithms are introduced that provide the same solution as Hartley and Sturm. The optimal two-measurement case can be solved as a quadratic equation in many common situations. The optimal many-measurement case may be solved without iteration as a linear system using the new Linear Optimal Sine Triangulation (LOST) method. The various triangulation algorithms are assessed with a few numerical examples, including planetary terrain relative navigation, angles-only optical navigation at Uranus, 3-D reconstruction of Notre-Dame de Paris, and angles-only relative navigation.

I. Introduction

Cameras, telescopes, and other optical instruments are an important source of information for modern space vehicles [1]. Information extracted from the images produced by these sensors may be used for many different purposes, with shape modeling [2, 3] and spacecraft navigation [4, 5] being two of the most common. In both of these applications, the objective is achieved by exploiting the geometry that relates the three-dimensional (3-D) location of objects in the observed scene to their apparent pixel locations in a digital image.

There are a variety of observables one might extract from an image and a variety of ways in which these observables may be interpreted. Perhaps the simplest situation is when one obtains line of sight (LOS) measurements from an optical instrument to a point in 3-D space. Oftentimes, the absolute location of either the camera or the observed point is known. When the camera location is known and the observed point's location is unknown, then this is a shape modeling (i.e., 3-D reconstruction) problem. Conversely, when the observed point's location is known and the camera location is unknown, this is a navigation problem. The geometry of these two problems is identical and the algorithms developed

*Graduate Research Assistant, Guggenheim School of Aerospace Engineering.

†Associate Professor, Guggenheim School of Aerospace Engineering. Associate Fellow AIAA.

for one are equally applicable to the other. For the sake of brevity and clarity, this work primarily develops algorithms from the navigation perspective (though all results are also valid for 3-D reconstruction).

Point localization using a collection of LOS measurements (or angles) is generically referred to as triangulation [for the specific application of spacecraft navigation this is also sometimes called “angles-only” optical navigation (OPNAV)]. In recent years, there has been substantial interest in the utility of triangulation methods for spacecraft localization in cislunar space using sightings of other well-known satellites [6, 7] or for interplanetary exploration using sightings of asteroids/planets [7–11]. The concepts of triangulation, however, apply to a much broader class of spaceflight navigation problems. For example, some of these other applications include terrain relative navigation (TRN) with known landmarks [12], angles-only relative navigation (RelNav) [13], and star-based interstellar navigation [14].

This work reviews the present state of triangulation algorithms with applicability to space exploration. Special consideration is given to the relationships between the different algorithms, and some algorithms are shown to be equivalent under certain conditions. Many of the most popular methods (e.g., the Direct Linear Transform) are geometrically exact, but do not produce statistically optimal localization estimates when provided noisy LOS measurements. When there are only two LOS measurements, the classic method of Hartley and Sturm [15] finds the statistically optimal answer as the solution to a polynomial of degree six. This work shows how Hartley and Sturm’s solution can be simplified to a polynomial of degree two when all of the LOS measurements come from a single image (as happens with monocular vision-based navigation). Unfortunately, the extension of Hartley and Sturm’s method to three or more LOS measurements is not practical [16] and past work has relied on iterative numerical schemes to perform statistically optimal triangulation with many measurements. To address this problem, the new Linear Optimal Sine Triangulation (LOST) method is introduced in Section V.B. The LOST method solves the statistically optimal triangulation problem without iteration as the solution to a linear system. When only two measurements are available the error covariance of the triangulated point is exactly the same for the LOST method and the Hartley and Sturm method. Moreover, as compared to the Hartley and Sturm method, the LOST method is faster (small linear system instead of a polynomial of degree six) and scalable (can directly find optimal solution for any number of measurements as a linear system). This work concludes with a number of examples to illustrate the similarities, advantages, and disadvantages of the various triangulation methods.

II. Background and the Lexicon of Triangulation

The idea of using optical observations to find an object’s location is not new. A sophisticated understanding of the underlying geometry was known in antiquity, and has been used for over two thousand years by navigators, cartographers, astronomers, civil engineers, and many others. Unfortunately, many critical ideas have been forgotten and rediscovered over the centuries—with this apparent forgetfulness being strangely prevalent today. Harry S. Truman famously said “There is nothing new in the world except the history you do not know.” It will soon become apparent that Truman’s

astute observation certainly applies to the field of triangulation.

To begin, let the term *triangulation* refer to the task of localizing a point using the angles that describe a triangle (see Fig. 1). In the simplest formulation there are two points of known position (forming two vertices of the triangle), such that the angles describing a triangle uniquely determine the position of an unknown point (the third vertex of the triangle). Note that the “tri” in triangulation refers to the use of triangles and not to the number of points. Thus, the term triangulation remains precise when observations of many known points are used to localize a single unknown point, since the solution then consists of many triangles.

The origins of triangulation are difficult to establish, largely due to the loss of primary sources from antiquity. Indeed, attribution of primacy seems to depend as much on whose works survived to the modern era as it does on who was truly the first to “discover” an idea. Regardless, a few things are known. The concept of using triangles to estimate distance and size was known as early as the 16th century BC, as can be seen by the problem/solution sets (especially P57-P60) in the Rhind Mathematical Papyrus [17] from the Second Intermediate Period of ancient Egypt. Sophistication of understanding increased significantly by 6th century BC, when the Greek mathematician Thales purportedly used triangles to estimate the height of the Egyptian pyramids and the distance to ships at sea [18]. All of the geometric

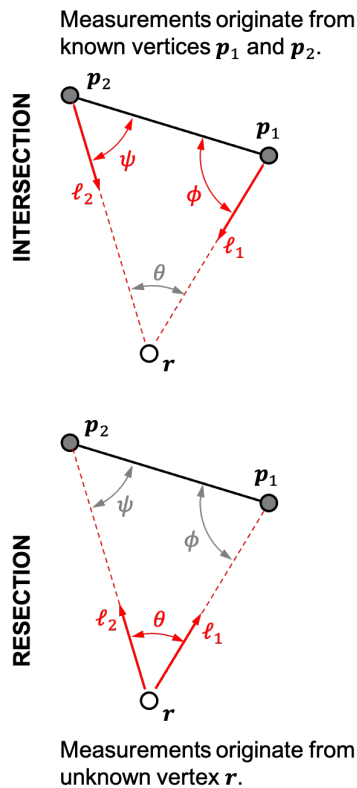


Fig. 1 Illustration of intersection (top) and resection (bottom) forms of the triangulation problem. The location of vertices p_1 and p_2 are known and the objective is to solve for the unknown location of vertex r . Measurements are shown in red.

principals necessary for point localization by triangulation were known by the 3rd century BC, when they were clearly laid out in Euclid’s *Elements* [19, 20]. Moreover, by the 2nd century BC, Hipparchus (amongst the first known to possess a trigonometric table [21]) used triangulation principles to estimate the distance to the Sun and Moon (as described by Ptolemy in the *Almagest* Book V) [22, 23]. Thus, there can be little doubt that the classical Greek geometers were quite familiar with how triangles and a known baseline could be used to infer the location of a point at a distance. While this line of study continued to flourish in the Islamic world during the first millennium CE [24], the knowledge was lost to European scholars for over a thousand years (until Euclid’s *Elements* was translated from Arabic into Latin in the 12th century CE [20, 24]). The modern understanding of triangulation (e.g., Fig. 2) can be traced to a booklet published in 1533 by Gemma Frisius [25–27]. Notable improvements in the practice were made by Snellius in 1617 as part of his effort to measure the circumference of the Earth [27, 28], and triangulation was put into a least squares framework by Gauss himself while conducting a survey of Hanover in the 1820s [29, 30]. At a conceptual level, the work of Frisius, Snellius, and Gauss brings us to the modern era—where new sensors, computational resources, and applications have made room for additional innovations.

The modern triangulation problem takes on one of two forms: intersection or resection [31]. This is illustrated in Fig. 1. The first form is *intersection*, which occurs when angle measurements collected by observers at two (or more) known locations are used to estimate the location of an unknown point. The intersection form of triangulation has many practical applications, such as satellite orbit determination [32, 33] and 3-D scene reconstruction from multiple images [15, 34, 35]. The second form is *resection*, which occurs when an observer estimates its unknown location using angle measurements to two (or more) points at known locations. The resection form of triangulation describes the vehicle

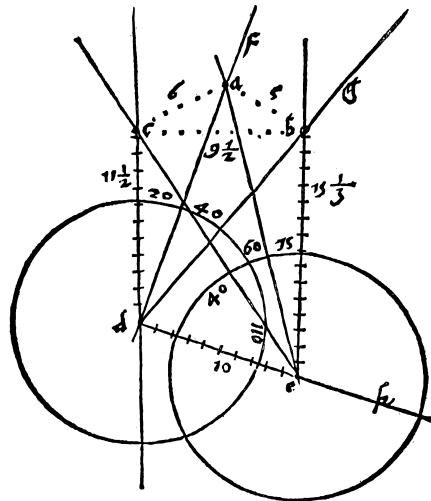


Fig. 2 Illustration by G. Frisius (c. 1533) showing how to determine the location of unknown (or inaccessible) points a, b, c using only the bearings from two known points (d and e) separated by a known baseline. This is an example of the intersection form of the triangulation problem. Reproduced from Ref. [25] as it appears at the end of Ref. [26].

(e.g., robot, ship, aircraft, spacecraft) localization problem that commonly appears in navigation applications [9, 36]. The intersection and resection problems have the same underlying geometry, with the primary difference being whether the triangle vertex of unknown location is the observer or is being observed.

Both the intersection and resection forms of the triangulation problem find the location of the unknown triangle vertex (denoted as \mathbf{r} in Fig. 1) relative to the locations of the known triangle vertices (denoted as \mathbf{p}_1 and \mathbf{p}_2 in Fig. 1). Thus, one typically chooses to express the known locations of \mathbf{p}_1 and \mathbf{p}_2 in a common frame and then triangulation usually results in an estimate of \mathbf{r} this same frame. The frame in which all this occurs is generically called the *localization frame*. The choice of the localization frame depends on the application (see Section VII for three different choices), but common examples for spacecraft localization include an inertial frame (e.g., International Celestial Reference Frame [37–39]), planet-fixed frame, spacecraft-fixed frame, or the orbital local-vertical, local-horizontal (LVLH) frame.

The angles in the triangulation problem often come from optical instruments. For example, in land surveying and laboratory metrology applications the optical instrument is commonly a theodolite. In spacecraft navigation applications the angles usually come from camera or telescope images. The angles themselves are often referred to as *bearings* and come in pairs for 3-D problems (e.g., azimuth and elevation, right ascension and declination). Regardless of the application, the angle measurements (i.e., the bearings) produced by such optical instruments describe the direction from the sensor to an observed point (i.e., the direction from one triangle vertex to another). This direction corresponds to a straight line connecting two points that is commonly referred to as the *line of sight* (LOS).

Crucially important is the frame(s) in which the measured LOS directions may be expressed. Most optical instruments fundamentally measure the LOS direction in a frame fixed to the sensor, referred to here as the *sensor frame*. If the orientation of this sensor frame relative to the localization frame is known, then it is possible to transform the LOS direction from the sensor frame (where it is measured) into the localization frame (where the locations of the reference points are known). When expressed in the localization frame, these measurements are referred to as *absolute* LOS directions. For usual optical instruments, the absolute LOS is coincident with the *line of position* (LOP)—where the LOP describes a straight line in the localization frame on which the unknown point must lie. Moreover, following the terminology of Kaplan [40], define *absolute triangulation* as triangulation performed exclusively with absolute LOS directions and having a solution at the intersection of two (or more) LOPs. Most spacecraft have excellent attitude knowledge (e.g., from star trackers [41–43]) and so the absolute triangulation problem occurs frequently in spaceflight applications. Absolute triangulation is the primary topic of this manuscript and numerous algorithms are presented to accomplish this task (see Sections IV and V).

Although absolute triangulation is the subject of the technical discussions that follow, additional insight may be gained (and common mistakes avoided) by also understanding what absolute triangulation is not. Thus, consider the alternative case where the orientation of the optical instrument is not known and the absolute LOS directions cannot be found—instead, only the triangle interior angles may be measured. In this case, the differences between the intersection

and resection forms of the triangulation problem are especially important. For example, consider a two-dimensional (2-D) system. In this example, the intersection form of the triangulation problem may be solved with a single triangle using observations of the unknown point from two known observer locations. This is because measurement of the angles ϕ and ψ (see top diagram in Fig. 1) produce two LOS directions relative to the known observer baseline that intersect at a unique 2-D point. This, however, is not the case for the resection problem with two known points. If absolute orientation is unknown and the only measurement is the angle θ , then the observer's unknown location is somewhere along a circular arc (see Fig. 3) called the *circle of position* (COP). This is a well-known result. The observer position may be made unique in the 2-D resection problem by measuring angle pairs between three points, which is classically referred to as the *three-point resection problem* or the *Snellius-Pothenot problem* (named after Snellius's seminal 1617 work mentioned earlier [27, 28]). As an example, consider Fig. 4 where Snellius documented how he found the location of point o (roof of his house) using only measured angles $\angle yoi = 32^\circ 57'$ and $\angle you = 64^\circ 40'$ to the known points y (Pieterskerk), i (Town Hall), u (Hooglandse Kerk) in Leiden. Clearly shown are the two COPs (one from the baseline yi and the other from the baseline yu) that intersect at the unique location of o . Even after 400 years, the Snellius-Pothenot problem remains an important problem in land surveying, with various algorithms still being published today [44].

Spacecraft and other aerospace vehicles operate in a 3-D world, and so it is instructive to expand upon the intuitive 2-D results from the Snellius-Pothenot problem. The 3-D case of resection, where a sensor of unknown attitude lies at the point of unknown location, has sometimes been called the *space resection problem* in land surveying and photogrammetry applications. The astute roboticist, engineer, or computer scientist will recognize this as identical to the *perspective- n -point (PnP) problem*. When $n = 3$ one has the famous P3P problem, which admits 4 unique solutions with a direct (non-iterative) method existing as early as 1841 [45]. Since then, driven in large part by interest from the computer vision community, there have been great improvements in algorithms for the P3P [46, 47], P4P [48], and PnP [49–52] problems. Similar problems (i.e., position and attitude from LOS measurements to points) have been

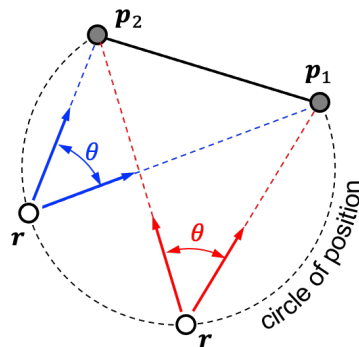


Fig. 3 Illustration of the 2-D resection problem with unknown instrument orientation. The observer lies somewhere on a circle of position (COP) when only the apparent angle between the LOS directions to two known stations is measured.

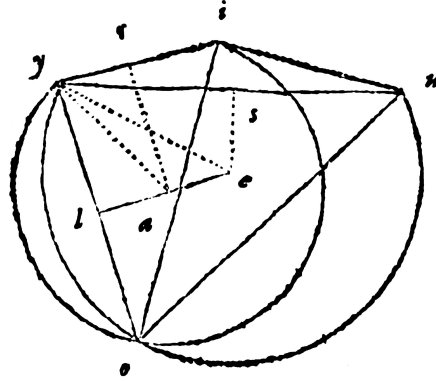


Fig. 4 Illustration by W. Snellius (c. 1617) showing how to determine the location of unknown observer point o using only measured angles $\angle yoi$ and $\angle you$ to the three known points y, i, u . This is a 2-D example of the resection form of the triangulation problem. Reproduced from Ref. [28], p. 204, and digitally restored by the authors of this manuscript.

considered within the space community for some time [53]. Note that the PnP problem simply describes a particular means of solving the *pose estimation problem*. Pose estimation is the general problem of finding the position and attitude of an object, which may be achieved with optical observations of points (e.g., PnP problem) or with other sensors (e.g., LIDAR point cloud registration [54, 55]). Finally, the reader should note that the pose estimation problem cannot be solved for the intersection form of the triangulation problem since the measured angles (collected by observers at the triangle's known points) do not depend on the orientation of the unknown point. Hence, the unknown point's location may be found, but the attitude of the object residing at the unknown point is unobservable by triangulation alone.

The triangulation problems discussed so far imply that the point of unknown location is either (1) stationary or (2) that the LOS measurements are obtained at the same instant in time. Spacecraft, however, are not stationary vehicles. Moreover, while it is possible in many situations to obtain (nearly) simultaneous LOS measurements, this is not always the case. Fortunately, the tools of triangulation may also be used for a moving observer—a concept referred to here as *dynamic triangulation*. The ideas of dynamic triangulation were pioneered for maritime applications, such as ship navigation [36] and bearings-only target motion analysis (BO-TMA) [56]. The topic gained much attention after the wide-spread deployment of radar systems in the 1940s and 1950s, where it immediately became apparent that a ship moving along a straight line cannot navigate by bearings to a single station [57]. Likewise, a single observer that is either stationary or moving along a straight line cannot uniquely determine the trajectory of a target ship with bearings alone. In these cases, it is impossible to distinguish between the object's true trajectory and an infinite number of *homothetic trajectories*. Any one of the homothetic trajectories is related to the true trajectory by a homothety [58], which is described by a contraction or expansion of the true trajectory about the homothetic center. Thus, the observer is left with scale ambiguity on the trajectory, as illustrated on Fig. 5. The usual solution is to collect LOS observations from multiple stations or to maneuver the observer [59, 60].

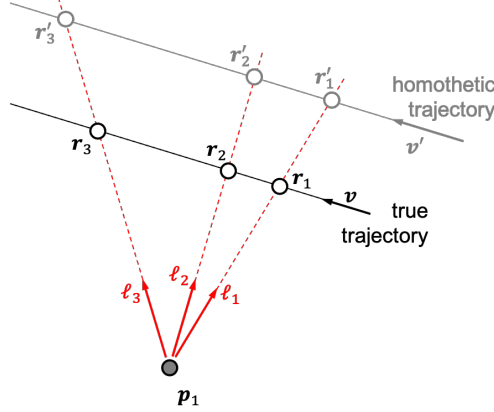


Fig. 5 If the motion between two particles is governed by linear dynamics, then then LOS measurements from one particle to the other can be explained by an infinite number of homothetic trajectories.

Dynamic triangulation plays a central role in spacecraft “angles-only” relative navigation (RelNav). Recall that two spacecraft in near circular orbits that are close to one another exhibit nearly linear dynamics (e.g., as described with the Clohessy-Wiltshire equations [61]). Due to the linear dynamics, the exact same observability challenges found for the BO-TMA problem were found to exist for problems of spacecraft angles-only RelNav [13, 62]. Unsurprisingly, the solutions (e.g., maneuvering the observer) for space applications are largely the same as for maritime applications. Indeed, many of the novel approaches for spacecraft angles-only RelNav are actually rediscoveries of the dynamic triangulation techniques known for decades within the context maritime BO-TMA.

III. Projective Geometry, Camera Models, and Images

Proper development and analysis of triangulation methods requires a model of the instrument used to acquire the LOS measurements. This work assumes an optical instrument obeying projective geometry and its mathematical representation is referred to here as the *camera model*. The subsections that follow first develop the camera model from the perspective of algebraic projective geometry [63] and then consider the measurement statistics.

A. Ideal Camera Model

Suppose a spacecraft at position \mathbf{r} views an object located as position \mathbf{p}_i with an optical instrument. In many cases the sensor only provides a measurement of the LOS direction $\boldsymbol{\ell}_i$

$$\boldsymbol{\ell}_i \propto \mathbf{p}_i - \mathbf{r} \quad (1)$$

Here, $\boldsymbol{\ell}_i$ is of arbitrary scale and describes a point in \mathbb{P}^2 . For additional information on projective space (e.g., $\mathbb{P}^2, \mathbb{P}^3, \mathbb{P}^n$), see Refs. [5, 49, 64]. The relationship in Eq. (1) is true in any consistent frame.

When the optical instrument is a camera (or telescope) obeying projective geometry, the LOS direction $\boldsymbol{\ell}_i$ is produced

by back-projecting a ray out of the camera that corresponds to a specific pixel coordinate $\mathbf{u}_i^T = [u_i, v_i]$ in a digital image. Although formation of the LOS direction ℓ_i may be accomplished in any frame, it is convenient to choose the sensor frame (which, in this case, is the *camera frame*). The most popular camera frame convention—and the one chosen here—places the origin at the center of the camera’s entrance pupil (i.e., apparent pinhole location to an observer outside the camera). The camera frame z -axis is along the camera boresight direction (positive out of the camera). The orientation of the x - and y -axes vary in the literature, but this work adopts the convention of Ref. [5] that aligns the x -axis with the image u -direction and the y -axis with the image v -direction. Details and diagrams are provided in Ref. [5].

Now, in the case where the camera attitude is known, it is possible to express everything in the camera frame. Different normalizations of the direction ℓ_i in the camera frame (denoted by the subscript C) describe the pinhole camera geometry [5], such that

$$\begin{bmatrix} x_i \\ y_i \\ 1 \end{bmatrix} = \bar{\mathbf{x}}_i \propto \mathbf{a}_{C_i} \propto \ell_{C_i} \propto \mathbf{p}_{C_i} - \mathbf{r}_C \quad (2)$$

where $\mathbf{a}_{C_i} = \ell_{C_i} / \|\ell_{C_i}\|$ is a unit vector pointing from the camera to the observed object and where $\mathbf{x}_i^T = [x_i, y_i]$ are the 2-D coordinates where the direction ℓ_{C_i} pierces the camera frame’s $z = 1$ plane (which is sometimes called the image plane). The 3-D camera frame coordinates of the $z = 1$ image plane intersection point is the same as \mathbf{x}_i written in homogeneous coordinates, which is denoted here as $\bar{\mathbf{x}}_i^T = [\mathbf{x}_i^T, 1]$. As will become apparent, efficiently moving between the different choices of normalization in Eq. (2) provides numerous algorithmic benefits and insights.

Contemporary space cameras most commonly produce a digital image. A 2-D point $\mathbf{x}_i^T = [x_i, y_i]$ on the image plane corresponds to a 2-D point $\mathbf{u}_i^T = [u_i, v_i]$ in the digital image. Writing \mathbf{u}_i in homogeneous coordinates, $\bar{\mathbf{u}}_i^T = [\mathbf{u}_i^T, 1]$, the affine transformation between the two image point representations is given by,

$$\begin{bmatrix} u_i \\ v_i \\ 1 \end{bmatrix} = \bar{\mathbf{u}}_i = \mathbf{K}\bar{\mathbf{x}}_i \quad (3)$$

where \mathbf{K} is the so-called *camera calibration matrix* (or, sometimes, the camera intrinsics matrix),

$$\mathbf{K} = \begin{bmatrix} d_x & \alpha & u_p \\ 0 & d_y & v_p \\ 0 & 0 & 1 \end{bmatrix} \quad (4)$$

In most cases $\alpha \approx 0$ and this transformation simply shifts the origin (u_p and v_p) and converts from units of length to units of pixels (d_x and d_y). More details are provided in Ref. [5].

The matrix \mathbf{K} is almost always known for space cameras. The five calibration terms contained within this matrix may be estimated prior to launch, and it is straightforward to recalibrate the camera on-orbit using images of starfields [43, 65, 66]. When \mathbf{K} is known, the apparent pixel coordinates of a point (e.g., star, distant celestial body, surface landmark) in an image may be transformed to the camera frame LOS direction ℓ_{C_i} as

$$\ell_{C_i} \propto \mathbf{a}_{C_i} \propto \bar{\mathbf{x}}_i = \mathbf{K}^{-1} \bar{\mathbf{u}}_i \quad (5)$$

where the matrix inverse \mathbf{K}^{-1} may be analytically computed as discussed in Ref. [5].

B. LOS Representations and Measurement Models

The choice of LOS representation and its covariance model is one of the most important decisions the designer of a triangulation algorithm must make. A good choice will often allow for an elegant and statistically optimal solution. Conversely, a poor choice will lead to a complicated (and usually iterative) solution.

The most common choice of LOS representation for spacecraft navigation is a unit vector. The popularity of this choice can be traced to the great success of unit vectors for star-based attitude determination. The problem of spacecraft attitude determination from unit vectors in correspondence was posed by Grace Wahba in 1965 [67] and a number of elegant solutions have been proposed since then [43, 68–70]. These algorithms are the workhorse of modern star-based attitude determination and play a central role in commercially available star trackers.

Proceeding in a similar way, consider the LOS direction represented by the unit vector \mathbf{a} . Let the noisy measurement of that unit vector be $\tilde{\mathbf{a}} = \mathbf{a} + \boldsymbol{\eta}$, where $\boldsymbol{\eta} \sim \mathcal{N}(\mathbf{0}_{3 \times 1}, \mathbf{R}_{QMM})$. In what is now known as the QUEST measurement model (QMM), the covariance of a unit vector (to first order) with isotropic direction uncertainty is [69]

$$\mathbf{R}_{QMM} = E[\boldsymbol{\eta}\boldsymbol{\eta}^T] = \sigma_\theta^2 (\mathbf{I}_{3 \times 3} - \mathbf{a}\mathbf{a}^T) \quad (6)$$

where σ_θ^2 is the variance of the unit vector pointing direction (in radians). This is true regardless of the frame in which \mathbf{a} is expressed. Since both \mathbf{a} and $\tilde{\mathbf{a}}$ are constrained to be unit vectors, the covariance matrix \mathbf{R}_{QMM} is rank two and describes a plane tangent to the unit sphere at the point \mathbf{a} . Importantly, solutions to Wahba's problem are known to provide a maximum likelihood estimate (MLE) of the attitude when unit vector measurements are assumed to follow the QMM [71]. This justifiably led to widespread adoption of the unit vector and QMM convention.

Building on past successes with spacecraft attitude determination, it would seem logical to represent LOS directions for spacecraft triangulation with the unit vector \mathbf{a} and covariance from Eq. (6). However, these are generally poor choices

in practice. There are two problems. The first problem is that the QMM constrains $\boldsymbol{\eta}$ to lie on the unit sphere's tangent plane such that $\tilde{\boldsymbol{a}}$ is not a unit vector (specifically, $\|\tilde{\boldsymbol{a}}\| > 1$). Although it is a second-order effect, these difficulties with additive noise are well-known and have led some to consider a multiplicative error model [72]. Avoiding the (usually) artificial unit vector normalization eliminates the need for the multiplicative error model. The second (and more important) problem is that the QMM from Eq. (6) is not the correct noise model when the sensor is a camera or telescope.

To build the correct error covariance for an LOS measurement, begin by considering how these measurements are constructed from a digital image. Recall that LOS directions originate as image points with pixel coordinates $\{u_i, v_i\}_{i=1}^n$. Depending on the type of object and image processing technique used (e.g., centroiding of an unresolved celestial body [73], cross-correlation of a terrain maplet [2, 74], localization of a SIFT keypoint [75]), there will be some uncertainty in the pixel coordinates $[u_i, v_i]$ used to create the LOS measurement. Therefore, let the pixel coordinate $\boldsymbol{u}_i^T = [u_i, v_i]$ produce the camera frame LOS measurement ℓ_{C_i} using Eq. (5). Describe the zero-mean, Gaussian measurement noise in the image point location by $\boldsymbol{v}_i \sim \mathcal{N}(0, \boldsymbol{R}_{u_i})$, such that

$$\tilde{\boldsymbol{u}}_i = \boldsymbol{u}_i + \boldsymbol{v}_i \quad (7)$$

where the measurement covariance $\boldsymbol{R}_{u_i} = E[\boldsymbol{v}_i \boldsymbol{v}_i^T]$ is a 2×2 matrix. Thus, following Eq. (5),

$$\tilde{\ell}_{C_i} \propto \tilde{\boldsymbol{x}}_i = \boldsymbol{K}^{-1} \tilde{\boldsymbol{u}}_i = \boldsymbol{K}^{-1} \bar{\boldsymbol{u}}_i + \boldsymbol{K}^{-1} \boldsymbol{S}^T \boldsymbol{v}_i \quad (8)$$

where

$$\begin{bmatrix} \tilde{\boldsymbol{u}}_i \\ \tilde{v}_i \\ 1 \end{bmatrix} = \tilde{\boldsymbol{u}}_i = \bar{\boldsymbol{u}}_i + \boldsymbol{S}^T \boldsymbol{v}_i \quad (9)$$

$$\boldsymbol{S} = \begin{bmatrix} \boldsymbol{I}_{2 \times 2} & \mathbf{0}_{2 \times 1} \end{bmatrix} \quad (10)$$

Moreover, defining $\boldsymbol{w}_i = \boldsymbol{K}^{-1} \boldsymbol{S}^T \boldsymbol{v}_i$, one has

$$\tilde{\boldsymbol{x}}_i = \bar{\boldsymbol{x}}_i + \boldsymbol{w}_i \quad (11)$$

Thus, making use of Eq. (8), it follows that the error covariance of $\tilde{\boldsymbol{x}}$ is

$$\boldsymbol{R}_{\tilde{\boldsymbol{x}}_i} = E[\boldsymbol{w}_i \boldsymbol{w}_i^T] = \boldsymbol{K}^{-1} \boldsymbol{S}^T \boldsymbol{R}_{u_i} \boldsymbol{S} \boldsymbol{K}^{-T} \quad (12)$$

Since $\mathbf{x} = S\bar{\mathbf{x}}$, the 2×2 covariance on the image plane is

$$\mathbf{R}_{\mathbf{x}_i} = S\mathbf{R}_{\bar{\mathbf{x}}_i}S^T = SK^{-1}S^T\mathbf{R}_{\mathbf{u}_i}SK^{-T}S^T \quad (13)$$

Finally, as was shown in Ref. [76], the covariance of the unit vector LOS direction is given by

$$\mathbf{R}_{\mathbf{a}_i} = \begin{pmatrix} \partial\mathbf{a}_i \\ \partial\mathbf{x}_i \end{pmatrix} \mathbf{R}_{\mathbf{x}_i} \begin{pmatrix} \partial\mathbf{a}_i \\ \partial\mathbf{x}_i \end{pmatrix}^T \quad (14)$$

where the Jacobian $\partial\mathbf{a}_i/\partial\mathbf{x}_i$ is the 3×2 matrix

$$\frac{\partial\mathbf{a}_i}{\partial\mathbf{x}_i} = \left(\frac{1}{\|\bar{\mathbf{x}}_i\|} \mathbf{I}_{3 \times 3} - \frac{1}{\|\bar{\mathbf{x}}_i\|^3} \bar{\mathbf{x}}_i \bar{\mathbf{x}}_i^T \right) S^T = \frac{-1}{\|\bar{\mathbf{x}}_i\|} [\mathbf{a}_i \times]^2 S^T \quad (15)$$

and where $[\cdot \times]$ is the skew-symmetric cross-product matrix, $[\mathbf{a} \times] \mathbf{b} = \mathbf{a} \times \mathbf{b}$. It was shown in Ref. [76] that $\mathbf{R}_{QMM} \geq \mathbf{R}_a$, suggesting that the QMM provides a conservative bound of the measurement uncertainty. However, to use the QMM is to assume measurement statistics that are inconsistent with the optical instrument's actual behavior—ultimately leading to reduced state estimation performance.

The development of the triangulation methods that follow can be equivalently achieved with any normalization of the LOS direction ℓ_i and its corresponding error covariance. The authors prefer to use $\bar{\mathbf{x}}_i = K^{-1}\bar{\mathbf{u}}_i$ in almost all cases, since this is often easier than working with the unit vector \mathbf{a}_i .

IV. Trigonometric Solutions

Simple trigonometric relations may be used to develop two of the classical solutions to the triangulation problem. Referred to here as the *trigonometric solutions*, one solution method follows from the Law of Sines and the other follows from the Law of Cosines. Both of these solutions have found widespread use in computer vision.

In the discussions that follow, the development for both of the trigonometric solutions are first presented from a vector analysis perspective. This is done since the vector interpretation has clear algorithmic advantages. These solutions are then shown to be equivalent to either the Law of Sines or Law of Cosines. The reader is reminded that idea behind the Law of Sines was understood by the classical Greek geometers (Euclid's *Elements*, Prop. I.18 and I.19 [19]) and was known in its modern form by at least the 13th century CE (when it appears in the work of Nasir al-Din al-Tusi, "Treatise on the Quadrilateral" [77]). Similarly, the idea underpinning the Law of Cosines is also found in Euclid's *Elements* (Prop II.12 and II.13[19]) and appeared in its modern form by at least the 15th century CE (notably in the work Jamshīd al-Kāshī [78]). Thus, while the vector notation used here is modern, the fundamental relationships necessary to construct the trigonometric solutions to the triangulation problem would have been quite familiar to classical Greek, medieval Islamic, and Renaissance European geometers.

The trigonometric solutions are geometrically exact and produce a perfect solution when provided perfect (noise free) measurements. They have the advantage of not requiring any *a priori* position knowledge, admitting a closed-form solution, and being easily scalable to many ($n > 2$) measurements (with the methods based on Law of Sines being considerably better at scaling than the Law of Cosines). The classical trigonometric solutions both have the disadvantage of being statistically suboptimal when challenged with noisy measurements obtained from a camera, telescope, or other optical sensor. This suboptimality arises because they are conventionally written as an ordinary (unweighted) least squares problems, though the Law of Sines method may be easily modified to overcome this drawback (see Section V.B). Finally, under consistent normalization assumptions, the two trigonometric solutions produce identical results. Thus, of the two methods, the Law of Sines approach is usually preferred since it is simpler and scales better with many LOS measurements.

The discussions that follow are primarily written from the perspective of a resection problem (e.g., spacecraft navigation). If desired, a simple change in notation will transform these results into the intersection problem (e.g., 3-D reconstruction).

A. Law of Sines: The Direct Linear Transform (DLT)

Optical instruments such as cameras and telescopes measure LOS directions ℓ_i . However, the distance between the instrument and the observed object along that LOS direction is not directly measured—thus giving rise to the proportional relationship in Eq. (1). Rather than attempting to explicitly solve for these unknown distances, it is sometimes easier to remove them entirely by use of the Direct Linear Transform (DLT) [49, 79]. In recent years, this approach has been considered for both camera-based navigation with planetary landmarks (a resection problem) [80] and for orbit determination from ground-based telescope observations (an intersection problem) [40].

1. Development by Vector Analysis

The DLT is the simplest of the triangulation algorithms and its development consists of a few steps. To begin, consider the case where one obtains $n \geq 2$ LOS measurements $\{\ell_i\}_{i=1}^n$ to points with known 3-D locations $\{p_i\}_{i=1}^n$. Now, to remove the scale (i.e., range) ambiguity in Eq. (1), take the cross-product of both sides with the known LOS direction ℓ_i

$$[\ell_i \times] \ell_i \propto [\ell_i \times] (p_i - r) = \mathbf{0}_{3 \times 1} \quad (16)$$

Both Eq. (1) and Eq. (16) are true in any consistent frame, and so no frame-specific notation is required. Thus, after simplification,

$$[\ell_i \times] r = [\ell_i \times] p_i \quad (17)$$

If many LOS measurements $\{\ell_i\}_{i=1}^n$ are available, they may be stacked into a linear system as

$$\begin{bmatrix} [\ell_1 \times] \\ [\ell_2 \times] \\ \vdots \\ [\ell_n \times] \end{bmatrix} \mathbf{r} = \begin{bmatrix} [\ell_1 \times] \mathbf{p}_1 \\ [\ell_2 \times] \mathbf{p}_2 \\ \vdots \\ [\ell_n \times] \mathbf{p}_n \end{bmatrix} \quad (18)$$

This linear system may be solved in the least squares sense for the estimated spacecraft position $\hat{\mathbf{r}}$. The DLT equations [e.g., Eq. (17) or Eq. (18)] are the same for both resection and intersection forms of the triangulation problem since $\ell_i \propto \mathbf{p}_i - \mathbf{r} \propto \mathbf{r} - \mathbf{p}_i$. Though Eq. (18) is true in any frame, some frame choices have algorithmic advantages in certain situations.

It is desirable for a triangulation algorithm to produce a consistent solution regardless of the choice of localization frame [15]. This condition is satisfied for the DLT regardless of the frame chosen. To see this, suppose that one knows the locations of the n observed points $\{\mathbf{p}_{I_i}\}_{i=1}^n$ as expressed in some localization frame denoted by I . Further suppose the triangulation τ produces the solution $\bar{\mathbf{r}}_I = \tau(\{\bar{\mathbf{u}}_i\}_{i=1}^n, \{\bar{\mathbf{p}}_i\}_{i=1}^n)$, where $\bar{\mathbf{r}}_I^T = [\mathbf{r}_I^T, 1]$ and $\bar{\mathbf{p}}_i^T = [\mathbf{p}_{I_i}^T, 1]$. If \mathbf{M}_A^I is a 4×4 matrix describing a general frame transformation (rotation and translation) between two different localization frames I and A , then a consistent triangulation solution would imply $\mathbf{M}_A^I \bar{\mathbf{r}}_I = \tau(\{\bar{\mathbf{u}}_i\}_{i=1}^n, \mathbf{M}_A^I \{\bar{\mathbf{p}}_i\}_{i=1}^n)$. Simple substitution will show this condition to be satisfied for Eq. (18).

Since almost any reasonable frame convention may be used with Eq. (18), a simple convention is usually best. As an example, the specific convention preferred by the authors is now provided. Following the sensor model from Section III.A, the LOS measurements originate as pixel coordinates $\bar{\mathbf{u}}_i$ in a digital image. These image points produce a LOS measurements in the camera frame as described by Eq. (5). Recognizing that different LOS measurements may come from different cameras, denote the camera frame producing image point $\bar{\mathbf{u}}_i$ as C_i and the corresponding camera calibration matrix as \mathbf{K}_i . If all the measurements come from one image, then they all come from the same camera and $C = C_i$, $\mathbf{K} = \mathbf{K}_i \forall i$. Thus, taking the most straightforward approach, one may write

$$[\mathbf{K}_i^{-1} \bar{\mathbf{u}}_i \times] \mathbf{T}_{C_i}^I \mathbf{r}_I = [\mathbf{K}_i^{-1} \bar{\mathbf{u}}_i \times] \mathbf{T}_{C_i}^I \mathbf{p}_{I_i} \quad (19)$$

where $\mathbf{T}_{C_i}^I$ is the attitude transformation matrix that transforms a vector expressed in frame I to that same vector expressed in frame C_i . The result in Eq. (19) makes use of the LOS normalization $\ell_{C_i} \propto \bar{\mathbf{x}}_i = \mathbf{K}_i^{-1} \bar{\mathbf{u}}_i$. Although any LOS normalization may be used, some care is required since (re)normalization acts as a weighting on the affected rows of the linear system from Eq. (18). Inconsistent normalization can result in inconsistent weighting of the measurements, which can result in poor triangulation performance. This observation is the motivation for the statistically optimal

algorithm presented in Section V.B.

If many image points $\{\bar{\mathbf{u}}_i\}_{i=1}^n$ are available, the corresponding vector equations from Eq. (19) may be stacked into a linear system as

$$\begin{bmatrix} [\mathbf{K}_1^{-1}\bar{\mathbf{u}}_1 \times] \mathbf{T}_{C_1}^I \\ [\mathbf{K}_2^{-1}\bar{\mathbf{u}}_2 \times] \mathbf{T}_{C_2}^I \\ \vdots \\ [\mathbf{K}_n^{-1}\bar{\mathbf{u}}_n \times] \mathbf{T}_{C_n}^I \end{bmatrix} \mathbf{r}_I = \begin{bmatrix} [\mathbf{K}_1^{-1}\bar{\mathbf{u}}_1 \times] \mathbf{T}_{C_1}^I \mathbf{p}_{I_1} \\ [\mathbf{K}_2^{-1}\bar{\mathbf{u}}_2 \times] \mathbf{T}_{C_2}^I \mathbf{p}_{I_2} \\ \vdots \\ [\mathbf{K}_n^{-1}\bar{\mathbf{u}}_n \times] \mathbf{T}_{C_n}^I \mathbf{p}_{I_n} \end{bmatrix} \quad (20)$$

This linear system may be solved in the least squares sense for the estimated spacecraft position $\hat{\mathbf{r}}_I$. An analytic expression for the covariance of this position estimate is given in the Appendix.

2. Relationship to Law of Sines

It was shown in Ref. [80] that the key relation from Eq. (17) is simply the Law of Sines in disguise. Making use of the angles from Fig. 6, write the Law of Sines for the triangle formed by the localization frame origin, \mathbf{p}_i , and \mathbf{r} ,

$$\frac{\sin \alpha_i}{\|\mathbf{r}\|} = \frac{\sin \beta_i}{\|\mathbf{p}_i\|} \quad (21)$$

which is the same as

$$\|\mathbf{r}\| \sin \beta_i = \|\mathbf{p}_i\| \sin \alpha_i \quad (22)$$

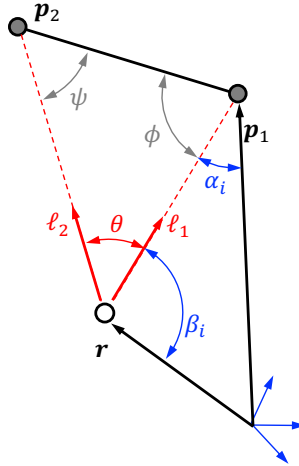


Fig. 6 The DLT is a vector representation of the Law of Sines using angles α_i and β_i .

This expression is true regardless of the frame in which the vector quantities are expressed. Recalling that $\|\mathbf{a} \times \mathbf{b}\| = \|\mathbf{a}\| \|\mathbf{b}\| \sin \theta$ and accounting for the sign of the cross-product,

$$\|\mathbf{r}\| \sin \beta_i = \|\mathbf{r}\| \frac{\boldsymbol{\ell}_i \times \mathbf{r}}{\|\mathbf{r}\| \|\boldsymbol{\ell}_i\|} = \|\mathbf{p}_i\| \frac{\boldsymbol{\ell}_i \times \mathbf{p}_i}{\|\boldsymbol{\ell}_i\| \|\mathbf{p}_i\|} = \|\mathbf{p}_i\| \sin \alpha_i \quad (23)$$

Simplifying the middle two terms yields

$$\boldsymbol{\ell}_i \times \mathbf{r} = \boldsymbol{\ell}_i \times \mathbf{p}_i \quad (24)$$

which is exactly the same as Eq. (17). Hence, the familiar DLT solution is a vector representation of the Law of Sines.

3. Relationship to the Collinearity Equations

There are other ways of representing the triangulation problem as a linear system, and some of these other representations are the same as the DLT. For example, consider triangulation with the collinearity equations.

To arrive at the collinearity equations, rewrite the pinhole camera model from Eq. (2) in homogeneous coordinates and remove the proportionality constraint by introducing the scaling $\alpha_i \neq 0$

$$\alpha_i \bar{\mathbf{x}}_i = \mathbf{T}_{C_i}^l (\mathbf{p}_{I_i} - \mathbf{r}_I) \quad (25)$$

or, equivalently,

$$\begin{bmatrix} \alpha_i x_i \\ \alpha_i y_i \\ \alpha_i \end{bmatrix} = \begin{bmatrix} -\mathbf{T}_{C_i}^l & \mathbf{T}_{C_i}^l \mathbf{p}_{I_i} \end{bmatrix} \begin{bmatrix} \mathbf{r}_I \\ 1 \end{bmatrix} \quad (26)$$

Define the rows of $\mathbf{T}_{C_i}^l$ as

$$\mathbf{T}_{C_i}^l = \begin{bmatrix} \mathbf{t}_1^T \\ \mathbf{t}_2^T \\ \mathbf{t}_3^T \end{bmatrix} \quad (27)$$

and the elements of $\mathbf{T}_{C_i}^l \mathbf{p}_{I_i}$ as

$$\mathbf{T}_{C_i}^l \mathbf{p}_{I_i} = \begin{bmatrix} p_1 & p_2 & p_3 \end{bmatrix}^T \quad (28)$$

The three rows of the pinhole camera model are now

$$\alpha_i x_i = -\mathbf{t}_1^T \mathbf{r}_I + p_1 \quad (29a)$$

$$\alpha_i y_i = -\mathbf{t}_2^T \mathbf{r}_I + p_2 \quad (29b)$$

$$\alpha_i = -\mathbf{t}_3^T \mathbf{r}_I + p_3 \quad (29c)$$

Dividing Eqs. (29a) and (29b) by Eq. (29c) gives the classical collinearity equations seen in textbooks and widely-used in a variety of applications (e.g., the so-called CAHVOR model for planetary photogrammetry [81, 82])

$$x_i = \frac{-\mathbf{t}_1^T \mathbf{r}_I + p_1}{-\mathbf{t}_3^T \mathbf{r}_I + p_3} = \frac{\mathbf{t}_1^T (\mathbf{p}_{I_i} - \mathbf{r}_I)}{\mathbf{t}_3^T (\mathbf{p}_{I_i} - \mathbf{r}_I)} \quad (30a)$$

$$y_i = \frac{-\mathbf{t}_2^T \mathbf{r}_I + p_2}{-\mathbf{t}_3^T \mathbf{r}_I + p_3} = \frac{\mathbf{t}_2^T (\mathbf{p}_{I_i} - \mathbf{r}_I)}{\mathbf{t}_3^T (\mathbf{p}_{I_i} - \mathbf{r}_I)} \quad (30b)$$

Within the context of triangulation, the collinearity equations may be used to construct a linear system for \mathbf{r}_I . To do this, substitute Eq. (29c) into Eqs. (29a) and (29b)

$$x_i(-\mathbf{t}_3^T \mathbf{r}_I + p_3) = -\mathbf{t}_1^T \mathbf{r}_I + p_1 \quad (31a)$$

$$y_i(-\mathbf{t}_3^T \mathbf{r}_I + p_3) = -\mathbf{t}_2^T \mathbf{r}_I + p_2 \quad (31b)$$

Rearranging this pair of equations and stacking them into matrix form yields (writing the equation for y_i first) a linear system that may be solved for \mathbf{r}_I

$$\begin{bmatrix} y_i \mathbf{t}_3^T - \mathbf{t}_2^T \\ \mathbf{t}_2^T - x_i \mathbf{t}_3^T \end{bmatrix} \mathbf{r}_I = \begin{bmatrix} y_i p_3 - p_2 \\ p_1 - x_i p_3 \end{bmatrix} \quad (32)$$

Which is easily verified to be the same as

$$\mathbf{S} [\bar{\mathbf{x}} \times] \mathbf{T}_{C_i}^T \mathbf{r}_I = \begin{bmatrix} y_i \mathbf{t}_3^T \mathbf{r}_I - \mathbf{t}_2^T \mathbf{r}_I \\ \mathbf{t}_2^T \mathbf{r}_I - x_i \mathbf{t}_3^T \mathbf{r}_I \end{bmatrix} = \begin{bmatrix} y_i p_3 - p_2 \\ p_1 - x_i p_3 \end{bmatrix} = \mathbf{S} [\bar{\mathbf{x}} \times] \mathbf{T}_{C_i}^T \mathbf{p}_{I_i} \quad (33)$$

where \mathbf{S} is from Eq. (10). Hence, comparing this result to Eq. (19) and recalling that $\bar{\mathbf{x}}_i = \mathbf{K}_i^{-1} \bar{\mathbf{u}}_i$, the collinearity equations for each measured image point are exactly the first two rows of the corresponding part of the DLT. Since the skew-symmetric matrix $[\bar{\mathbf{x}} \times]$ is only rank two, the third row is redundant (linearly dependent on the first two). Thus, solving the DLT is equivalent to solving the collinearity equations (and vice versa).

4. Relationship to Plücker Coordinates

Given the algebraic projective geometry framework considered here, it is logical to consider triangulation through the use of Plücker coordinates. Introduced in 1865 [83], the so-called Plücker coordinates are a way of representing a 3-D line in \mathbb{P}^3 using the ratios between six parameters (a point in \mathbb{P}^5). This representation of 3-D lines has become popular for a variety of computer vision applications [15].

The LOS direction $\ell_i \in \mathbb{P}^2$ is formed by the line passing through the origin (camera location in the camera frame) and the camera-relative point location $\mathbf{p}_i - \mathbf{r}$. The corresponding LOP is a 3-D line (not necessarily passing through the origin) passing through two points $\mathbf{r} \in \mathbb{R}^3$ and $\mathbf{p}_i \in \mathbb{R}^3$. Therefore, consider the triangulation problem as expressed in \mathbb{P}^3 . In this case, let the spacecraft position be denoted by $\bar{\mathbf{r}}^T = [\mathbf{r}^T, 1]$ and the known point's position be denoted by $\bar{\mathbf{p}}_i^T = [\mathbf{p}_i^T, 1]$. Describe the LOP as the line in \mathbb{P}^3 formed by the join of the points $\bar{\mathbf{r}} \in \mathbb{P}^3$ and $\bar{\mathbf{p}}_i \in \mathbb{P}^3$, which may be written directly using the Plücker matrix L_i [15]

$$L_i \propto \bar{\mathbf{r}}\bar{\mathbf{p}}_i^T - \bar{\mathbf{p}}_i\bar{\mathbf{r}}^T \quad (34)$$

The present application requires the dual representation L_i^* , which may be computed as

$$L_i^* \propto \begin{bmatrix} [(\mathbf{r} - \mathbf{p}_i) \times] & (\mathbf{p}_i \times \mathbf{r}) \\ (\mathbf{r} \times \mathbf{p}_i)^T & 0 \end{bmatrix} \quad (35)$$

Since the same line is formed by any two points along the line, one may use the relation from Eq. (1) to find

$$L_i^* \propto \begin{bmatrix} [\ell_i \times] & (\mathbf{p}_i \times \ell_i) \\ (\ell_i \times \mathbf{p}_i)^T & 0 \end{bmatrix} \quad (36)$$

This solution is valid in any frame, and one may easily choose to express this problem in the camera frame, localization frame, or any other frame. Now, recall that any point $\bar{\mathbf{q}}^T \propto [\mathbf{q}^T, 1] \in \mathbb{P}^3$ lies on the line when $L_i^* \bar{\mathbf{q}} = \mathbf{0}_{4 \times 1}$. Thus, it follows that

$$L_i^* \bar{\mathbf{r}} = \mathbf{0}_{4 \times 1} \quad (37)$$

The matrix L_i^* has rank two. Hence when $n \geq 2$ unique LOS measurements are available one may construct the linear system

$$\begin{bmatrix} L_1^* \\ \vdots \\ L_n^* \end{bmatrix} \bar{\mathbf{r}} = \mathbf{0}_{4n \times 1} \quad (38)$$

The result in Eq. (38) is a null space problem and the least squares solution for $\bar{\mathbf{r}}$ may be found directly via the Singular Value Decomposition (SVD). The resulting $\hat{\mathbf{r}} \in \mathbb{P}^3$ is a 4×1 vector with ambiguous scale (it represents the null space direction) and one may recover the camera location $\hat{\mathbf{r}} \in \mathbb{R}^3$ by scaling the fourth component to unity.

It is now observed that the Plücker coordinate solution shown here is the same as the DLT solution. To see this, begin by noting that the first three rows of Eq. (37) are

$$\begin{bmatrix} [\ell_i \times] & (\mathbf{p}_i \times \ell_i) \end{bmatrix} \begin{bmatrix} \mathbf{r} \\ 1 \end{bmatrix} = \mathbf{0}_{3 \times 1} \quad (39)$$

which is the same as

$$[\ell_i \times] \mathbf{r} + (\mathbf{p}_i \times \ell_i) = \mathbf{0}_{3 \times 1} \quad (40)$$

$$[\ell_i \times] \mathbf{r} = [\ell_i \times] \mathbf{p}_i \quad (41)$$

which, in turn, is identical to the foundational DLT expression from Eq. (17). Moreover, the fourth row in Eq. (37) is linearly dependent on the first three rows and simply says that \mathbf{r} must lie in the plane spanned by the origin and the 3D LOS (i.e., the line connecting \mathbf{p}_i and \mathbf{r}). To arrive at this result, observe that the normal to this plane as expressed in the camera frame is given by $\ell_i \times \mathbf{p}_i$. Since the camera location \mathbf{r} lies along the LOS, it must lie in this plane. Hence $(\ell_i \times \mathbf{p}_i)^T \mathbf{r} = 0$, which is the fourth row in Eq. 37.

B. Law of Cosines: Explicit Range Estimation

The missing piece of information for each measurement is the unknown range $\rho_i = \|\mathbf{p}_i - \mathbf{r}\|$, and so it is understandable that one might wish to explicitly estimate these unknown ranges. Following this line of reasoning, the unknown scale in Eq. (1) may be made explicit by introducing the range,

$$\rho_i \mathbf{a}_i = \mathbf{p}_i - \mathbf{r} \propto \ell_i \quad (42)$$

which is true in any consistent frame. Solving the triangulation problem by finding the unknown ranges $\{\rho_i\}_{i=1}^n$ has been suggested within the context of spacecraft navigation by a number of authors [8, 11, 84].

1. Development by Vector Analysis

As before, consider the case where one obtains $n \geq 2$ LOS measurements $\{\ell_i\}_{i=1}^n$ to points with known 3-D locations $\{\mathbf{p}_i\}_{i=1}^n$. Choose to normalize the LOS measurements to be the unit vectors $\{\mathbf{a}_i\}_{i=1}^n$. Thus, by rearrangement of Eq. (42),

$$\mathbf{r} = \mathbf{p}_i - \rho_i \mathbf{a}_i \quad (43)$$

where the objective is to find \mathbf{r} without any *a priori* knowledge of ρ_i . Since \mathbf{r} is the same for all measurements, the relation from Eq. (43) may be used to equate any pair of measurements $i \neq j$,

$$\mathbf{p}_i - \rho_i \mathbf{a}_i = \mathbf{r} = \mathbf{p}_j - \rho_j \mathbf{a}_j \quad (44)$$

which can be rearranged to find

$$\rho_j \mathbf{a}_j - \rho_i \mathbf{a}_i = \mathbf{p}_j - \mathbf{p}_i \quad (45)$$

Now, let \mathbf{d}_{ij} be the vector from \mathbf{p}_i to \mathbf{p}_j ,

$$\mathbf{d}_{ij} = \mathbf{p}_j - \mathbf{p}_i \quad (46)$$

Substituting for \mathbf{d}_{ij} and left-multiplying by either \mathbf{a}_i^T or \mathbf{a}_j^T leads to a pair of equations that are linear in the unknown ranges ρ_i and ρ_j

$$(\mathbf{a}_i^T \mathbf{a}_j) \rho_j - \rho_i = \mathbf{a}_i^T \mathbf{d}_{ij} \quad (47)$$

$$\rho_j - (\mathbf{a}_j^T \mathbf{a}_i) \rho_i = \mathbf{a}_j^T \mathbf{d}_{ij} \quad (48)$$

It is possible to construct such a pair of equations for every $\{i, j\}$ satisfying $i < j \leq n$, ultimately producing a total of $2 \binom{n}{2}$ relationships with n unknown range values. The resulting equations may be stacked to create a linear least squares problem that may be solved for the n unknown ranges. For example, the case of $n = 3$ leads to the following linear system

$$\begin{bmatrix} -1 & \mathbf{a}_1^T \mathbf{a}_2 & 0 \\ -\mathbf{a}_2^T \mathbf{a}_1 & 1 & 0 \\ -1 & 0 & \mathbf{a}_1^T \mathbf{a}_3 \\ -\mathbf{a}_3^T \mathbf{a}_1 & 0 & 1 \\ 0 & -1 & \mathbf{a}_2^T \mathbf{a}_3 \\ 0 & -\mathbf{a}_3^T \mathbf{a}_2 & 1 \end{bmatrix} \begin{bmatrix} \rho_1 \\ \rho_2 \\ \rho_3 \end{bmatrix} = \begin{bmatrix} \mathbf{a}_1^T \mathbf{d}_{12} \\ \mathbf{a}_2^T \mathbf{d}_{12} \\ \mathbf{a}_1^T \mathbf{d}_{13} \\ \mathbf{a}_3^T \mathbf{d}_{13} \\ \mathbf{a}_2^T \mathbf{d}_{23} \\ \mathbf{a}_3^T \mathbf{d}_{23} \end{bmatrix} \quad (49)$$

which may be solved in the least squares sense for the estimated ranges $\{\hat{\rho}_i\}_{i=1}^n$. Of note is that Eq. (49) is true in any consistent frame.

With the ranges known, it is possible to solve for \mathbf{r} directly using Eq. (43) for any one of the LOS measurements. In general, however, it may be more desirable to solve for the position as the average of all the LOS measurements. Since

the position is typically desired in the localization frame,

$$\hat{\mathbf{r}}_I = \frac{1}{n} \sum_{i=1}^n (\mathbf{p}_{I_i} - \hat{\rho}_i \mathbf{a}_{I_i}) \quad (50)$$

An analytic expression for the covariance of this position estimate is given in the Appendix.

2. Relationship to Law of Cosines

It may be shown that Eq. (47) and Eq. 48 [and, hence, the rows of the linear system in Eq. (49)] are nothing more than the Law of Cosines in disguise. Therefore, begin by writing the Law of Cosines as for each of the interior angles belonging to the triangle described by edges ρ_i , ρ_j , and $\|\mathbf{d}_{ij}\|$:

$$\|\mathbf{d}_{ij}\|^2 = \rho_i^2 + \rho_j^2 - 2\rho_i\rho_j\mathbf{a}_i^T\mathbf{a}_j \quad (51)$$

$$\rho_i^2 = \|\mathbf{d}_{ij}\|^2 + \rho_j^2 - 2\rho_j\mathbf{d}_{ij}^T\mathbf{a}_j \quad (52)$$

$$\rho_j^2 = \rho_i^2 + \|\mathbf{d}_{ij}\|^2 + 2\rho_i\mathbf{d}_{ij}^T\mathbf{a}_i \quad (53)$$

Use Eq. (51) to substitute for $\|\mathbf{d}_{ij}\|$ in Eq. (52) to find

$$\rho_i^2 = \left(\rho_i^2 + \rho_j^2 - 2\rho_i\rho_j\mathbf{a}_i^T\mathbf{a}_j \right) + \rho_j^2 - 2\rho_j\mathbf{d}_{ij}^T\mathbf{a}_j \quad (54)$$

Next, after eliminating ρ_i^2 ,

$$2\rho_j^2 - 2\rho_i\rho_j\mathbf{a}_i^T\mathbf{a}_j = 2\rho_j\mathbf{d}_{ij}^T\mathbf{a}_j \quad (55)$$

This simplifies to

$$\rho_j - \rho_i(\mathbf{a}_i^T\mathbf{a}_j) = \mathbf{d}_{ij}^T\mathbf{a}_j \quad (56)$$

and is identical to Eq. (48). Likewise, substitution of Eq. (51) into Eq. (53) will reproduce Eq. (47). Hence, the explicit range solution shown here is a vector representation of the Law of Cosines.

3. Difficulty with Scalability

Compared with other triangulation methods, the explicit range method does not scale well with a growing number of LOS measurements. In this method, the length of the state vector is dependent on the number of LOS measurements since the unknown range must be estimated for each measurement. Moreover, because the explicit range method depends on measurement pairs, the number of equations grows as $2\binom{n}{2}$ —which is nearly exponential for $n \gg 2$ —when every pairwise LOS combination is considered. For example, the consideration of only 20 LOS measurements would require

the solution to a least squares problem with a matrix of size 380×20 . To consider 192 measurements (which is the model point with the maximum number of measurements in the 3-D reconstruction example in Section VII.C) leads to a matrix of size $36,672 \times 192$. At best, the explicit range method would require inversion of a 192×192 matrix in this example—as compared to inversion of only a 3×3 matrix for either the DLT (Section IV.A) or the statistically optimal LOST algorithm (Section V.B). This rapid growth in problem size makes the explicit range estimation method comparatively undesirable for some applications.

C. Comparison of the Trigonometric Solutions

Both of the trigonometric solutions are exact when provided perfect measurements. Interestingly, with provided with noisy measurements, both the DLT method (Section IV.A) and the explicit range method (Section IV.B) produce an identical estimate of $\hat{\mathbf{r}}_I$ when a consistent LOS normalization is used. Specifically, this occurs when the LOS measurements in the DLT are scaled to be unit vectors [i.e., choose $\ell_i \propto \mathbf{a}_i$ in Eq. (18)]. This can be shown analytically for the case of two measurements, and a proof is provided in the Appendix. The results can also be observed in numerical experiments (see Section VII.A, especially Fig. 11). As compared to the DLT solution suggested in Eq. (20), this normalization weights points near the image center more and points near the image edges less (since $\|\bar{\mathbf{x}}_i\|^{-1}$ is larger near the image center). While point localization performance may indeed be better near the image center and worse near the image edges (e.g., empirical focal plane model from Ref. [85]), the relative weighting of these observations should be derived from the measurement statistics and not from an arbitrary normalization scheme. Proper accounting of this fact tends to favor the DLT solution over the explicit range solution.

From a practical standpoint, there are a few reasons to prefer the DLT solution over the explicit range solution. The DLT is (1) much simpler, (2) scales more elegantly with many measurements, and (3) allows for easy control of the normalization scheme. The DLT also forms the foundation for statistically optimal triangulation (i.e., LOST algorithm in Section V.B) and dynamic triangulation (Section VI). For these reasons, the DLT method (Law of Sines method) is almost always preferable to the explicit range method (Law of Cosines method).

V. Optimal Triangulation

The trigonometric solutions from Section IV do not usually provide a statistically optimal estimate of the unknown point's location. Though both of these solutions do solve a least squares optimization problem, they do not minimize the correct cost function. Proper formulation of the cost function requires consideration how LOS measurement errors are related to state estimation errors and a realization that some measurements provide better information than others. One appropriate way to proceed is with a maximum likelihood estimate (MLE) framework [86, 87]. The two-measurement case admits some interesting optimal solutions, though the classical approach requires finding the roots of a polynomial of degree six [15]. After first reviewing this special case, a more general approach—referred to here as the Linear

Optimal Sine Triangulation (LOST) algorithm—is shown to provide an equivalent estimate as the solution to a linear system. The new LOST algorithm is generally preferable to the classical polynomial solutions in that (1) it provides an equivalent solution without the need to solve a degree six polynomial and (2) it provides the MLE for an arbitrary number ($n \geq 2$) of LOS measurements as the solution to a linear system (with no iteration).

A. Two LOS Measurements: The Polynomial Methods

At least two absolute LOS measurements are necessary to triangulate the location of a camera and some interesting algorithms arise when exactly two LOS measurements exist. There are two different scenarios to consider here. The first scenario is when the two LOS measurements are collected from different cameras and extracted from different images, and so the two measured points generally lie in two different image planes. The second scenario is when both of the LOS measurements are collected by the same camera and extracted from the same image, and so the two measured points lie in the same image plane. These two scenarios lead to two different (but equivalent) optimal algorithms. The solution for two images involves solving a polynomial of degree six, while the solution for a single image involves solving only a quadratic equation.

Consider a collection of LOS measurements to n objects that were produced by optical instruments. Applying the measurement model from Section III.B,

$$\mathbf{u}_i = \mathbf{S}\tilde{\mathbf{u}}_i = h_i(\mathbf{r}) = \frac{\mathbf{S}\mathbf{K}\mathbf{T}_{C_i}^T(\mathbf{p}_{I_i} - \mathbf{r}_I)}{\mathbf{k}^T \mathbf{T}_{C_i}^T(\mathbf{p}_{I_i} - \mathbf{r}_I)} \quad (57)$$

and a noisy measurement of

$$\tilde{\mathbf{u}}_i = \mathbf{u}_i + \mathbf{v}_i = h_u(\mathbf{r}) + \mathbf{v}_i \quad (58)$$

As before, assuming $\mathbf{v}_i \sim \mathcal{N}(\mathbf{0}_{2 \times 1}, \mathbf{R}_{u_i})$ and that the additive noise on measurements i and j are uncorrelated (i.e., $E[\mathbf{v}_i^T \mathbf{v}_j] = \mathbf{0}_{2 \times 2}$), the MLE statement is

$$\max J(\mathbf{r}) = C \exp \left\{ - \sum_{i=1}^n [\tilde{\mathbf{u}}_i - h_i(\mathbf{r})]^T \mathbf{R}_{u_i}^{-1} [\tilde{\mathbf{u}}_i - h_i(\mathbf{r})] \right\} \quad (59)$$

which is the same as the minimization problem

$$\min J(\mathbf{r}) = \sum_{i=1}^n [\tilde{\mathbf{u}}_i - h_i(\mathbf{r})]^T \mathbf{R}_{u_i}^{-1} [\tilde{\mathbf{u}}_i - h_i(\mathbf{r})] \quad (60)$$

Thus, the MLE solution seeks to find the location \mathbf{r} that minimizes the reprojection errors as weighted by the measurement covariance. In many cases, the image point errors are isotropic and the measurement covariance is $\mathbf{R}_{u_i} \approx \sigma_{u_i}^2 \mathbf{I}_{2 \times 2}$. In

this case,

$$\min J(\mathbf{r}) = \sum_{i=1}^n \frac{1}{\sigma_{\mathbf{u}_i}^2} [\tilde{\mathbf{u}}_i - h_i(\mathbf{r})]^T [\tilde{\mathbf{u}}_i - h_i(\mathbf{r})] \quad (61)$$

Moreover, when there are only two LOS measurements ($n = 2$) and assuming similar uncertainty in each measurement (i.e., $\sigma_{\mathbf{u}_1} = \sigma_{\mathbf{u}_2}$), the cost function simplifies further to

$$\min_{\mathbf{r} \in \mathbb{R}^3} J(\mathbf{r}) = \|\tilde{\mathbf{u}}_1 - h_1(\mathbf{r})\|^2 + \|\tilde{\mathbf{u}}_2 - h_2(\mathbf{r})\|^2 \quad (62)$$

which is simply the sum of the squared reprojection errors. Since the two reprojected points $\mathbf{u}_1 = h_1(\mathbf{r})$ and $\mathbf{u}_2 = h_2(\mathbf{r})$ must satisfy the epipolar constraint, this is equivalent to

$$\begin{aligned} \min J(u_1, v_1, u_2, v_2) &= [(\tilde{u}_1 - u_1)^2 + (\tilde{v}_1 - v_1)^2] + [(\tilde{u}_2 - u_2)^2 + (\tilde{v}_2 - v_2)^2] \\ \text{s.t. } \tilde{\mathbf{u}}_2^T \mathbf{F} \tilde{\mathbf{u}}_1 &= 0 \end{aligned} \quad (63)$$

where \mathbf{F} is the fundamental matrix. This is the cost function suggested in the majority of the contemporary literature when seeking an “optimal” triangulation with two LOS measurements [15].

Further, for a calibrated camera with a known calibration matrix \mathbf{K} , the cost function may be rewritten in terms of the image plane coordinates. Assuming square pixels ($d_x = d_y$) and no detector skewness ($\alpha = 0$) the matrix \mathbf{K} simplifies and

$$\begin{aligned} \min J(x_1, y_1, x_2, y_2) &= w_1 [(\tilde{x}_1 - x_1)^2 + (\tilde{y}_1 - y_1)^2] + w_2 [(\tilde{x}_2 - x_2)^2 + (\tilde{y}_2 - y_2)^2] \\ \text{s.t. } \tilde{\mathbf{x}}_2^T \mathbf{E} \tilde{\mathbf{x}}_1 &= 0 \end{aligned} \quad (64)$$

where $w_i = 1/\sigma_{x_i}^2 = d_{x_i}^2/\sigma_{\mathbf{u}_i}^2$ and where \mathbf{E} is the essential matrix. Note that this form has reintroduced the possibility of a different uncertainty for the two different LOS measurements. This cost function can be used to produce optimal triangulation algorithms for special case of two LOS measurements.

1. Measurements from Different Images

Consider the situation where each LOS measurement comes from a different image. This is a necessary condition for the intersection form of the triangulation problem. The situation is less common for resection, but does still occur for a few important problems (e.g., triangulation with two objects whose angular separation is larger than a single optical instruments field of view). The optimal solution for the intersection problem was developed by Hartley and Sturm in 1997 [15] and involves finding the roots of a polynomial of degree six. It is possible to show that the resection problem is identical to the intersection problem, and that the optimal solution from Ref. [15] may be used for both forms.

The first task is to establish the equivalence between the intersection and resection form of the two-image triangulation problem. This may be accomplished by considering the geometry illustrated in Fig. 7. The geometry of the intersection form is shown in the top frame of Fig. 7 and it is this configuration that is considered in Ref. [15]. The resection problem may seem very different at first, but the bottom frame of Fig. 7 illustrates how resection with two images is equivalent to intersection with two images. Specifically, consider a camera located at the unknown point r viewing the known point p_i . If one creates an imaginary camera of the same attitude but located at p_i the LOS direction ℓ_i intersects the new image plane at exactly the same place—but the point r is *behind* the imaginary camera. Since the triangulation algorithms do not depend on the observed point’s chirality [88], it does not matter that the triangulated point lies behind these imaginary camera locations. Moreover, when using the two imaginary cameras in the bottom frame of Fig. 7, the triangulation of the unknown point r is now an intersection (and not a resection) problem—thus the solution from Ref. [15] may be used directly.

The solution procedure will now be briefly summarized with only limited derivation (the reader interested in the details is directed to Ref. [15]) using a notation consistent with the present work. Begin by computing the image plane

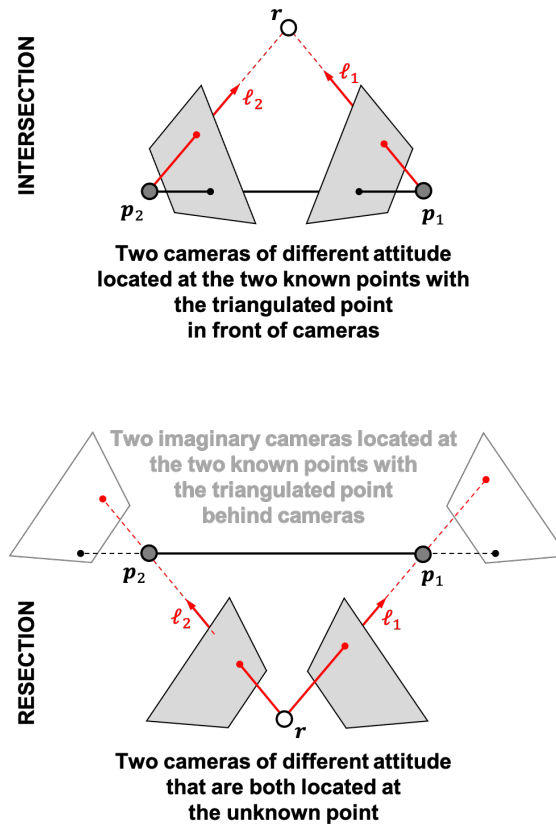


Fig. 7 Illustration of the equivalence between intersection and resection geometry for two LOS measurements.

coordinates of the two epipoles (black dots on the image planes in Fig. 7),

$$\mathbf{e}_1 \propto \mathbf{T}_{C_1}^I(\mathbf{p}_{I_2} - \mathbf{p}_{I_1}) \quad \text{and} \quad \mathbf{e}_2 \propto \mathbf{T}_{C_2}^I(\mathbf{p}_{I_1} - \mathbf{p}_{I_2}) \quad (65)$$

Given the epipoles \mathbf{e}_1 and \mathbf{e}_2 , compute the rotations α_1 and α_2 as

$$\begin{bmatrix} \sin \alpha_i \\ \cos \alpha_i \\ \cdot \end{bmatrix} \propto \mathbf{e}_i \times \tilde{\mathbf{x}}_i \quad (66)$$

where the left-hand side scale may be found by recalling $\sin^2 \alpha_i + \cos^2 \alpha_i = 1$. From here, one may directly compute the mapping \mathbf{M}_i

$$\mathbf{M}_i = \begin{bmatrix} \cos \alpha_i & -\sin \alpha_i & y_i \sin \alpha_i - x_i \cos \alpha_i \\ \sin \alpha_i & \cos \alpha_i & -y_i \cos \alpha_i - x_i \sin \alpha_i \\ 0 & 0 & 1 \end{bmatrix} \quad (67)$$

that results in

$$\begin{bmatrix} 1 \\ 0 \\ f_i \end{bmatrix} \propto \mathbf{e}'_i \propto \mathbf{M}_i \mathbf{e}_i \quad (68)$$

Consider now the epipolar constraint written in terms of the essential matrix

$$\tilde{\mathbf{x}}_2^T \mathbf{E} \tilde{\mathbf{x}}_1 = 0 \quad (69)$$

where \mathbf{E} is

$$\mathbf{E} \propto \mathbf{T}_{C_2}^I \mathbf{T}_{I_1}^{C_1} [\mathbf{e}_1 \times] \quad (70)$$

Note that the original work of Hartley and Sturm writes this in terms of the fundamental matrix, but this difference is not important here. Using the mappings \mathbf{M}_1 and \mathbf{M}_2 , one computes the simplified form of \mathbf{E}'

$$\mathbf{E}' \propto \mathbf{M}_2^{-T} \mathbf{E} \mathbf{M}_1^{-1} \propto \begin{bmatrix} f_1 f_2 d & -f_2 c & -f_2 d \\ -f_1 b & a & b \\ -f_1 d & c & d \end{bmatrix} \quad (71)$$

The elements a, b, c, d, f_1, f_2 from E' may be used to form epipolar lines and to directly write the constrained image plane reprojection error from Eq. (64) in terms of the single parameter t . Making the appropriate substitutions (see Ref. [15]) the cost function becomes

$$\min_{t \in \mathbb{R}} J(t) = w_1 \frac{t^2}{1 + (tf_1)^2} + w_2 \frac{(ct + d)^2}{(at + b)^2 + f_2^2(ct + d)^2} \quad (72)$$

where the solution presented here departs slightly from Hartley and Sturm by the introduction of different weightings of the two measurements (the solution from Ref. [15] weights the measurements equally). Applying the first differential condition $\partial J / \partial t = 0$ yields a polynomial of degree six in t ,

$$w_1 \frac{2t}{[1 + (tf_1)^2]^2} - w_2 \frac{2(ad - bc)(at + b)(ct + d)}{[(at + b)^2 + f_2^2(ct + d)^2]^2} = 0 \quad (73)$$

which is also

$$w_1 t [(at + b)^2 + f_2^2(ct + d)^2]^2 - w_2 [1 + (tf_1)^2]^2 (ad - bc)(at + b)(ct + d) = 0 \quad (74)$$

or, equivalently,

$$\sum_{k=0}^6 g_k t^k = 0 \quad (75)$$

where this polynomial's seven coefficients $\{g_k\}_{k=0}^6$ may be readily computed. Solve for the six roots of Eq. (75) and evaluate the real roots (there are often more than one) using Eq. (72) to find which one minimizes the cost function. Checking the roots is necessary since the degree six polynomial may have multiple local minima. Denote the optimal root as \hat{t} .

With \hat{t} known, the optimal epipolar lines are

$$\hat{\mathbf{m}}'_1 \propto \begin{bmatrix} \hat{t}f \\ 1 \\ -\hat{t} \end{bmatrix} \quad \hat{\mathbf{m}}'_2 \propto \begin{bmatrix} -f_2(c\hat{t} + d) \\ a\hat{t} + b \\ c\hat{t} + d \end{bmatrix} \quad (76)$$

Since the points were shifted to the origin by \mathbf{M}_i , the goal is to find the point on these lines closest to the origin. It follows that

$$\begin{bmatrix} \hat{x}'_1 \\ \hat{y}'_1 \\ 1 \end{bmatrix} \propto \begin{bmatrix} -(\hat{t}f)(-\hat{t}) \\ -1(-\hat{t}) \\ (\hat{t}f)^2 + 1^2 \end{bmatrix} = \begin{bmatrix} f\hat{t}^2 \\ \hat{t} \\ f^2\hat{t}^2 + 1 \end{bmatrix} \quad (77)$$

$$\begin{bmatrix} \hat{x}'_2 \\ \hat{y}'_2 \\ 1 \end{bmatrix} \propto \begin{bmatrix} -(-f_2(c\hat{t} + d))(c\hat{t} + d) \\ -(a\hat{t} + b)(c\hat{t} + d) \\ (-f_2(c\hat{t} + d))^2 + (a\hat{t} + b)^2 \end{bmatrix} = \begin{bmatrix} f_2(c\hat{t} + d)^2 \\ -(a\hat{t} + b)(c\hat{t} + d) \\ f_2^2(c\hat{t} + d)^2 + (a\hat{t} + b)^2 \end{bmatrix} \quad (78)$$

which may each be mapped back to the final point according to

$$\hat{\mathbf{x}}_i = \begin{bmatrix} \hat{x}_i \\ \hat{y}_i \\ 1 \end{bmatrix} \propto \mathbf{M}_i^{-1} \begin{bmatrix} \hat{x}'_i \\ \hat{y}'_i \\ 1 \end{bmatrix} \quad (79)$$

Once the estimated image points $\{\hat{\mathbf{x}}_i\}_{i=1}^2$ are known, the location of $\hat{\mathbf{r}}$ may be found with any of the trigonometric solutions from Section IV. Since $\{\hat{\mathbf{x}}_i\}_{i=1}^2$ are constrained to exactly satisfy the epipolar constraint the resulting triangulation problem is now exact.

2. Measurements from the Same Image

A simpler solution is possible in the case when measurements come from the same camera (for resection) or from two cameras of the same attitude (for intersection). To simplify the discussion, and without loss of generality, focus on the resection form of the triangulation problem. To find the triangulation constraint, first recognize that $\boldsymbol{\ell}_C$, $\boldsymbol{\ell}_2$, and \mathbf{d}_{12} are linearly dependent and all lie in a common plane. Thus, since the vector $\mathbf{d}_{12} \times \boldsymbol{\ell}_2$ is perpendicular to the this plane, it follows that

$$\boldsymbol{\ell}_1^T [\mathbf{d}_{12} \times] \boldsymbol{\ell}_2 = 0 \quad (80)$$

Recalling that in the camera frame $\boldsymbol{\ell}_{C_i} \propto \bar{\mathbf{x}}_i$, one may also write

$$\bar{\mathbf{x}}_1^T [\mathbf{d}_{C_{12}} \times] \bar{\mathbf{x}}_2 = 0 \quad (81)$$

which is the same thing as the epipolar constraint. Recalling $\bar{\mathbf{x}}_i^T = [x_i, y_i, 1]$ and defining $\mathbf{d}^T = [d, e, f]$, the constraint develops as

$$\bar{\mathbf{x}}_1^T [\mathbf{d}_{C_{12}} \times] \bar{\mathbf{x}}_2 = x_1 (e - fy_2) + y_1 (fx_2 - d) + (dy_2 - ex_2) = 0 \quad (82)$$

Thus, the triangulation (epipolar) constraint may be adjoined to the cost function from Eq. (64) with a Lagrange multiplier, λ

$$\min J(x_1, y_1, x_2, y_2, \lambda) = \sum_{i=1}^2 w_i [(\tilde{x}_i - x_i)^2 + (\tilde{y}_i - y_i)^2] + \lambda (\bar{\mathbf{x}}_1^T [\mathbf{d}_{C_{12}} \times] \bar{\mathbf{x}}_2) \quad (83)$$

Table 1 Coefficients of the polynomial expressions of the state variable with respect to λ .

	D	N_{x_1}	N_{y_1}	N_{x_2}	N_{y_2}
γ_2	f^2	df	ef	df	ef
γ_1	0	$2w_2(e - f\tilde{y}_2)$	$2w_2(f\tilde{x}_2 - d)$	$2w_1(f\tilde{y}_1 - e)$	$2w_1(d - f\tilde{x}_1)$
γ_0	$-4w_1w_2$	$-4w_1w_2\tilde{x}_1$	$-4w_1w_2\tilde{y}_1$	$-4w_1w_2\tilde{x}_2$	$-4w_1w_2\tilde{y}_2$

Applying the first differential condition yields

$$\frac{\partial J}{\partial x_1} = 2w_1(x_1 - \tilde{x}_1) - \lambda(fy_2 - e) = 0 \quad (84a)$$

$$\frac{\partial J}{\partial y_1} = 2w_1(y_1 - \tilde{y}_1) + \lambda(fx_2 - d) = 0 \quad (84b)$$

$$\frac{\partial J}{\partial x_2} = 2w_2(x_2 - \tilde{x}_2) + \lambda(fy_1 - e) = 0 \quad (84c)$$

$$\frac{\partial J}{\partial y_2} = 2w_2(y_2 - \tilde{y}_2) - \lambda(fx_1 - d) = 0 \quad (84d)$$

Additionally, $\partial J/\partial \lambda = 0$ gives the constraint at Eq. (82) as a fifth equation to solve.

Solving Eq. (84a) to (84d) yields an expression of each image plane coordinate as a function of λ . Given the symmetry between each coordinate, all of their solutions take the form of a rational fraction where both the numerator and denominator are polynomials of degree two:

$$(\cdot) = \frac{N_{(\cdot)}}{D} = \frac{\gamma_2\lambda^2 + \gamma_1\lambda + \gamma_0}{\gamma_2\lambda^2 + \gamma_1\lambda + \gamma_0} \quad (85)$$

with coefficients from Table 1. Note that the denominator is the same for each coordinate. For example, the fraction for the optimal value of x_1 takes the form

$$\hat{x}_1 = \frac{N_{x_1}}{D} = \frac{[df]\lambda^2 + [2w_2(e - f\tilde{y}_2)]\lambda + [-4w_1w_2\tilde{x}_1]}{[f^2]\lambda^2 + [0]\lambda + [-4w_1w_2]} \quad (86)$$

The constraint from Eq. (82) may now be rewritten in terms of λ only as

$$f \frac{N_{y_1}N_{x_2} - N_{x_1}N_{y_2}}{D^2} + \frac{eN_{x_1} - dN_{y_1} + dN_{y_2} - eN_{x_2}}{D} = 0 \quad (87)$$

or equivalently

$$fN_{y_1}N_{x_2} - N_{x_1}N_{y_2} + eN_{x_1}D - dN_{y_1}D + dN_{y_2}D - eN_{x_2}D = 0 \quad (88)$$

The terms within the coefficients of λ^4 and λ^3 cancel out, such that Eq. (88) simplifies into a polynomial of degree two

$$h_2\lambda^2 + h_1\lambda + h_0 = 0 \quad (89)$$

with coefficients

$$h_2 = f^2 w_1 w_2 [f(\tilde{x}_2 \tilde{y}_1 - \tilde{x}_1 \tilde{y}_2) + e(\tilde{x}_1 - \tilde{x}_2) + d(\tilde{y}_2 - \tilde{y}_1)] \quad (90)$$

$$h_1 = -2w_1 w_2 [f^2(w_1 \tilde{x}_1^2 + w_1 \tilde{y}_1^2 + w_2 \tilde{x}_2^2 + w_2 \tilde{y}_2^2) - 2f(dw_1 \tilde{x}_1 + dw_2 \tilde{x}_2 + ew_1 \tilde{y}_1 + ew_2 \tilde{y}_2) + (d^2 + e^2)(w_1 + w_2)] \quad (91)$$

$$h_0 = 4w_1 w_2 \frac{h_2}{f^2} \quad (92)$$

The solution in the general case is given by

$$\lambda = \frac{-h_1 \pm \sqrt{h_1^2 - 4h_2 h_0}}{2h_2} \quad (93)$$

In practice, the algorithm proposed first solves the quadratic equation to find the two roots. It then computes the image plane coordinates for each root with Eq. (85). The set of coordinates that minimizes Eq. (64) is selected as the solution.

It is important to consider the case where $f = 0$, because $h_2 = 0$ yields an undefined solution if it is solved with Eq. (93). In that case, the solution is much simpler to compute from the Lagrangian, or the unique root can be computed from the existing coefficients as

$$\begin{aligned} \lambda_{f \rightarrow 0} &= \lim_{f \rightarrow 0} \left(-\frac{h_0}{h_1} \right) \\ &= \frac{2w_1 w_2 [e(\tilde{x}_1 - \tilde{x}_2) + d(\tilde{y}_2 - \tilde{y}_1)]}{(d^2 + e^2)(w_1 + w_2)} \end{aligned} \quad (94)$$

For a numerical implementation, it is important to switch to the solution from Eq. 94 whenever h_2 is very small compared to the other coefficients.

3. Comparison of Solutions for the Single Image Case

When there is only one camera (resection) or two cameras of the same attitude (intersection), the classical solution from Hartley and Sturm [15] reviewed in Section V.A.1 always provides exactly the same solution as the quadratic solution introduced in Section V.A.2. Thus, since solving a quadratic equation is simpler than solving a polynomial of degree six, the new method from Section V.A.2 is to be preferred in this case. This equivalence is best illustrated with a small numerical example.

Without loss of generality, assume a camera is located at the origin of the localization frame and has an attitude of

$T_C^I = I_{3 \times 3}$. Let this camera observe two objects at the known positions

$$p_{I_1} = \begin{bmatrix} 50 \\ 25 \\ 2100 \end{bmatrix} \quad p_{I_2} = \begin{bmatrix} -50 \\ -25 \\ 2000 \end{bmatrix}$$

Supposing the camera in this example has image centroiding performance of about $\sigma_{x_i} = 8.73 \times 10^{-5}$, consider the case with the following additive noise (see Eq. (11)):

$$w_1 = \begin{bmatrix} -3.6876 \times 10^{-5} \\ -1.5482 \times 10^{-4} \\ 0 \end{bmatrix} \quad w_2 = \begin{bmatrix} -6.3361 \times 10^{-6} \\ 1.0428 \times 10^{-4} \\ 0 \end{bmatrix}$$

With this particular realization of measurement noise and assuming the measurements are weighted equally ($w_1 = w_2$), the sixth order polynomial of Hartley and Sturm presented in Eq. 75 gives six roots,

$$t_1 = 1.6199 \times 10^4, \quad t_2 = -7.3533 \times 10^{-5}, \\ t_{3,4} = -0.7527 \pm 0.7904i, \quad \text{and} \quad t_{5,6} = 0.7526 \pm 0.7903i$$

Amongst the two real roots, the minimum of the cost function from Eq. (72) occurs for the root $t_2 = -7.3533 \times 10^{-5}$ and produces estimated image plane coordinates of

$$\hat{x}_1 = \begin{bmatrix} 0.02386 \\ 0.01186 \end{bmatrix} \quad \hat{x}_2 = \begin{bmatrix} -0.02483 \\ -0.01249 \end{bmatrix}$$

As a comparison, the same noisy image centroids produces a second order polynomial from Eq. 89 with two real roots,

$$\lambda_1 = -1.5582 \times 10^2 \quad \text{and} \quad \lambda_2 = -6.4175 \times 10^{-7}$$

The minimum cost occurs for the root $\lambda_2 = -6.4175 \times 10^{-7}$ and produces the estimate image plane coordinates

$$\hat{x}_1 = \begin{bmatrix} 0.02386 \\ 0.01186 \end{bmatrix} \quad \hat{x}_2 = \begin{bmatrix} -0.02483 \\ -0.01249 \end{bmatrix}$$

Using a standard root solver (without extra root polishing), the difference between the estimated coordinates is of the order of 10^{-13} . Therefore, in the case of a single camera with only two measurements, it is equivalent (and faster) to triangulate by solving the second order polynomial in Eq. 89 instead of the sixth order polynomial in Eq. 75.

B. More than Two LOS Measurements: The Linear Optimal Sine Triangulation (LOST) Method

Solving the MLE triangulation problem by explicit minimization of the reprojection errors does not easily scale to more than two LOS measurements. This was attempted in Ref. [16] for three LOS measurements ($n = 3$) and was found to require the solution to a system of polynomials possessing 47 roots. To attempt this for $n \geq 4$ is completely unreasonable. In light of these challenges, it is commonly argued that to obtain the MLE solution for n views requires one to iteratively solve a non-linear least squares problem (so-called *bundle adjustment*). This, however, is not true. It is possible to create a MLE solution to \mathbf{r} as the solution to a linear system by a double applications of the Law of Sines. The resulting method is referred to here as the Linear Optimal Sine Triangulation (LOST) algorithm.

Begin with the first application of the Law of Sines as written in the form of the DLT. Rewrite Eq. (19) as

$$[\bar{\mathbf{x}}_i \times] \mathbf{T}_{C_i}^l (\mathbf{r}_I - \mathbf{p}_{I_i}) = \mathbf{0}_{3 \times 1} \quad (95)$$

This condition is only satisfied with perfect measurements. When only the noisy measurements $\tilde{\mathbf{x}}_i = \mathbf{K}^{-1} \tilde{\mathbf{u}}$ are available, the right-hand side is no longer exactly zero. Instead, one finds that

$$[\tilde{\mathbf{x}}_i \times] \mathbf{T}_{C_i}^l (\mathbf{r}_I - \mathbf{p}_{I_i}) = \boldsymbol{\epsilon}_i \quad (96)$$

Recalling from Eq. (11) that $\tilde{\mathbf{x}}_i = \bar{\mathbf{x}}_i + \mathbf{w}_i$, the residual vector $\boldsymbol{\epsilon}_i$ is found to be

$$\boldsymbol{\epsilon}_i = \left[\mathbf{T}_{C_i}^l (\mathbf{p}_{I_i} - \mathbf{r}_I) \times \right] \mathbf{w}_i \quad (97)$$

with covariance

$$\mathbf{R}_{\boldsymbol{\epsilon}_i} = E[\boldsymbol{\epsilon}_i \boldsymbol{\epsilon}_i^T] = - \left[\mathbf{T}_{C_i}^l (\mathbf{p}_{I_i} - \mathbf{r}_I) \times \right] \mathbf{R}_{\bar{\mathbf{x}}_i} \left[\mathbf{T}_{C_i}^l (\mathbf{p}_{I_i} - \mathbf{r}_I) \times \right] \quad (98)$$

where $\mathbf{R}_{\bar{\mathbf{x}}_i} = E[\mathbf{w}_i \mathbf{w}_i^T]$ is from Eq. (12). The leading negative sign in Eq. (98) is a result of the identity $[\cdot \times]^T = -[\cdot \times]$. It is possible to rewrite $\mathbf{R}_{\bar{\mathbf{x}}_i}$ explicitly in terms of the corresponding measurement $\bar{\mathbf{u}}_i$ and unknown range ρ_i by substitution from Eq. (5) and Eq. (42)

$$\mathbf{R}_{\boldsymbol{\epsilon}_i} = - \frac{\rho_i^2}{\|\mathbf{K}_i^{-1} \bar{\mathbf{u}}_i\|^2} \left[\mathbf{K}_i^{-1} \bar{\mathbf{u}}_i \times \right] \mathbf{R}_{\bar{\mathbf{x}}_i} \left[\mathbf{K}_i^{-1} \bar{\mathbf{u}}_i \times \right] \quad (99)$$

Therefore, one may write the MLE problem as

$$\min J(\mathbf{r}_I) = \sum_{i=1}^n \boldsymbol{\epsilon}_i^T \mathbf{R}_{\boldsymbol{\epsilon}_i}^{-1} \boldsymbol{\epsilon}_i \quad (100)$$

which, after substituting for $\boldsymbol{\epsilon}_i$ using Eq. (96), becomes

$$\min J(\mathbf{r}_I) = \sum_{i=1}^n -(\mathbf{r}_I - \mathbf{p}_i)^T \mathbf{T}_I^{C_i} [\tilde{\mathbf{x}}_i \times] \mathbf{R}_{\boldsymbol{\epsilon}_i}^{-1} [\tilde{\mathbf{x}}_i \times] \mathbf{T}_{C_i}^T (\mathbf{r}_I - \mathbf{p}_i) \quad (101)$$

There are three apparent issues here—all of which relate to the practical computation of $\mathbf{R}_{\boldsymbol{\epsilon}_i}^{-1}$. First is that $\mathbf{R}_{\boldsymbol{\epsilon}_i}$ depends on the ideal pixel coordinates $\bar{\mathbf{u}}_i$ when only the measured pixel coordinates $\tilde{\mathbf{u}}_i$ are available in practice. Second is that the 3×3 matrix $\mathbf{R}_{\boldsymbol{\epsilon}_i}$ is only rank two and, therefore, not invertable. Third is that $\mathbf{R}_{\boldsymbol{\epsilon}_i}$ depends on the unknown distance ρ_i between points \mathbf{r} and \mathbf{p}_i . All three of these issues may be avoided.

Begin with addressing the use of the noisy measurements $\tilde{\mathbf{u}}_i$ in place of the perfect $\bar{\mathbf{u}}_i$ in Eq. (99). This is a common problem in navigation. Indeed, a measurement's error covariance is dependent on the measurement itself for all but the simplest sensor models. When approximating the error covariance of $\boldsymbol{\epsilon}_i$ with the measurement $\tilde{\mathbf{u}}_i$, denote the noisy covariance as $\tilde{\mathbf{R}}_{\boldsymbol{\epsilon}_i}$, where

$$\tilde{\mathbf{R}}_{\boldsymbol{\epsilon}_i} = -\frac{\hat{\rho}_i^2}{\|\mathbf{K}_i^{-1} \tilde{\mathbf{u}}_i\|^2} [\mathbf{K}_i^{-1} \tilde{\mathbf{u}}_i \times] \mathbf{R}_{\tilde{\mathbf{x}}_i} [\mathbf{K}_i^{-1} \tilde{\mathbf{u}}_i \times] \quad (102)$$

Using the measurement in place of the truth when computing the covariance is correct to first order and has been studied before for image-based LOS measurements [76, 85]. Moreover, using measurements or estimates is the only choice since the true values will never be known. This approximation is acceptable in practice since the covariance $\mathbf{R}_{\boldsymbol{\epsilon}_i}$ is only used to weight the different residual vectors $\boldsymbol{\epsilon}_i$. The numerical results in Section VII confirm this assertion. Thus, proceed using $\tilde{\mathbf{R}}_{\boldsymbol{\epsilon}_i}$ in place of $\mathbf{R}_{\boldsymbol{\epsilon}_i}$.

Next, address the computation of $\tilde{\mathbf{R}}_{\boldsymbol{\epsilon}_i}^{-1}$. Observe from Eq. (102) that the null space of $\tilde{\mathbf{R}}_{\boldsymbol{\epsilon}_i}$ is in the direction of $\mathbf{K}_i^{-1} \tilde{\mathbf{u}}_i = \tilde{\mathbf{x}}_i$. Observe also that $[\tilde{\mathbf{x}}_i \times]$ has a null space in the same direction. Thus, because of the alignment of the null spaces, the central term in the cost function of Eq. (101) may be replaced with the identity

$$[\tilde{\mathbf{x}}_i \times] \tilde{\mathbf{R}}_{\boldsymbol{\epsilon}_i}^{-1} [\tilde{\mathbf{x}}_i \times] = [\tilde{\mathbf{x}}_i \times] \tilde{\mathbf{R}}_{\boldsymbol{\epsilon}_i}^\dagger [\tilde{\mathbf{x}}_i \times] \quad (103)$$

where the superscript \dagger indicates the pseudoinverse. It is always possible to find pseudoinverse numerically with the SVD of the 3×3 matrix $\tilde{\mathbf{R}}_{\boldsymbol{\epsilon}_i}$. In most cases, however, this is not the preferred approach. Instead, the pseudoinverse may usually be computed analytically as discussed in the Appendix.

Finally, address the issue of the unknown range ρ_i . Dealing with this unknown range was a central issue for the trigonometric solutions presented in Section IV, where it was either avoided [e.g., DLT: see Eq. (16)] or directly

estimated [e.g., explicit range: see Eq. (49)]. Thus, the unmitigated dependence on ρ_i (or on \mathbf{r}) would seem to suggest an iterative algorithm, where the unknown range is derived from the previous iteration. Another option is to attempt some kind of approximation in special situations [89]. However, the unknown range ρ_i may be constructed directly from the measurements themselves. Interestingly, the solution for how to obtain the unknown range was suggested by Frisius in 1533 in the same booklet [25] that (re)introduced the idea of triangulation to the modern world. Making use of Haasbroek’s translation of the original Latin, Frisius observes “that the distances can also be computed ‘with the tables of sine, but I omitted this intentionally as it is too difficult for the common man’ ” [27]. To the modern (and *uncommon!*) [wo]man, Frisius’s suggestion is most straightforwardly mechanized by employing the Law of Sines,

$$\frac{\|\mathbf{d}_{ij}\|}{\sin \theta_{ij}} = \frac{\rho_i}{\sin \psi_{ij}} \quad (104)$$

with angles as defined in Fig. 6. It follows then that

$$\rho_i = \frac{\|\mathbf{d}_{ij}\| \sin \psi_{ij}}{\sin \theta_{ij}} = \frac{\|\mathbf{d}_{ij} \times \mathbf{a}_j\|}{\|\mathbf{a}_i \times \mathbf{a}_j\|} \quad (105)$$

where everything on the right-hand side is known. This expression for ρ_i is true in any consistent frame. Since LOS directions \mathbf{a}_i and \mathbf{a}_j may come from different cameras having different frames (C_i and C_j), one may perform the cross products in the localization frame

$$\tilde{\rho}_i = \frac{\|\mathbf{T}_I^{C_i} \mathbf{K}_i^{-1} \tilde{\mathbf{u}}_i\| \|\mathbf{T}_I^{C_j} \mathbf{K}_j^{-1} \tilde{\mathbf{u}}_j\| \|\mathbf{d}_{I_{ij}} \times \mathbf{T}_I^{C_j} \mathbf{K}_j^{-1} \tilde{\mathbf{u}}_j\|}{\|\mathbf{T}_I^{C_j} \mathbf{K}_j^{-1} \tilde{\mathbf{u}}_j\| \|\mathbf{T}_I^{C_i} \mathbf{K}_i^{-1} \tilde{\mathbf{u}}_i \times \mathbf{T}_I^{C_j} \mathbf{K}_j^{-1} \tilde{\mathbf{u}}_j\|} = \frac{\|\mathbf{K}_i^{-1} \tilde{\mathbf{u}}_i\| \|\mathbf{d}_{I_{ij}} \times \mathbf{T}_I^{C_j} \mathbf{K}_j^{-1} \tilde{\mathbf{u}}_j\|}{\|\mathbf{T}_I^{C_i} \mathbf{K}_i^{-1} \tilde{\mathbf{u}}_i \times \mathbf{T}_I^{C_j} \mathbf{K}_j^{-1} \tilde{\mathbf{u}}_j\|} \quad (106)$$

where, once again, the measured $\tilde{\mathbf{u}}_i$ is used in place of the true $\bar{\mathbf{u}}_i$ (this is acceptable when the approximation is *only* used for approximating the covariance \mathbf{R}_{ϵ_i}). Thus, applying these observations to Eq. (99) yields an expression for $\tilde{\mathbf{R}}_{\epsilon_i}$ that is written entirely in terms of known (or measured) quantities

$$\tilde{\mathbf{R}}_{\epsilon_i} = -\gamma_i^2 [\mathbf{K}_i^{-1} \tilde{\mathbf{u}}_i \times] \mathbf{R}_{\tilde{\mathbf{x}}_i} [\mathbf{K}_i^{-1} \tilde{\mathbf{u}}_i \times] \quad (107)$$

where

$$\gamma_i = \frac{\tilde{\rho}_i}{\|\mathbf{K}_i^{-1} \tilde{\mathbf{u}}_i\|} = \frac{\|\mathbf{d}_{I_{ij}} \times \mathbf{T}_I^{C_j} \mathbf{K}_j^{-1} \tilde{\mathbf{u}}_j\|}{\|\mathbf{T}_I^{C_i} \mathbf{K}_i^{-1} \tilde{\mathbf{u}}_i \times \mathbf{T}_I^{C_j} \mathbf{K}_j^{-1} \tilde{\mathbf{u}}_j\|} \quad (108)$$

Finally, for any given any LOS measurement $\tilde{\ell}_i \propto \mathbf{K}_i^{-1} \tilde{\mathbf{u}}_i$, there is some ambiguity in which additional LOS measurement $\tilde{\ell}_j \propto \mathbf{K}_j^{-1} \tilde{\mathbf{u}}_j$ (for $i \neq j$) to use for computing γ_i with Eq. (108). Experience has shown that any reasonable scheme (even a random one) provides essentially the same triangulation performance in practice (i.e., small variations in γ_i do not change the relative measurement weightings in the MLE enough to matter). Efforts to find the “optimal” choice of a

companion measurement j do not appear to be worth the additional computational effort.

Now, to find the optimal solution, return to Eq. (101) and apply the first differential condition

$$\sum_{i=1}^n -2(\hat{\mathbf{r}}_I - \mathbf{p}_{I_i})^T \mathbf{T}_I^{C_i} [\tilde{\mathbf{x}}_i \times] \tilde{\mathbf{R}}_{\epsilon_i}^\dagger [\tilde{\mathbf{x}}_i \times] \mathbf{T}_{C_i}^I = 0 \quad (109)$$

Substituting for $\tilde{\mathbf{x}}_i = \mathbf{K}_i^{-1} \tilde{\mathbf{u}}$ and rearranging gives

$$\left(\sum_{i=1}^n \mathbf{T}_I^{C_i} [\mathbf{K}_i^{-1} \tilde{\mathbf{u}}_i \times] \tilde{\mathbf{R}}_{\epsilon_i}^\dagger [\mathbf{K}_i^{-1} \tilde{\mathbf{u}}_i \times] \mathbf{T}_{C_i}^I \right) \hat{\mathbf{r}}_I = \sum_{i=1}^n \mathbf{T}_I^{C_i} [\mathbf{K}_i^{-1} \tilde{\mathbf{u}}_i \times] \tilde{\mathbf{R}}_{\epsilon_i}^\dagger [\mathbf{K}_i^{-1} \tilde{\mathbf{u}}_i \times] \mathbf{T}_{C_i}^I \mathbf{p}_{I_i} \quad (110)$$

As expected, this final result is nothing more than the normal equations for an optimally weighted DLT (with weighting $\mathbf{W}_i = \mathbf{R}_{\epsilon_i}^\dagger \sim \mathbf{R}_{\epsilon_i}^{-1}$). Following the usual approach for solving any least squares system [90], the numerical stability may be improved by avoiding explicit formation of the normal equations and instead solving (e.g., with QR factorization)

$$\begin{bmatrix} \mathbf{B}_1 [\mathbf{K}_1^{-1} \tilde{\mathbf{u}}_1 \times] \mathbf{T}_{C_1}^I \\ \mathbf{B}_2 [\mathbf{K}_2^{-1} \tilde{\mathbf{u}}_2 \times] \mathbf{T}_{C_2}^I \\ \vdots \\ \mathbf{B}_n [\mathbf{K}_n^{-1} \tilde{\mathbf{u}}_n \times] \mathbf{T}_{C_n}^I \end{bmatrix} \mathbf{r}_I = \begin{bmatrix} \mathbf{B}_1 [\mathbf{K}_1^{-1} \tilde{\mathbf{u}}_1 \times] \mathbf{T}_{C_1}^I \mathbf{p}_{I_1} \\ \mathbf{B}_2 [\mathbf{K}_2^{-1} \tilde{\mathbf{u}}_2 \times] \mathbf{T}_{C_2}^I \mathbf{p}_{I_2} \\ \vdots \\ \mathbf{B}_n [\mathbf{K}_n^{-1} \tilde{\mathbf{u}}_n \times] \mathbf{T}_{C_n}^I \mathbf{p}_{I_n} \end{bmatrix} \quad (111)$$

which makes use of the factorization $\tilde{\mathbf{R}}_i^\dagger = \mathbf{B}_i^T \mathbf{B}_i$. In the case that $\mathbf{R}_{x_i} = \sigma_{x_i}^2 \mathbf{I}_{2 \times 2}$, the results of the Appendix show that

$$\mathbf{B}_i = \frac{q_i}{\|\mathbf{K}_i^{-1} \tilde{\mathbf{u}}_i\|^2} \mathbf{S} [\mathbf{K}_i^{-1} \tilde{\mathbf{u}}_i \times]^2 \quad (112)$$

where

$$q_i = \frac{1}{\sigma_{x_i} \gamma_i} = \frac{\|\mathbf{K}_i^{-1} \tilde{\mathbf{u}}_i\|}{\sigma_{x_i} \rho_i} = \frac{\|\mathbf{T}_I^{C_i} \mathbf{K}_i^{-1} \tilde{\mathbf{u}}_i \times \mathbf{T}_I^{C_i} \mathbf{K}_j^{-1} \tilde{\mathbf{u}}_j\|}{\sigma_{x_i} \|\mathbf{d}_{I_{ij}} \times \mathbf{T}_I^{C_j} \mathbf{K}_j^{-1} \tilde{\mathbf{u}}_j\|} \quad (113)$$

Recalling identity $[\mathbf{b} \times]^3 = -\|\mathbf{b}\|^2 [\mathbf{b} \times]$, it follows that the above simplifies to

$$\begin{bmatrix} q_1 \mathbf{S} [\mathbf{K}_1^{-1} \tilde{\mathbf{u}}_1 \times] \mathbf{T}_{C_1}^I \\ q_2 \mathbf{S} [\mathbf{K}_2^{-1} \tilde{\mathbf{u}}_2 \times] \mathbf{T}_{C_2}^I \\ \vdots \\ q_n \mathbf{S} [\mathbf{K}_n^{-1} \tilde{\mathbf{u}}_n \times] \mathbf{T}_{C_n}^I \end{bmatrix} \mathbf{r}_I = \begin{bmatrix} q_1 \mathbf{S} [\mathbf{K}_1^{-1} \tilde{\mathbf{u}}_1 \times] \mathbf{T}_{C_1}^I \mathbf{p}_{I_1} \\ q_2 \mathbf{S} [\mathbf{K}_2^{-1} \tilde{\mathbf{u}}_2 \times] \mathbf{T}_{C_2}^I \mathbf{p}_{I_2} \\ \vdots \\ q_n \mathbf{S} [\mathbf{K}_n^{-1} \tilde{\mathbf{u}}_n \times] \mathbf{T}_{C_n}^I \mathbf{p}_{I_n} \end{bmatrix} \quad (114)$$

Note here that the matrix $\mathbf{S} = [\mathbf{I}_{2 \times 2}, \mathbf{0}_{2 \times 1}]$ removes the redundant third row for each of the measurements. The reader

is reminded that the two remaining rows were shown in Section IV.A.3 to be equivalent to the collinearity equations. Moreover, substituting from Eq. (113), observe that

$$q_i \mathbf{S} [\mathbf{K}_i^{-1} \tilde{\mathbf{u}}_i \times] \mathbf{T}_{C_i}^l = \frac{\|\mathbf{K}_i^{-1} \tilde{\mathbf{u}}_i\|^2}{\sigma_{x_i} \rho_i} \mathbf{S} [\tilde{\mathbf{a}}_{C_i} \times] \mathbf{T}_{C_i}^l \quad (115)$$

it is observed that a particular LOS measurement is weighted less as either the measurement error (σ_i) or the range (ρ_i) increase. This also allows the LOST algorithm to be written in terms of the measured unit vector $\tilde{\mathbf{a}}_{C_i}$ if that normalization is preferred to the analyst (as opposed to directly using the measured pixel coordinates $\tilde{\mathbf{u}}_i$).

Whether it is ultimately best to solve for $\hat{\mathbf{r}}_l$ via the normal equations [Eq. (110)] or by QR factorization [Eq. (114)] depends on the problem at hand and the priorities of the analyst. The normal equations solution requires less memory and fewer computations (when n is large), while the QR factorization tends to have slightly better numerical stability. The numerical stability of the QR factorization approach becomes more important as the angle(s) between the LOS measurements become smaller.

Since the weighting is statistically optimal, the covariance may be computed as

$$\mathbf{P}_r = - \left(\sum_{i=1}^n \mathbf{T}_i^{C_i} [\mathbf{K}_i^{-1} \tilde{\mathbf{u}}_i \times] \tilde{\mathbf{R}}_{\epsilon_i}^\dagger [\mathbf{K}_i^{-1} \tilde{\mathbf{u}}_i \times] \mathbf{T}_{C_i}^l \right)^{-1} \quad (116)$$

where, again, the leading negative sign is a result of the identity $[\cdot \times]^T = -[\cdot \times]$. In the case of $\mathbf{R}_{x_i} = \sigma_{x_i}^2 \mathbf{I}_{2 \times 2}$ computing the pseudoinverse can be avoided and

$$\mathbf{P}_r = - \left(\sum_{i=1}^n q_i^2 \mathbf{T}_i^{C_i} [\mathbf{K}_i^{-1} \tilde{\mathbf{u}}_i \times] \mathbf{S}^T \mathbf{S} [\mathbf{K}_i^{-1} \tilde{\mathbf{u}}_i \times] \mathbf{T}_{C_i}^l \right)^{-1} \quad (117)$$

where q_i is from Eq. (113). Since \mathbf{K}_i^{-1} may be written directly (see Ref. [5]), computing the covariance \mathbf{P}_r only requires a single matrix inverse. This is fast to compute since the inverse is of a symmetric 3×3 matrix.

Finally, though the authors are unaware of prior weighted DLT methods that are both optimal and direct (non-iterative), the LOST method proposed here will likely seem obvious to the contemporary practitioner of estimation theory. What becomes clear, however, is that the widespread claims of suboptimality of the DLT are often misplaced. The suboptimality is not a shortcoming of the DLT itself, but a shortcoming of the choice to solve the resulting equations as an unweighted least squares problem. Accounting for the different uncertainty in different measurements is essential to any estimation problem—be that triangulation with the DLT, navigating a spacecraft, or estimating anything else. Indeed, handling the the relative weighting of observations was one of Fisher's original complaints against the method of ordinary least squares that led to the development of the MLE approach between 1912 and 1922 [91]. Thus, the authors make no claim that the concepts behind the LOST method are especially novel. The LOST algorithm is simply

the natural consequence of applying the MLE framework to the DLT algorithm, while recognizing the Law of Sines may be used to efficiently acquire the measurement covariance.

VI. Dynamic Triangulation

The concepts from triangulation are not confined to concurrent measurements (or to static systems). Triangulation with moving objects was pioneered for maritime navigation and tracking after widespread deployment of radar systems in the 1940s—largely under the name bearings-only target motion analysis (BO-TMA) [56]. Similar concepts were considered for applications in spacecraft orbit determination by Kaplan [40], though these historical presentations often obscure elegant relations to triangulation (especially the DLT from Section IV.A). As with other triangulation methods, there is no meaningful difference between the algorithms to address the intersection (e.g., orbit determination) and resection (e.g., navigation) forms of the dynamic triangulation problem.

Consider a camera aboard a vehicle whose state ξ evolves according the linear dynamics

$$\dot{\xi}(t) = \mathbf{A}(t) \xi(t) \quad (118)$$

Such a dynamical system exhibits a solution of the form [92]

$$\xi_i = \Phi(t_i, t_0) \xi_0 \quad (119)$$

where $\Phi(t_i, t_0)$ is the state transition matrix (STM) that advances the state from t_0 to t_i . Suppose that one of the dynamical states within ξ is the vehicle's position r . Let the rows of the STM Φ corresponding to r be denoted by Φ_r such that

$$r_i = \Phi_r(t_i, t_0) \xi_0 \quad (120)$$

Thus the LOS measurement at any point in time is given by

$$\ell_i \propto p_i - r_i = p_i - \Phi_r(t_i, t_0) \xi_0 \quad (121)$$

Following the same approach as for the DLT in Section IV.A, take the cross product with the measured LOS direction,

$$[\ell_i \times] p_i - [\ell_i \times] \Phi_r(t_i, t_0) \xi_0 = \mathbf{0}_{3 \times 1} \quad (122)$$

such that

$$[\ell_i \times] \Phi_r(t_i, t_0) \xi_0 = [\ell_i \times] p_i \quad (123)$$

Stacking these equations for many measurements leads to a modified version of the DLT,

$$\begin{bmatrix} [\ell_1 \times] \Phi_r(t_1, t_0) \\ \vdots \\ [\ell_n \times] \Phi_r(t_n, t_0) \end{bmatrix} \xi_0 = \begin{bmatrix} [\ell_1 \times] p_1 \\ \vdots \\ [\ell_n \times] p_n \end{bmatrix} \quad (124)$$

which is true in any consistent frame. This formulation is nothing more than a specialized form of classical batch estimation, which is widely used in astrodynamics applications [87].

For a STM $\Phi_r(t_i, t_0)$ of general form and LOS measurements to a variety of different points $p_i \neq 0$, one may usually solve for the full state vector ξ_0 . However, under certain degeneracies in dynamics, sampling times, or point configurations, it is sometimes not possible to solve for ξ_0 without ambiguity. The variations of degeneracies are many and their full enumeration is not practical. However, the most common degeneracy occurs when all LOS measurements are between a moving point and a single reference point at the origin [or a reference point that can be shifted to the origin while maintaining the linear dynamics of Eq. (119)], which leads to a family of homothetic solutions characterized by an unobservable scale (e.g., Fig. 5). As an example of this, the common case of spacecraft relative navigation is discussed in Section VII.D.

VII. Example Applications

A. Terrain Relative Navigation (TRN)

Imaging and triangulation play a crucial role in Terrain Relative Navigation (TRN). While TRN does have a variety of terrestrial applications, it is particularly important in interplanetary space exploration where few other navigation observables are available. Specific examples include orbit determination from landmarks [12, 80, 93] and precision landing [74, 94–96]. TRN often takes the form of absolute triangulation since the camera-to-terrain attitude may be obtained using knowledge of the spacecraft’s inertial attitude (e.g., from star trackers [41–43]) and the celestial body’s inertial attitude (e.g., from ephemeris files [97, 98]).

As an example, consider a simulated lander descending from an altitude of 2,000 m to an altitude of 200 m. During this time, a camera onboard the lander observes two points (either natural or artificial) on the surface of the celestial body. Suppose the lander’s camera is similar to the Mars 2020 LCAM [99], having a FOV of 90×90 deg and a detector with 1024×1024 pixels. At regular intervals along a simulated descent trajectory, a Monte Carlo simulation is performed with 1,000 sample points generated by Eq. (8) with standard deviation of $\sigma_{u_i} = 0.1$ pixel. Here, a comparison is made between the two trigonometric solutions (DLT and explicit range) and the optimal polynomial solution from Section V.A.2. For each of these three methods, the analytic covariance (see Appendix) is compared with the Monte Carlo sample covariance. These comparisons are made for two different scenarios.

In a first scenario, consider a downward (nadir) pointed camera that observes two objects placed on the ground. This is illustrated in the left-hand frame of Fig. 8. The two points are placed 300 m apart and centered beneath the lander. One point (p_1) has an elevation of 30 m above the other point (p_2). As the lander descends, the apparent angular separation of the two objects increases—and so their distance to one another on the image plane also increases. Now, define the total standard deviation of the position estimate σ_r as

$$\sigma_r = \sqrt{\text{Tr} [\mathbf{P}_r]} \quad (125)$$

where $\text{Tr}[\cdot]$ is the trace operator and \mathbf{P}_r is the error covariance of the triangulated position \hat{r} . This answer is the same in any frame since $\text{Tr} [\mathbf{P}_r] = \text{Tr} [\mathbf{T}\mathbf{P}_r\mathbf{T}^T]$. Figure 9 shows σ_r for each of the triangulation methods (left-hand frame) and the relative increase in standard deviation (or loss in precision) of the two trigonometric methods against the optimal polynomial method (right-hand frame). In this particular case, there is nearly no difference between the optimal solution (labeled QUAT), the DLT, and the explicit range. This follows the intuition gained from Section V.B which explains how the optimal weighting of the DLT is inversely proportional to the measurement uncertainty and the range. Since both the measurement uncertainty and the range are about the same for both measurements (due to the symmetry of this example scenario) the DLT and explicit range methods happen to have a nearly optimal weighting (by luck rather than design). As the lander continues to descend, the small 30 m altitude difference between p_1 and p_2 accounts for a larger percentage of the range, and so small differences begin to arise at very low altitudes (e.g., below about 600 m in the right-hand frame of Fig. 9). This motivates a second scenario with larger range differences.

In a second scenario, illustrated in Fig. 8, the camera is pointed 45 deg off nadir and observes two objects on the ground. The two objects are located at 3,000 m and 300 m from the point on the ground beneath the lander. As with the first scenario, triangulation performance is evaluated for the two triangulation methods (DLT and explicit range) and for the optimal polynomial method and results are shown in Fig. 10. The improvement of the optimal solution triangulation is more pronounced in this case, with nearly 12% of gain in relative precision over the DLT at 400 m. The

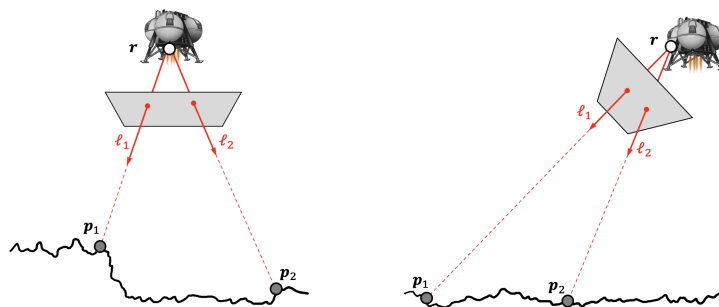


Fig. 8 Illustration of a lander using two surface points for TRN. The first scenario is for a nadir pointed camera (left) and the second scenario is for a camera pointed 45 deg off-nadir (right).

small difference between the DLT and explicit range method is a result of the normalization chosen. If all the LOS measurements in the DLT are converted to unit vectors, then the DLT and explicit range methods produce identical estimates as shown in Fig. 11. That the DLT and explicit range methods are identical under such a normalization was discussed in Section IV.C and proven analytically in the Appendix. This provides a numerical validation of this fact.

The second scenario may also be used to illustrate the practical equivalence between the Hartley and Sturm method (labeled HS, see Ref. [15] and Section V.A.1), the new quadratic polynomial method (labeled QUAT, see Section V.A.2),

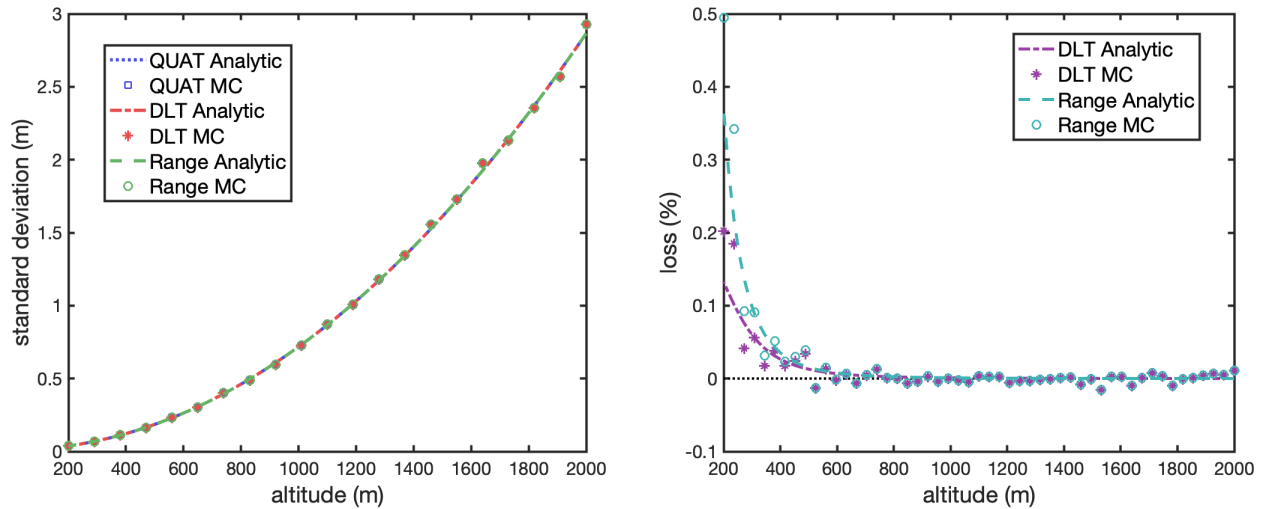


Fig. 9 Analytical (lines) and Monte Carlo (dots) total standard deviation of the triangulated position for the first TRN scenario (nadir camera). Left frame shows the standard deviation for all methods. Right frame shows the percentage of increase in standard deviation (loss in precision) of the trigonometric solutions as compared to the quadratic polynomial (QUAT) method.

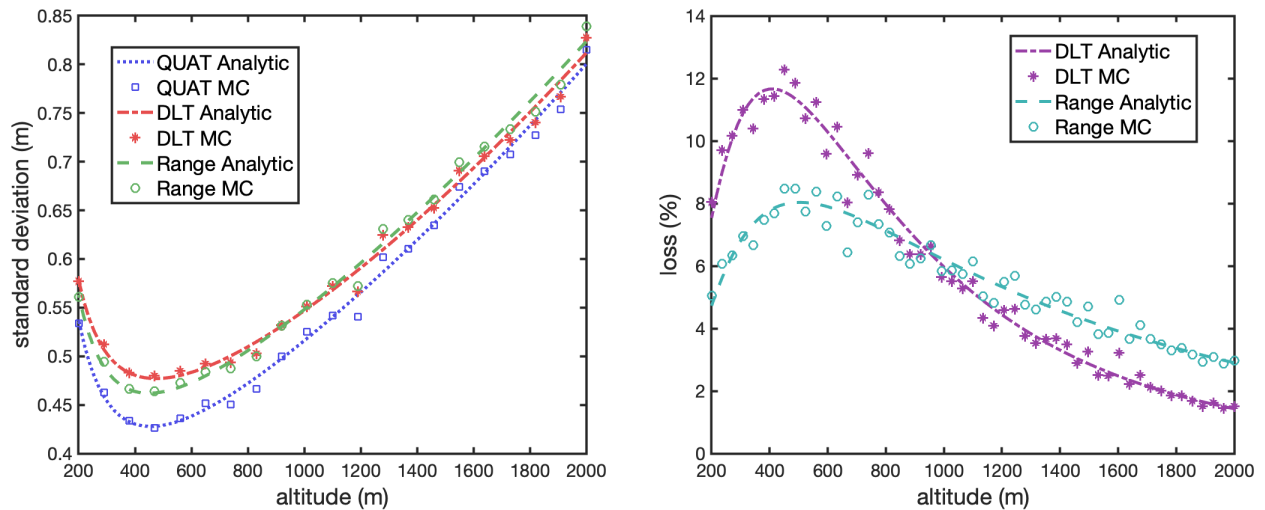


Fig. 10 Analytical (lines) and Monte Carlo (dots) total standard deviation of the triangulated position for the second TRN scenario (45 deg off-nadir camera). Left frame shows the standard deviation for all methods. Right frame shows the percentage of increase in standard deviation (loss in precision) of the trigonometric solutions as compared to the quadratic polynomial (QUAT) method.

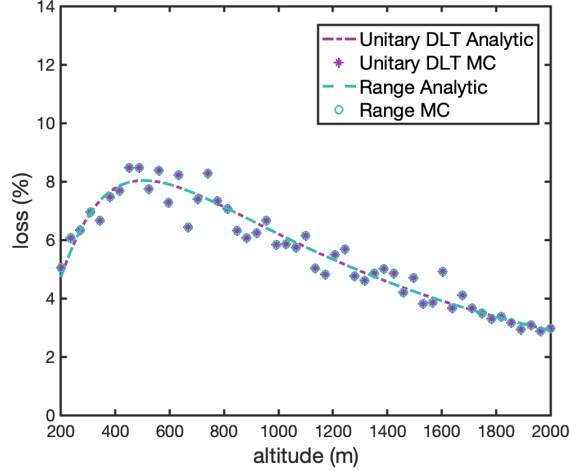


Fig. 11 The DLT with unit vector LOS measurements provides the exact same result as the and the explicit range method. Results are for the second TRN scenario (45 deg off-nadir camera).

Table 2 TRN triangulation residual statistics for scenario two (45 deg off-nadir camera) at an altitude of 1,000 m.

	HS vs TRUE	QUAT vs TRUE	LOST vs TRUE	QUAT vs HS	LOST vs HS
mean x (m)	-5.2118×10^{-4}	-5.2118×10^{-4}	-4.6149×10^{-4}	4.6997×10^{-11}	5.9695×10^{-5}
mean y (m)	-4.2484×10^{-5}	-4.2484×10^{-5}	-4.2484×10^{-5}	-3.6710×10^{-11}	2.4340×10^{-12}
mean z (m)	7.3771×10^{-4}	7.3771×10^{-4}	6.7233×10^{-4}	-5.1492×10^{-11}	-6.5378×10^{-5}
standard dev (m)	4.3804×10^{-1}	4.3804×10^{-1}	4.3804×10^{-1}	1.0414×10^{-7}	1.2507×10^{-4}

and the new LOST method (see Section V.B). At an altitude of 1 km, a 1-million sample Monte Carlo analysis was performed and the results are summarized in Table 2. As compared to the truth, the standard deviation of all three methods (HS, QUAT, LOST) are identical to the reported precision. All three are functionally zero mean, having mean errors about three orders of magnitude smaller than the standard deviation. When compared to one another, the HS and QUAT algorithms are identical to about 10 digits (standard deviation of difference on the order of 10^{-7} m on a position vector of length 10^3 m). This is considered numerically equivalent when accounting for the fact that the HS solution relies on numerically finding the roots of a polynomial of degree six. The difference between the LOST and HS methods (standard deviation of 1.25×10^{-4} m) is about three orders of magnitude smaller than the difference of either of these with respect to the truth (standard deviation of 4.38×10^{-1} m). Such a difference is practically inconsequential. This can be made explicit by considering a scatter plot of the errors for each (see Fig. 12), which clearly shows that one method is no better than the other. In this Monte Carlo analysis the LOST method was closer to the truth for 50.05% of the cases, while the HS method was closer to the truth for 49.95% of the cases.

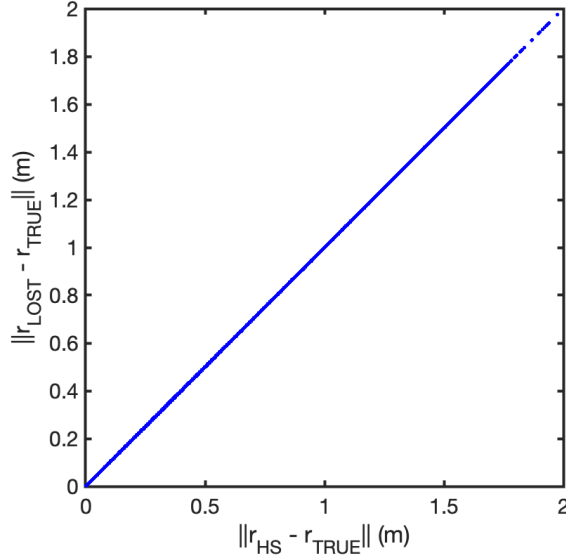


Fig. 12 The position errors are essentially the same for the the Hartley & Sturm method and the LOST method. Results are for TRN scenario two (45 deg off-nadir camera) at an altitude of 1,000 m.

B. Interplanetary Exploration

Triangulation is expected to play an important role in future exploration missions to the outer planets. Both the gas giants (Jupiter and Saturn) and the ice giants (Uranus and Neptune) have a large number of moons, and it is possible to use LOS measurements to these moons to triangulate a spacecraft’s location. The U.S. National Academies have identified the Uranus Orbiter and Probe (UOP) as “the highest-priority new Flagship mission for initiation in the decade 2023-2032” [100], which makes Uranus a prime candidate for further study. A simulated scenario is created where a spacecraft observes the moons Titania and Oberon, with a different camera pointing in the direction of each of the moons. An illustration of this is found in Fig. 13.

Supposing an epoch of 1 January 2050 00:00:0.0 UTC, the known locations of Titania (p_1) and Oberon (p_2) relative

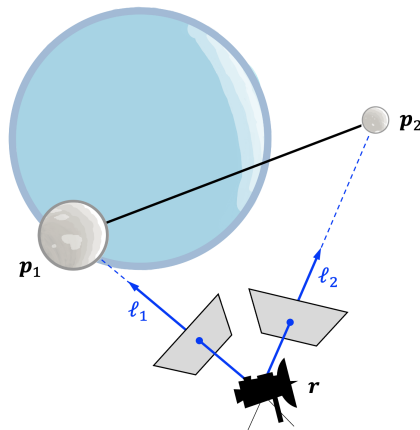


Fig. 13 Spacecraft determining its position by triangulation using two moons around Uranus.

to Uranus are

$$\mathbf{p}_1 = \begin{bmatrix} 2.8607 \times 10^5 \\ -3.2961 \times 10^5 \\ -3.3944 \times 10^2 \end{bmatrix} \text{ km} \quad \mathbf{p}_2 = \begin{bmatrix} 5.0811 \times 10^5 \\ -2.8608 \times 10^5 \\ -9.0978 \times 10^2 \end{bmatrix} \text{ km}$$

These positions were obtained from the URA111 ephemeris files [101] and processed using the SPICE toolkit [97, 98]. These two moons are then viewed by simulated cameras aboard a simulated spacecraft residing somewhere in the equatorial plane of Uranus. Although the true spacecraft location is in the equatorial plane, the moons Titania and Oberon are not in this plane—and, thus, the triangulation problem considered here is fully 3-D. Moreover, this specific arrangement and choice of epoch allows for qualitative comparison of these results with the moon-based localization study provided in Ref. [102].

It is not possible to practically image a specific moon from everywhere in the Uranian system. Thus, following a similar approach as Ref. [102], a number of visibility constraints are adopted. For a moon to be visible, it cannot be blocked from view in any way by Uranus, and needs to have at least 5% of FOV clearance from Uranus. Additionally, the moon is not visible if it occupies more than 80% of the FOV. Finally, the spacecraft is not able to see the moon if the LOS to the sun is within 30 deg of the LOS to the moon. The triangulation is only performed in the case where both moons are visible. To facilitate easy comparison, this analysis uses the mid-resolution camera from Ref. [102], with a FOV of 7 degrees and an IFOV of 60 μ rad.

This simulated scenario (of practical relevance to future interplanetary exploration) may be used to illustrate a number of important observations about triangulation algorithms. These observations are facilitated by the evaluation of results from a Monte Carlo analysis. Specifically, consider a $(3 \times 10^6) \times (3 \times 10^6)$ km region centered around Uranus. At each point within this region, a Monte Carlo analysis was performed with LOS errors generated according to Eq. (8). These noisy LOS data are used to triangulate the spacecraft position using the DLT method from Section IV.A, Hartley and Sturm (HS) polynomial method from Ref. [15] (and Section V.A.1), and the new LOST method from Section V.B.

The first use of the Monte Carlo analysis is to validate the analytic covariance models. Exceptional agreement between the analytic and sample covariances were seen in all cases. To summarize these results, contours of the total standard deviation σ_r [see Eq. (125)] are shown for the LOST method in Fig. 14 and for the DLT method in Fig. 15. The contours for the HS method are visually indistinguishable from the LOST method, and so a separate figure is not necessary. Indeed, the covariance for the HS and LOST methods are identical to machine precision for the analytic case and the total standard deviation agrees to better than 0.1% everywhere for the numerical case (which is consistent with the expected uncertainty in the numerically computed covariance with a finite number of Monte Carlo samples).

A few observations are immediately apparent from Figs. 14 and 15. and agree with simple intuition. First, triangulation performance is best (localization error is smallest) when the angle between the LOS directions and the

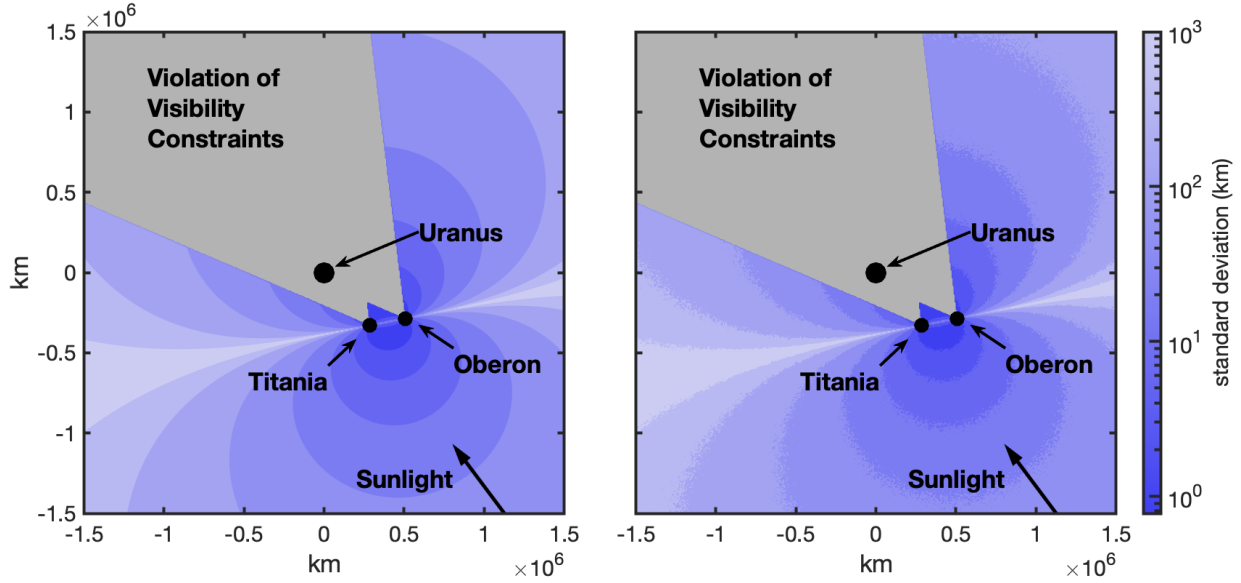


Fig. 14 Analytical (left) and Monte Carlo (right) standard deviations of the spacecraft position with the LOST method.

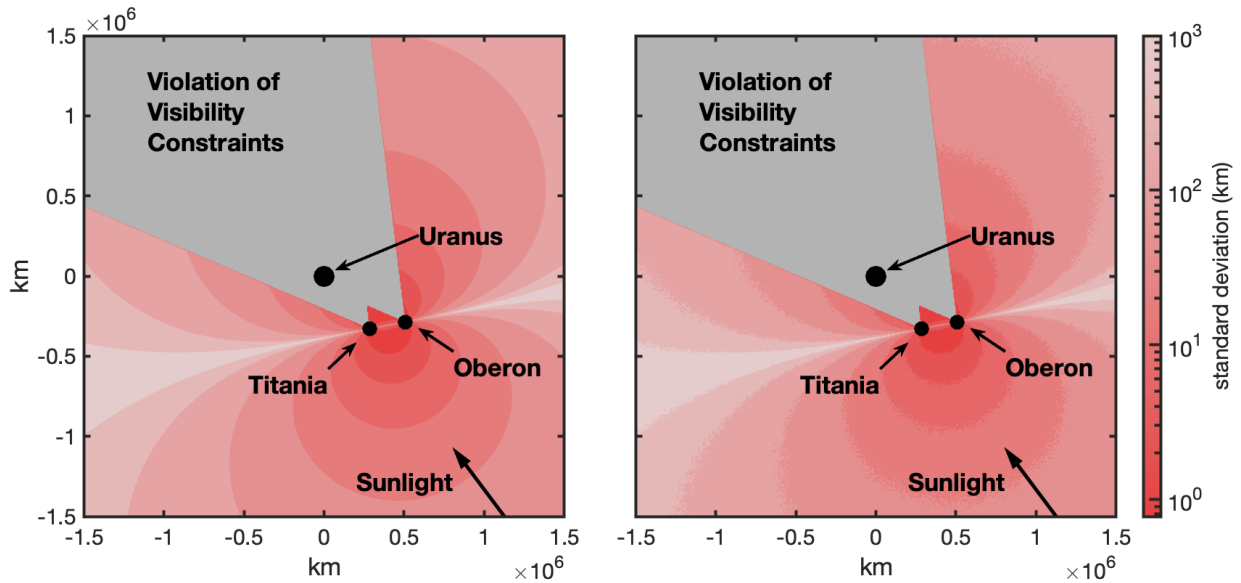


Fig. 15 Analytical (left) and Monte Carlo (right) standard deviations of the spacecraft position with the DLT method.

baseline d_{12} is large. Conversely, performance is worst (localization error is largest) when this angle is small. Second, triangulation performance is best when close to the moons and this performance deteriorates as the distance to the observed moons increases. Third, the analytic covariance for the LOST (and HS) method is always smaller than the DLT method, as can be seen in Fig. 16. The improved performance obtained with LOST as compared to the DLT is only significant when the distances between the observed points is very different.

The second use of the Monte Carlo analysis is further investigate the statistical equivalence of the HS and LOST

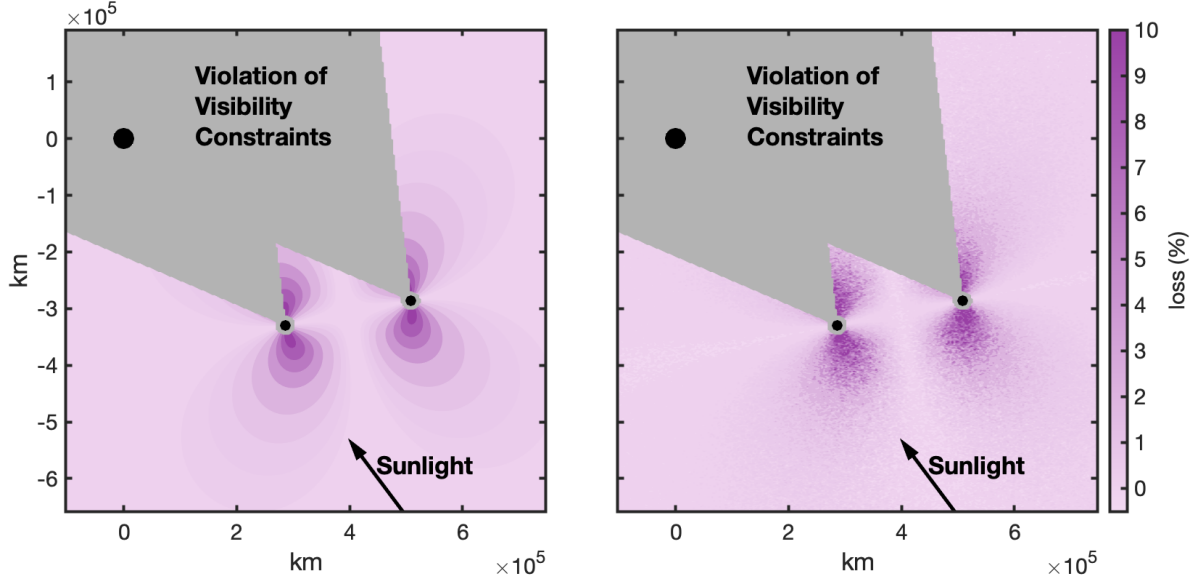


Fig. 16 Analytical (left) and Monte Carlo (right) percentage increase in standard deviation (loss in precision) of DLT compared to LOST. The analytical loss never goes under zero.

methods. The covariance of these two methods has already been shown to be equivalent—to within machine precision for the analytic result and to within the expected error for the Monte Carlo result. Having an equivalent covariance, however, does not imply that the HS and LOST methods provide the exact same estimate for any particular realization of measurement noise. Two additional analyses are performed to address this question. First, the total standard deviation of the residual $\Delta \mathbf{r} = \mathbf{r}_{LOST} - \mathbf{r}_{DLT}$ is computed and then contours of the ratio $\sigma_{\Delta \mathbf{r}} / \sigma_{LOST}$ shown in the left-hand frame of Fig. 17 (for comparison, contours of σ_{LOST} are as shown in Fig. 14). Second, at every point where a Monte Carlo analysis is performed, the number of cases is recorded where each method (LOST or HS) is best. The results are summarized in the right-hand frame of Fig. 17, where a point is colored dark blue if the LOST algorithm was closer to the truth for more than half of the cases (or gray if HS was closer to the truth for more than half). Two things are now clear. First, the standard deviation of the residual $\sigma_{\Delta \mathbf{r}}$ is usually 3–4 orders of magnitude smaller than the total standard deviation $\sigma_{\mathbf{r}}$ (and at least one order of magnitude smaller everywhere). Second, there is no apparent structure in which method is closer to the truth, suggesting that there is no viewing geometry that systematically makes the LOST method better (or worse) than HS method. Moreover, each algorithm was found to be “best” with about the same frequency (the LOST algorithm was better for about 50.1% of the points evaluated). Thus, not only do the LOST and HS methods have exactly the same covariance, but neither of the methods is more likely to produce a better estimate than the other.

While the HS and LOST algorithms have equivalent localization performance, the LOST algorithm has a few notable advantages. First, for the two-measurement case, the solution to LOST takes the form of a small linear system, which is easier (and faster) to solve than the polynomial of degree six in the HS method. Second, the LOST method retains its linear form for $n \geq 3$ LOS measurements—thus allowing for statistically optimal triangulation for a very large number

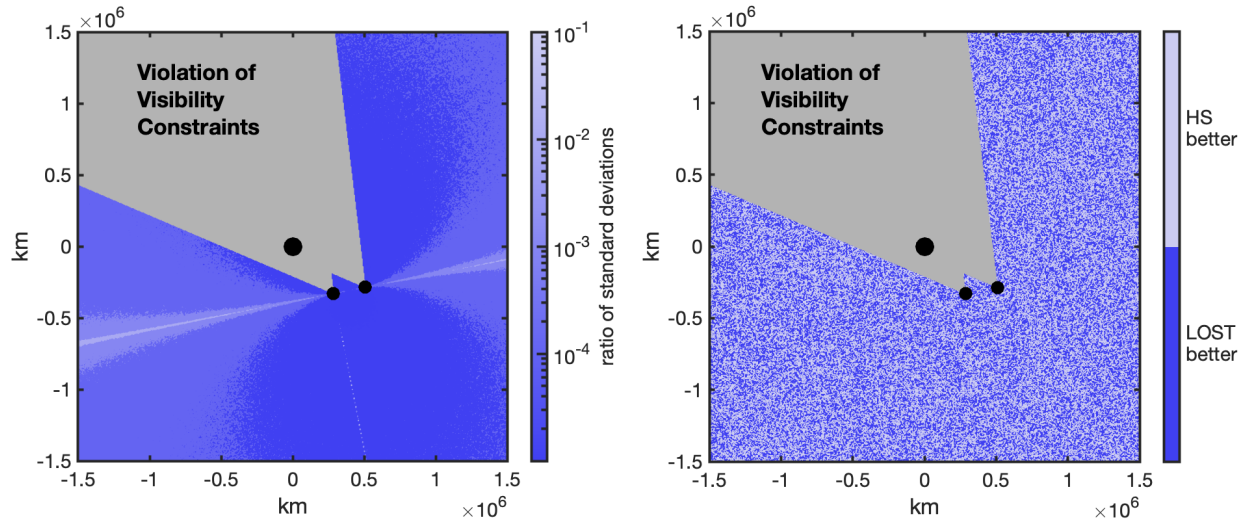


Fig. 17 The Hartley and Sturm (HS) and LOST algorithms have equivalent performance. Monte Carlo results show the ratio of $\sigma_{\Delta}/\sigma_{LOST}$ (left) and the pattern of where each algorithm performed best (right).

of measurements as the direct solution to a linear system (and without the need for iteratively solving a nonlinear least squares problem). By comparison, the optimal HS method does not scale to more than two LOS measurements.

C. Three-Dimensional Reconstruction

Shape modeling and 3-D reconstruction is an important problem for the exploration of small bodies in the Solar System [2, 3]. Such a reconstruction may be accomplished by triangulation. Rather than demonstrate the capability on a space object, an example is presented using a standard benchmark dataset.

The Notre-Dame de Paris cathedral lies on the Île de la Cité in Paris and the main body of the cathedral was built between about 1160 and 1245 [103]. Notre-Dame is widely regarded as the preeminent surviving example of French Gothic architecture and is amongst the most visited (and photographed) structures in France. As a result of its popularity, there are a large number of public-domain photographs—making Notre-Dame a natural choice (amongst others) for demonstration of the ground-breaking image-based 3-D reconstruction work by Snavely, Seitz, and Szeliski [35, 104]. A 3-D cloud of 127,431 points originating from 715 pictures (and as many cameras) obtained from Ref. [104]* may be used to reconstruct the west facade of the cathedral. This is an example of the intersection form of the triangulation problem. The solutions of the DLT and the LOST are compared to the reference model included in the benchmark dataset. As illustrated in Fig. 18, the distinction between the reference model and the LOST reconstruction is hardly distinguishable to the naked eye. The histogram presented in Fig. 19 confirms what the eye can (or cannot) see, the majority of the point positions found by LOST are within a centimeter or less from the reference model. Figure 19 also highlights that the residuals are one order of magnitude lower when using the LOST instead of the DLT, for the majority of the points.

*Supplementary data for Ref. [104] available from: <http://phototour.cs.washington.edu/datasets/>.

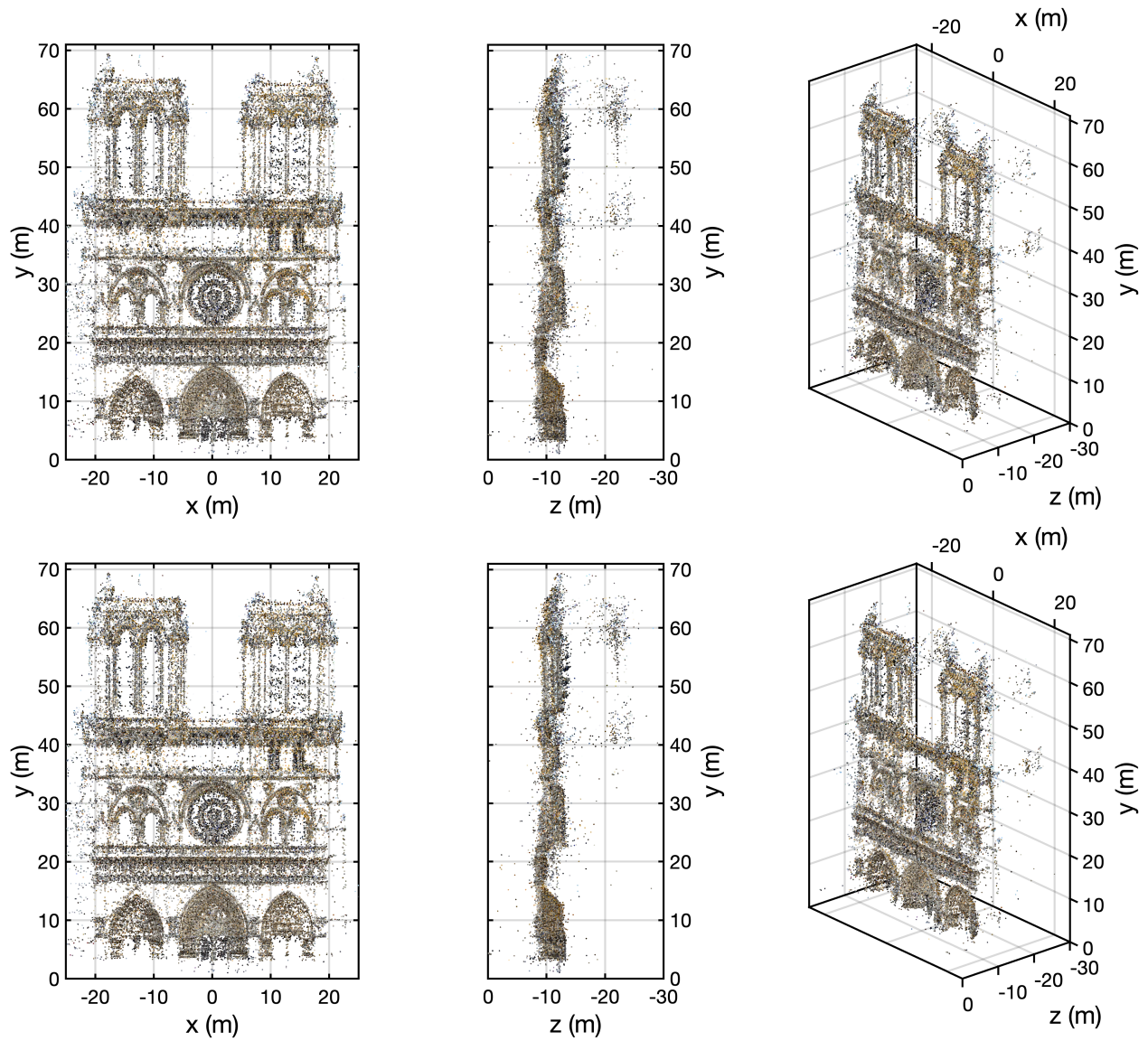


Fig. 18 Point cloud reconstruction of the west facade of Notre-Dame de Paris. The top row shows the reference model from [104] while the bottom row is the solution found with the LOST method.

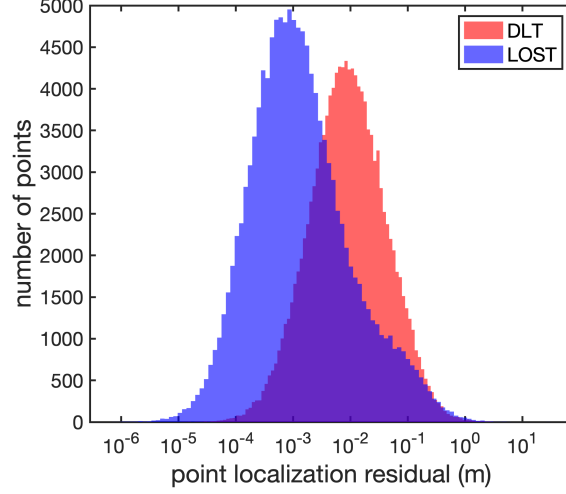


Fig. 19 Position residuals for the 3-D reconstruction of Notre-Dame de Pairs using the DLT and LOST methods as compared to the reference model.

D. Rendezvous, Proximity Operations, and Docking (RPOD)

Rendezvous, Proximity Operations, and Docking (RPOD) is a critical capability for a variety of spaceflight applications [105], including human exploration [106–108], interplanetary exploration [109], and satellite servicing [110]. When two spacecraft in nearly circular orbits are close to one another, their relative dynamics are nearly linear and may be described by the Clohessy-Wiltshire (CW) equations [61]. It has been known for some time that the relative state between two particles is unobservable under CW dynamics when only LOS measurements are available [13, 62]. There are two ways to reintroduce observability during coasting flight (i.e., with no maneuvers). The first is to consider the nonlinear dynamics [111]. The second is to alter the triangulation geometry. This brief example focuses only on the latter of these solutions.

Consider the situation where the origin of an LVLH frame fixed to a chief spacecraft in a circular orbit. The relative motion of a nearby deputy spacecraft in this same LVLH frame is governed by the CW equations having a solution of the form:

$$\xi_i = \begin{bmatrix} \mathbf{r}_i \\ \mathbf{v}_i \end{bmatrix} = \begin{bmatrix} \Phi_{rr}(t_i, t_0) & \Phi_{rv}(t_i, t_0) \\ \Phi_{vr}(t_i, t_0) & \Phi_{vv}(t_i, t_0) \end{bmatrix} \begin{bmatrix} \mathbf{r}_0 \\ \mathbf{v}_0 \end{bmatrix} = \Phi(t_i, t_0) \xi_0 \quad (126)$$

where \mathbf{r}_i and \mathbf{v}_i are LVLH position and velocity of the deputy relative to the chief at time t_i . The equations for $\Phi(t_i, t_0)$ may be found in Ref. [61] or a contemporary astrodynamics textbook (e.g., [112]).

Using the notation from Section VI, let Φ_r denote the rows of the STM that produce the position vector,

$$\Phi_r(t_i, t_0) = \begin{bmatrix} \Phi_{rr}(t_i, t_0) & \Phi_{rv}(t_i, t_0) \end{bmatrix} \quad (127)$$

which is a 3×6 matrix in this case.

Suppose for a moment that LOS measurements are collected between the chief and deputy spacecraft (the same equations result regardless of the vehicle on which the camera resides). Since the chief spacecraft is at the origin, this implies that $\mathbf{p}_{I_i} = 0, \forall t_i$. Hence, substituting this scenario into Eq. (124), one arrives at

$$\begin{bmatrix} [\ell_1 \times] \Phi_r(t_1, t_0) \\ \vdots \\ [\ell_n \times] \Phi_r(t_n, t_0) \end{bmatrix} \begin{bmatrix} \mathbf{r}_0 \\ \mathbf{v}_0 \end{bmatrix} = \mathbf{0}_{3n \times 1} \quad (128)$$

Since the result is a homogeneous linear system, it follows that both ξ_0 and $\alpha \xi_0$ (for $\alpha \neq 0$) provide equally acceptable solutions to the linear system. There are infinitely many homothetic solutions $\alpha \xi_0$ that represent an expansion or contraction of the figure (i.e., true deputy's trajectory) about the homothetic center (i.e., the chief's location at the origin of the LVLH frame). This is nothing more than a triangulation interpretation of the well-known scale ambiguity associated with angles-only RelNav that is usually shown by other means (e.g., Ref. [62]).

It is obvious now that scale observability may be introduced by making the right-hand side of Eq. (128) non-zero. This may be practically achieved by introducing a known offset in the location of either the camera (on the deputy) or the observed point (on the chief). Such a situation may occur when either of the spacecraft are not small when compared to the scale of the relative motion.

To see this, suppose there is a camera aboard the deputy spacecraft with a known offset of $\delta \mathbf{r}_i$ at time t_i . In this case, the LOS measurement is

$$\ell_i \propto \mathbf{p}_i - (\mathbf{r}_i + \delta \mathbf{r}_i) \quad (129)$$

and so the DLT equation becomes

$$[\ell_i \times] \mathbf{r}_i = [\ell_i \times] (\mathbf{p}_i - \delta \mathbf{r}_i) \quad (130)$$

Therefore, after mapping \mathbf{r}_i to time t_0 ,

$$[\ell_i \times] \Phi(t_i, t_0) \xi_0 = [\ell_i \times] (\mathbf{p}_i - \delta \mathbf{r}_i) \quad (131)$$

Letting the localization frame be the LVLH frame (denoted by L) and using the normalization $\ell_{C_i} \propto \mathbf{K}^{-1} \bar{\mathbf{u}}_i$,

$$[\mathbf{K}^{-1} \bar{\mathbf{u}}_i \times] \mathbf{T}_{C_i}^L \Phi(t_i, t_0) \xi_0 = [\mathbf{K}^{-1} \bar{\mathbf{u}}_i \times] \mathbf{T}_{C_i}^L (\mathbf{p}_{L_i} - \delta \mathbf{r}_{L_i}) \quad (132)$$

When more than one measurement is available at more than one time, this expression may be stacked in the usual way to

form a linear system

$$\begin{bmatrix} [\mathbf{K}^{-1}\bar{\mathbf{u}}_1 \times] \mathbf{T}_{C_1}^L \Phi(t_1, t_0) \\ \vdots \\ [\mathbf{K}^{-1}\bar{\mathbf{u}}_i \times] \mathbf{T}_{C_i}^L \Phi(t_i, t_0) \end{bmatrix} \xi_0 = \begin{bmatrix} [\mathbf{K}^{-1}\bar{\mathbf{u}}_1 \times] \mathbf{T}_{C_1}^L (\mathbf{p}_{L_1} - \delta \mathbf{r}_{L_1}) \\ \vdots \\ [\mathbf{K}^{-1}\bar{\mathbf{u}}_i \times] \mathbf{T}_{C_i}^L (\mathbf{p}_{L_i} - \delta \mathbf{r}_{L_i}) \end{bmatrix} \quad (133)$$

So long as the offsets (and measurement times) are chosen to avoid $[\mathbf{K}^{-1}\bar{\mathbf{u}}_i \times] \mathbf{T}_{C_i}^L (\mathbf{p}_{C_i} - \delta \mathbf{r}_{C_i}) = 0$ for all of the observation times then the problem becomes observable. In most cases this condition is the same as ensuring $\mathbf{p}_{C_i} \neq \delta \mathbf{r}_{C_i}$. The idea of introducing observability by an offset in just the point aboard the deputy (i.e., $\mathbf{p}_{C_i} = 0$ and $\delta \mathbf{r}_{C_i} \neq 0$) was explored in Ref. [113]. The result above demonstrates that an equivalent solution could be achieved by introducing an offset on the chief (i.e., $\mathbf{p}_{C_i} \neq 0$ and $\delta \mathbf{r}_{C_i} = 0$).

VIII. Conclusions

Absolute line of sight (LOS) measurements from images may be used to solve both spacecraft navigation and three-dimensional (3-D) reconstruction problems via triangulation. The mathematical foundations necessary for triangulation have been understood since antiquity, and knowledge of this history enhances the versatility of the modern practitioner. This manuscript reviews the historical evolution of triangulation algorithms that ultimately led to the embodiments of the trigonometric solutions that are in widespread use today. Many variations on these trigonometric solutions [e.g, with the Direct Linear Transform (DLT), collinearity equations, or Plücker coordinates] are shown to be equivalent to one another. In the special case of two LOS observations, the statistically optimal solution of Hartley and Sturm [15] is summarized and the resulting polynomial of degree six is considered. When the two LOS observations come from the same camera (e.g., with monocular navigation), the derivation can be modified to produce a much simpler polynomial of degree two. Moreover, in the general case of many measurements (from one or many cameras), it is shown that a Maximum Likelihood Estimate (MLE) may be developed as the solution to a small linear system (of size $2n \times 3$ for n LOS measurements)—resulting in the so-called Linear Optimal Sine Triangulation (LOST) method. The non-iterative LOST method is shown to provide an equivalent solution to the classical Hartley and Sturm method, but has the comparative advantages of (1) being scalable to many measurements and (2) not requiring the solution to a polynomial of degree six. Finally, many of the triangulation results are also shown to be valid for dynamic systems, especially when the dynamics are linear. The various algorithms and analytic insights are validated through a variety of examples, including planetary terrain relative navigation (TRN), interplanetary optical navigation (OPNAV), 3-D reconstruction of Notre-Dame de Paris, and angles-only relative navigation (RelNav).

Appendix

A. Analytic Covariance Expressions

1. Direct Linear Transform

The DLT is formulated in Eq. (20) as an ordinary (unweighted) least squares problem. Given a problem $\mathbf{H}\mathbf{x} = \mathbf{y}$, recall that the covariance for a generic weighting is,

$$\mathbf{P} = (\mathbf{H}^T \mathbf{W} \mathbf{H})^{-1} (\mathbf{H}^T \mathbf{W} \mathbf{R} \mathbf{W}^T \mathbf{H}) (\mathbf{H}^T \mathbf{W} \mathbf{H})^{-1} \quad (134)$$

where \mathbf{R} is the measurement covariance and \mathbf{W} is the measurement weighting matrix. When $\mathbf{W} = \mathbf{R}^{-1}$ the result is the MLE solution. However, when $\mathbf{W} = \mathbf{I}_{n \times n}$, the result is the ordinary least squares solution having covariance

$$\mathbf{P} = (\mathbf{H}^T \mathbf{H})^{-1} (\mathbf{H}^T \mathbf{R} \mathbf{H}) (\mathbf{H}^T \mathbf{H})^{-1} \quad (135)$$

Substituting into this notation, it follows from Eq. (20), that

$$\mathbf{H} = \begin{bmatrix} [\mathbf{K}_1^{-1} \bar{\mathbf{u}}_1 \times] \mathbf{T}_{C_1}^I \\ \vdots \\ [\mathbf{K}_n^{-1} \bar{\mathbf{u}}_n \times] \mathbf{T}_{C_n}^I \end{bmatrix} \quad (136)$$

and, therefore,

$$\mathbf{H}^T \mathbf{H} = - \sum_{i=1}^n \mathbf{T}_I^{C_i} [\mathbf{K}_i^{-1} \bar{\mathbf{u}}_i \times]^2 \mathbf{T}_{C_i}^I \quad (137)$$

Moreover, obtaining \mathbf{R}_{ϵ_i} from Eq. (107) one finds that

$$\mathbf{P}_{DLT} = -(\mathbf{H}^T \mathbf{H})^{-1} \left(\sum_{i=1}^n \mathbf{T}_I^{C_i} [\mathbf{K}_i^{-1} \bar{\mathbf{u}}_i \times] \tilde{\mathbf{R}}_{\epsilon_i} [\mathbf{K}_i^{-1} \bar{\mathbf{u}}_i \times] \mathbf{T}_{C_i}^I \right) (\mathbf{H}^T \mathbf{H})^{-1} \quad (138)$$

where everything here is known. The leading negative sign is a result of the identity $[\cdot \times]^T = -[\cdot \times]$.

2. Explicit Range

Writing an analytic expression for the covariance of the explicit range method is difficult in general due to combinatorial nature of the problem. It is not generally clear which combinations of measurements should be used. Thus, the discussion that follows focuses only on the two-measurement case. Additional attention is not warranted since this method is rarely the preferred approach for triangulation.

To develop the covariance, begin with the expression from Eq. (50)

$$\mathbf{r}_I = \frac{1}{n} \sum_{i=1}^n \mathbf{p}_{I_i} - \rho_i \mathbf{a}_{I_i} \quad (139)$$

and then compute the differential

$$\delta \mathbf{r}_I = -\frac{1}{n} \sum_{i=1}^n \delta \rho_i \mathbf{a}_{I_i} + \rho_i \delta \mathbf{a}_{I_i} \quad (140)$$

For the case of $n = 2$, this may be written as

$$-2\delta \mathbf{r} = \mathbf{A}_{12} \begin{bmatrix} \delta \rho_1 \\ \delta \rho_2 \end{bmatrix} + \mathbf{B}_{12} \begin{bmatrix} \delta \mathbf{a}_{I_1} \\ \delta \mathbf{a}_{I_2} \end{bmatrix} \quad (141)$$

$$\mathbf{A}_{12} = \begin{bmatrix} \mathbf{a}_{I_1} & \mathbf{a}_{I_2} \end{bmatrix} \quad \text{and} \quad \mathbf{B}_{12} = \begin{bmatrix} \rho_1 \mathbf{I}_{3 \times 3} & \rho_2 \mathbf{I}_{3 \times 3} \end{bmatrix} \quad (142)$$

Similarly, taking the differential of Eq. (49) for $n = 2$, one obtains

$$\begin{bmatrix} -1 & \mathbf{a}_{I_1}^T \mathbf{a}_{I_2} \\ -\mathbf{a}_{I_2}^T \mathbf{a}_{I_1} & 1 \end{bmatrix} \begin{bmatrix} \delta \rho_1 \\ \delta \rho_2 \end{bmatrix} = \begin{bmatrix} \mathbf{d}_{I_{12}}^T \delta \mathbf{a}_{I_1} - \rho_2 (\mathbf{a}_{I_2}^T \delta \mathbf{a}_{I_1} + \mathbf{a}_{I_1}^T \delta \mathbf{a}_{I_2}) \\ \mathbf{d}_{I_{12}} \delta \mathbf{a}_{I_2} + \rho_1 (\mathbf{a}_{I_2}^T \delta \mathbf{a}_{I_1} + \mathbf{a}_{I_1}^T \delta \mathbf{a}_{I_2}) \end{bmatrix} \quad (143)$$

which may be rewritten as

$$\begin{bmatrix} \delta \rho_1 \\ \delta \rho_2 \end{bmatrix} = \mathbf{C}_{12} \begin{bmatrix} \delta \mathbf{a}_{I_1} \\ \delta \mathbf{a}_{I_2} \end{bmatrix} \quad (144)$$

$$\mathbf{C}_{12} = \frac{1}{(\mathbf{a}_{I_1}^T \mathbf{a}_{I_2})^2 - 1} \begin{bmatrix} 1 & -\mathbf{a}_{I_1}^T \mathbf{a}_{I_2} \\ \mathbf{a}_{I_2}^T \mathbf{a}_{I_1} & -1 \end{bmatrix} \begin{bmatrix} \mathbf{d}_{I_{12}}^T - \rho_2 \mathbf{a}_{I_2}^T & -\rho_2 \mathbf{a}_{I_1}^T \\ \rho_1 \mathbf{a}_{I_2}^T & \mathbf{d}_{I_{12}} + \rho_1 \mathbf{a}_{I_1} \end{bmatrix} \quad (145)$$

Substituting Eq. (144) into Eq. (141), it follows that

$$\delta \mathbf{r} = -\frac{1}{2} (\mathbf{A}_{12} \mathbf{C}_{12} + \mathbf{B}_{12}) \begin{bmatrix} \delta \mathbf{a}_{C_1} \\ \delta \mathbf{a}_{C_2} \end{bmatrix} \quad (146)$$

Also, computing $\partial \mathbf{a}_{C_i} / \partial \bar{\mathbf{x}}_i$, observe that

$$\begin{bmatrix} \delta \mathbf{a}_{C_1} \\ \delta \mathbf{a}_{C_2} \end{bmatrix} = -\mathbf{D}_{12} \begin{bmatrix} \delta \bar{\mathbf{x}}_1 \\ \delta \bar{\mathbf{x}}_2 \end{bmatrix} \quad (147)$$

$$\mathbf{D}_{12} = \begin{bmatrix} \|\bar{\mathbf{x}}_1^T\|^{-1} \mathbf{T}_I^{C_1} [\mathbf{a}_{C_1} \times]^2 & \mathbf{0}_{3 \times 3} \\ \mathbf{0}_{3 \times 3} & \|\bar{\mathbf{x}}_2^T\|^{-1} \mathbf{T}_I^{C_2} [\mathbf{a}_{C_2} \times]^2 \end{bmatrix} \quad (148)$$

Which, after substitution of Eq. (147) into Eq. (146), yields

$$\delta \mathbf{r} = \frac{1}{2} (\mathbf{A}_{12} \mathbf{C}_{12} + \mathbf{B}_{12}) \mathbf{D}_{12} \begin{bmatrix} \delta \bar{\mathbf{x}}_1 \\ \delta \bar{\mathbf{x}}_2 \end{bmatrix} \quad (149)$$

And, finally,

$$\mathbf{P}_{RNG} = E[\delta \mathbf{r} \delta \mathbf{r}^T] = \frac{1}{4} (\mathbf{A}_{12} \mathbf{C}_{12} + \mathbf{B}_{12}) \mathbf{D}_{12} \mathbf{R}_{\bar{\mathbf{x}}} \mathbf{D}_{12}^T (\mathbf{A}_{12} \mathbf{C}_{12} + \mathbf{B}_{12})^T \quad (150)$$

3. Hartley and Sturm Polynomial

To develop the analytic covariance for the Hartley and Sturm method, begin with the measurement model from Eq. (57)

$$\mathbf{u}_i = \frac{\mathbf{S} \mathbf{K}_i \mathbf{T}_{C_i}^l (\mathbf{p}_{I_i} - \mathbf{r}_I)}{\mathbf{k}^T \mathbf{K}_i \mathbf{T}_{C_i}^l (\mathbf{p}_{I_i} - \mathbf{r}_I)} \quad (151)$$

Since this method (as modified here) explicitly minimizes the covariance-weighted reprojection error, one obtains a covariance

$$\mathbf{P}_r = \left[\sum_{i=1}^2 \mathbf{A}_i^T \mathbf{R}_{u_i}^{-1} \mathbf{A}_i \right]^{-1} \quad (152)$$

where

$$\mathbf{A}_i = \frac{\partial \mathbf{u}_i}{\partial \mathbf{r}_I} = \frac{-\mathbf{S} \mathbf{K}_i \mathbf{T}_{C_i}^l}{\mathbf{k}^T \mathbf{K}_i \mathbf{T}_{C_i}^l (\mathbf{p}_{I_i} - \mathbf{r}_I)} \left(\mathbf{I}_{3 \times 3} - \frac{(\mathbf{p}_{I_i} - \mathbf{r}_I) \mathbf{k}^T \mathbf{K}_i \mathbf{T}_{C_i}^l}{\mathbf{k}^T \mathbf{K}_i \mathbf{T}_{C_i}^l (\mathbf{p}_{I_i} - \mathbf{r}_I)} \right) \quad (153)$$

This may be simplified somewhat by considering the structure of \mathbf{A}_i and \mathbf{R}_{u_i} . First, recognize that $\mathbf{k}^T \mathbf{K}_i = \mathbf{k}^T$. Also, making use of the identity $(\mathbf{a}^T \mathbf{b}) \mathbf{I}_{3 \times 3} - \mathbf{b} \mathbf{a}^T = [\mathbf{a} \times] [\mathbf{b} \times]$, one observes that that \mathbf{A}_i becomes

$$\mathbf{A}_i = \frac{1}{\gamma_i} \mathbf{S} \mathbf{K}_i \mathbf{T}_{C_i}^l \left[\mathbf{T}_I^{C_i} \mathbf{k} \times \right] \left[(\mathbf{p}_{I_i} - \mathbf{r}_I) \times \right] \quad (154)$$

Further, recognizing that $\bar{\mathbf{x}}_i = \mathbf{T}_{C_i}^l (\mathbf{p}_{I_i} - \mathbf{r}_I) / \gamma_i$,

$$\mathbf{A}_i = \frac{1}{\gamma_i} \mathbf{S} \mathbf{K}_i \mathbf{T}_{C_i}^l \left[\mathbf{T}_I^{C_i} \mathbf{k} \times \right] \left[\mathbf{T}_I^{C_i} \bar{\mathbf{x}}_i \times \right] \quad (155)$$

Factoring out the rotation $\mathbf{T}_{C_i}^l$

$$\mathbf{A}_i = \frac{1}{\gamma_i} \mathbf{S} \mathbf{K}_i [\mathbf{k} \times] [\bar{\mathbf{x}}_i \times] \mathbf{T}_{C_i}^l \quad (156)$$

If $\mathbf{R}_{u_i}^{-1} = \sigma_{u_i}^{-2} \mathbf{I}_{2 \times 2}$, substituting into

$$\mathbf{P}_r^{-1} = \sum_{i=1}^n \frac{1}{\sigma_{x_i}^2 \gamma_i^2} \mathbf{T}_I^{C_i} [\bar{x}_i \times] [\mathbf{k} \times] \mathbf{K}_i^T \mathbf{S}^T \mathbf{S} \mathbf{K}_i [\mathbf{k} \times] [\bar{x}_i \times] \mathbf{T}_{C_i}^I \quad (157)$$

Suppose that pixels are square ($d_x = d_y$) and that there is no detector skewness ($\alpha = 0$) when forming the camera calibration matrix \mathbf{K}_i . Under this condition, note that $[\mathbf{k} \times] \mathbf{K}_i^T \mathbf{S}^T \mathbf{S} \mathbf{K}_i [\mathbf{k} \times] = -d_{x_i}^2 \mathbf{S}^T \mathbf{S}$. Moreover, since $\bar{x}_i = \mathbf{K}_i^{-1} \bar{u}_i$,

$$\mathbf{P}_r^{-1} = - \sum_{i=1}^n \frac{d_{x_i}^2}{\sigma_{u_i}^2 \gamma_i^2} \mathbf{T}_I^{C_i} [\mathbf{K}_i^{-1} \bar{u}_i \times] \mathbf{S}^T \mathbf{S} [\mathbf{K}_i^{-1} \bar{u}_i \times] \mathbf{T}_{C_i}^I \quad (158)$$

Recognizing that $\sigma_{x_i} = \sigma_{u_i} / d_x$, this becomes

$$\mathbf{P}_r^{-1} = - \sum_{i=1}^n \frac{1}{\sigma_{x_i}^2 \gamma_i^2} \mathbf{T}_I^{C_i} [\mathbf{K}_i^{-1} \bar{u}_i \times] \mathbf{S}^T \mathbf{S} [\mathbf{K}_i^{-1} \bar{u}_i \times] \mathbf{T}_{C_i}^I \quad (159)$$

which is identical to Eq. (164). Hence, the analytic covariance for the HS and LOST methods is the same when

$$\mathbf{R}_{u_i} = \sigma_{u_i}^2 \mathbf{I}_{2 \times 2} = d_{x_i}^2 \sigma_{x_i}^2 \mathbf{I}_{2 \times 2} = d_{x_i}^2 \mathbf{R}_{x_i}.$$

4. LOST

The analytic LOST covariance is given from Eq. 116, repeated here as

$$\mathbf{P}_r = - \left(\sum_{i=1}^n \mathbf{T}_I^{C_i} [\mathbf{K}_i^{-1} \bar{u}_i \times] \mathbf{R}_{\epsilon_i}^\dagger [\mathbf{K}_i^{-1} \bar{u}_i \times] \mathbf{T}_{C_i}^I \right)^{-1} \quad (160)$$

The complicating term for analytic analysis is $\mathbf{R}_{\epsilon_i}^\dagger$. This is addressed first. Beginning with the definition of \mathbf{R}_{ϵ_i} from Eq. (107), which is written compactly as

$$\mathbf{R}_{\epsilon_i} = -\gamma_i^2 [\mathbf{K}_i^{-1} \bar{u}_i \times] \mathbf{R}_{\bar{x}_i} [\mathbf{K}_i^{-1} \bar{u}_i \times] \quad (161)$$

where γ_i is from Eq. (108). Under the case when $\mathbf{R}_{\bar{x}_i} = \sigma_{\bar{x}_i}^2 \mathbf{S}^T \mathbf{S}$, observe that

$$\mathbf{R}_{\epsilon_i}^\dagger = \frac{1}{\sigma_{\bar{x}_i}^2 \gamma_i^2 \|\mathbf{K}_i^{-1} \bar{u}_i\|^4} [\mathbf{K}_i^{-1} \bar{u}_i \times]^2 \mathbf{S}^T \mathbf{S} [\mathbf{K}_i^{-1} \bar{u}_i \times]^2 \quad (162)$$

Substituting this into the Eq. (160) leads to

$$\mathbf{P}_r^{-1} = - \sum_{i=1}^n \frac{1}{\sigma_{\bar{x}_i}^2 \gamma_i^2 \|\mathbf{K}_i^{-1} \bar{u}_i\|^4} \mathbf{T}_I^{C_i} [\mathbf{K}_i^{-1} \bar{u}_i \times]^3 \mathbf{S}^T \mathbf{S} [\mathbf{K}_i^{-1} \bar{u}_i \times]^3 \mathbf{T}_{C_i}^I \quad (163)$$

which simplifies to

$$\mathbf{p}_r^{-1} = - \sum_{i=1}^n \frac{1}{\sigma_{\hat{x}_i}^2 \gamma_i^2} \mathbf{T}_I^{C_i} [\mathbf{K}_i^{-1} \bar{\mathbf{u}}_i \times] \mathbf{S}^T \mathbf{S} [\mathbf{K}_i^{-1} \bar{\mathbf{u}}_i \times] \mathbf{T}_{C_i}^T \quad (164)$$

B. Equivalence of the Triangulation Solutions

For the 2×2 case, one can analytically find the position estimate by the explicit range as

$$\mathbf{r}_I = \frac{1}{2} \sum_{i=1}^2 (\mathbf{p}_i - \rho_i \mathbf{a}_i) \quad (165)$$

$$\mathbf{r}_I = \frac{1}{2} (\mathbf{p}_1 + \mathbf{p}_2) - \frac{1}{2} \begin{bmatrix} \mathbf{a}_{I_1} & \mathbf{a}_{I_2} \end{bmatrix} \begin{bmatrix} \rho_1 \\ \rho_2 \end{bmatrix} \quad (166)$$

$$\begin{aligned} \hat{\mathbf{r}}_I &= \frac{1}{2} (\mathbf{p}_1 + \mathbf{p}_2) - \frac{1}{2} \begin{bmatrix} \mathbf{a}_{I_1} & \mathbf{a}_{I_2} \end{bmatrix} \left(\frac{1}{(\mathbf{a}_{I_1}^T \mathbf{a}_{I_2})^2 - 1} \begin{bmatrix} 1 & -\mathbf{a}_{I_1}^T \mathbf{a}_{I_2} \\ \mathbf{a}_{I_2}^T \mathbf{a}_{I_1} & -1 \end{bmatrix} \begin{bmatrix} \mathbf{a}_{I_1}^T \mathbf{d}_{I_{12}} \\ \mathbf{a}_{I_2}^T \mathbf{d}_{I_{12}} \end{bmatrix} \right) \\ &= \frac{((\mathbf{a}_{I_1}^T \mathbf{a}_{I_2})^2 - 1) (\mathbf{p}_1 + \mathbf{p}_2) + \mathbf{a}_{I_1} (\mathbf{a}_{I_1}^T \mathbf{a}_{I_2} \mathbf{a}_{I_2}^T (\mathbf{p}_2 - \mathbf{p}_1) - \mathbf{a}_{I_1}^T (\mathbf{p}_2 - \mathbf{p}_1)) + \mathbf{a}_{I_2} (\mathbf{a}_{I_2}^T (\mathbf{p}_2 - \mathbf{p}_1) - \mathbf{a}_{I_2}^T \mathbf{a}_{I_1} \mathbf{a}_{I_1}^T (\mathbf{p}_2 - \mathbf{p}_1))}{2 ((\mathbf{a}_{I_1}^T \mathbf{a}_{I_2})^2 - 1)} \\ &= \frac{((\mathbf{a}_{I_1}^T \mathbf{a}_{I_2})^2 - 1) (\mathbf{p}_1 + \mathbf{p}_2) - \mathbf{a}_{I_1} \mathbf{a}_{I_1}^T (\mathbf{p}_2 - \mathbf{p}_1) + \mathbf{a}_{I_2} \mathbf{a}_{I_2}^T (\mathbf{p}_2 - \mathbf{p}_1) + \mathbf{a}_{I_1} \mathbf{a}_{I_1}^T \mathbf{a}_{I_2} \mathbf{a}_{I_2}^T (\mathbf{p}_2 - \mathbf{p}_1) - \mathbf{a}_{I_2} \mathbf{a}_{I_2}^T \mathbf{a}_{I_1} \mathbf{a}_{I_1}^T (\mathbf{p}_2 - \mathbf{p}_1)}{2 ((\mathbf{a}_{I_1}^T \mathbf{a}_{I_2})^2 - 1)} \end{aligned} \quad (167)$$

Now, consider the two-LOS version of the DLT from Eq. (18). Choose to describe the LOS measurement by $\ell_i = \alpha_i \mathbf{a}_i$, where $\alpha_i \neq 0$ is the scaling associated with the unit vector LOS \mathbf{a}_i , such that

$$\begin{bmatrix} \alpha_1 [\mathbf{a}_1 \times] \\ \alpha_2 [\mathbf{a}_2 \times] \end{bmatrix} \mathbf{r} = \begin{bmatrix} \alpha_1 [\mathbf{a}_1 \times] \mathbf{p}_1 \\ \alpha_2 [\mathbf{a}_2 \times] \mathbf{p}_2 \end{bmatrix} \quad (168)$$

Solving this linear system in the least squares sense for \mathbf{r} yields

$$\hat{\mathbf{r}} = \left(\sum_{i=1}^2 \alpha_i^2 [\mathbf{a}_i \times]^2 \right)^{-1} \sum_{i=1}^2 \alpha_i^2 [\mathbf{a}_i \times]^2 \mathbf{p}_i \quad (169)$$

Recalling that that if \mathbf{a} is a 3×1 unit vector then $-\mathbf{a} \times = \mathbf{I}_{3 \times 3} - \mathbf{a} \mathbf{a}^T$, then one may write

$$\frac{\left(\sum_{i=1}^2 \alpha_i^2 [\mathbf{a}_i \times]^2 \right)}{-(\alpha_1^2 + \alpha_2^2)} = \mathbf{I}_{3 \times 3} - \underbrace{\frac{\alpha_1^2}{\alpha_1^2 + \alpha_2^2} \mathbf{a}_{I_1}^T \mathbf{a}_{I_1}}_{\beta_1} - \underbrace{\frac{\alpha_2^2}{\alpha_1^2 + \alpha_2^2} \mathbf{a}_{I_2}^T \mathbf{a}_{I_2}}_{\beta_2} \quad (170)$$

The matrices $\mathbf{a}_i^T \mathbf{a}_i$ are both rank one, and it is possible to analytically invert this sum of matrices with the Sherman-Morrison formula (applied twice). It is also useful to consider that $1 + \beta_1 = -\beta_2$, so that the inverse finally becomes

$$\left(\frac{\left(\sum_{i=1}^2 \alpha_i^2 [\mathbf{a}_i \times]^2 \right)}{-(\alpha_1^2 + \alpha_2^2)} \right)^{-1} = \mathbf{I}_{3 \times 3} - \beta_1 \frac{\mathbf{a}_{I_1} \mathbf{a}_{I_1}^T}{1 + \beta_1} - \frac{\beta_2 \left(\mathbf{I}_{3 \times 3} - \beta_1 \frac{\mathbf{a}_{I_1} \mathbf{a}_{I_1}^T}{1 + \beta_1} \right) \mathbf{a}_{I_2} \mathbf{a}_{I_2}^T \left(\mathbf{I}_{3 \times 3} - \beta_1 \frac{\mathbf{a}_{I_1} \mathbf{a}_{I_1}^T}{1 + \beta_1} \right)}{1 + \beta_2 \mathbf{a}_{I_2}^T \left(\mathbf{I}_{3 \times 3} - \beta_1 \frac{\mathbf{a}_{I_1} \mathbf{a}_{I_1}^T}{1 + \beta_1} \right) \mathbf{a}_{I_2}} \quad (171)$$

When the two measurements are equally weighted (i.e., when $\alpha_1 = \alpha_2$), one finds that $\beta_1 = \beta_2 = -1/2$, so the expression in Eq. 171 becomes

$$\left(\frac{\left(\sum_{i=1}^2 \alpha_i^2 [\mathbf{a}_i \times]^2 \right)}{-(\alpha_1^2 + \alpha_2^2)} \right)^{-1} = - \frac{- \left((\mathbf{a}_{I_1}^T \mathbf{a}_{I_2})^2 - 1 \right) (\mathbf{a}_{I_1} \mathbf{a}_{I_1}^T + \mathbf{I}_{3 \times 3}) + (\mathbf{a}_{I_1} \mathbf{a}_{I_1}^T + \mathbf{I}_{3 \times 3}) \mathbf{a}_{I_2} \mathbf{a}_{I_2}^T (\mathbf{a}_{I_1} \mathbf{a}_{I_1}^T + \mathbf{I}_{3 \times 3})}{(\mathbf{a}_{I_1}^T \mathbf{a}_{I_2})^2 - 1} \quad (172)$$

Expanding Eq. (169), the position given by the DLT is therefore

$$\hat{\mathbf{r}} = \frac{1}{-(\alpha_1^2 + \alpha_2^2)} \left(\frac{\left(\sum_{i=1}^2 \alpha_i^2 [\mathbf{a}_i \times]^2 \right)}{-(\alpha_1^2 + \alpha_2^2)} \right)^{-1} \left(\alpha_1^2 [\mathbf{a}_{I_1} \times]^2 \mathbf{p}_1 + \alpha_2^2 [\mathbf{a}_{I_2} \times]^2 \mathbf{p}_2 \right) \quad (173)$$

which, under the assumption of $\alpha_1 = \alpha_2$ (i.e., $\beta_1 = \beta_2 = -1/2$) and after substitution from Eq. (172), becomes

$$\hat{\mathbf{r}} = \frac{\left((\mathbf{a}_{I_1}^T \mathbf{a}_{I_2})^2 - 1 \right) (\mathbf{p}_2 + \mathbf{p}_1) - \mathbf{a}_{I_1} \mathbf{a}_{I_1}^T (\mathbf{p}_2 - \mathbf{p}_1) + \mathbf{a}_{I_2} \mathbf{a}_{I_2}^T (\mathbf{p}_2 - \mathbf{p}_1) + \mathbf{a}_{I_1} \mathbf{a}_{I_1}^T \mathbf{a}_{I_2} \mathbf{a}_{I_2}^T (\mathbf{p}_2 - \mathbf{p}_1) - \mathbf{a}_{I_2} \mathbf{a}_{I_2}^T \mathbf{a}_{I_1} \mathbf{a}_{I_1}^T (\mathbf{p}_2 - \mathbf{p}_1)}{2 \left((\mathbf{a}_{I_1}^T \mathbf{a}_{I_2})^2 - 1 \right)} \quad (174)$$

Thus, the equally-weighted unit vector DLT [Eq. (174)] and the explicit range [Eq. (167)] give the same position for two LOS observations.

References

- [1] Christian, J. A., McMahon, J., DellaGuistina, D. N., Ernst, C. M., Russell, R. P., Golish, D. R., McCabe, J. S., S. K., Laurretta, D. S., Gay, P., and Schoch, P., "Resolved Imagery as a Tool for Space Science and Exploration," *NASA Exploration Science Forum*, 2019.
- [2] Gaskell, R. W., Barnouin-Jha, O. S., Scheers, D. J., and et al., "Characterizing and Navigating Small Bodies with Imaging Data," *Meteoritics & Planetary Science*, Vol. 43, No. 6, 2008, pp. 1049–1061. <https://doi.org/10.1111/j.1945-5100.2008.tb00692.x>.
- [3] Palmer, E. E., and et al., "Practical Stereophotoclinometry for Modeling Shape and Topography on Planetary Missions," *The Planetary Science Journal*, Vol. 3, 2022. <https://doi.org/10.3847/PSJ/ac460f>.

- [4] Owen, W., Duxbury, T., Acton, C., Synnott, S., Riedel, J., and Bhaskaran, S., “A Brief History of Optical Navigation at JPL,” *AAS Guidance and Control Conference*, 2008.
- [5] Christian, J. A., “A Tutorial on Horizon-Based Optical Navigation and Attitude Determination with Space Imaging Systems,” *IEEE Access*, 2021, pp. 19,819–19,853. <https://doi.org/10.1109/ACCESS.2021.3051914>.
- [6] Driedger, M., and Ferguson, P., “Feasibility Study of an Orbital Navigation Filter Using Resident Space Object Observations,” *Journal of Guidance, Control, and Dynamics*, Vol. 44, No. 3, 2021, pp. 622–628. <https://doi.org/10.2514/1.G005210>.
- [7] Bradley, N., Olikara, Z., Bhsakaran, S., and Young, B., “Cislunar Navigation Accuracy Using Optical Observations of Natural and Artificial Targets,” *Journal of Spacecraft and Rockets*, Vol. 57, No. 4, 2020, pp. 777–792. <https://doi.org/10.2514/1.A34694>.
- [8] Karimi, R. R., and Mortari, D., “Interplanetary Autonomous Navigation Using Visible Planets,” *Journal of Guidance, Control, and Dynamics*, Vol. 38, No. 6, 2015, pp. 1151–1156. <https://doi.org/10.2514/1.G000575>.
- [9] Broschart, S. B., Bradley, N., and Bhsakaran, S., “Kinematic Approximation of Position Accuracy Achieved Using Optical Observations of Distant Asteroids,” *Journal of Spacecraft and Rockets*, Vol. 56, No. 5, 2019, pp. 1383–1392. <https://doi.org/10.2514/1.A34354>.
- [10] Hinga, M. B., “Cis-Lunar Autonomous Navigation via Implementation of Optical Asteroid Angle-Only Measurements,” *21st Advanced Maui Optical and Space Surveillance Technologies (AMOS) Conference*, Maui, HI, 2020.
- [11] Franzese, V., and Topputo, F., “Deep-Space Optical Navigation Exploiting Multiple Beacons,” *The Journal of the Astronautical Sciences*, 2022. <https://doi.org/10.1007/s40295-022-00303-5>.
- [12] Cheng, Y., Johnson, A., Matthies, L., and Olson, C., “Optical Landmark Detection for Spacecraft Navigation,” *AAS/AIAA Astrodynamics Specialist Conference*, 2003.
- [13] Woffinden, D. C., and Geller, D. K., “Observability Criteria for Angles-Only Navigation,” *IEEE Transactions on Aerospace and Electronic Systems*, Vol. 45, No. 3, 2009, pp. 1194–1208. <https://doi.org/10.1109/TAES.2009.5259193>.
- [14] McKee, P., Kowalski, J., and Christian, J. A., “Navigation and star identification for an interstellar mission,” *Acta Astronautica*, Vol. 192, 2022, pp. 390–401. <https://doi.org/10.1016/j.actaastro.2021.12.007>.
- [15] Hartley, R. I., and Sturm, P., “Triangulation,” *Computer Vision and Image Understanding*, Vol. 68, No. 2, 1997, pp. 146–157. <https://doi.org/10.1006/cviu.1997.0547>.
- [16] Stewénius, H., Schaffalitzky, F., and Nistér, D., “How Hard is 3-View Triangulation Really?” *IEEE International Conference on Computer Vision (ICCV’05)*, 2005. <https://doi.org/10.1109/ICCV.2005.115>.
- [17] Chace, A. B., and Manning, H. P., *The Rhind Mathematical Papyrus, British Museum 10057 and 10058, Vol. 1: Free Translation and Commentary*, Mathematical Association of America, Oberlin, OH, 1927, pp. 96–99. URL <https://hdl.handle.net/2027/mdp.39015017389894>.

- [18] Molinsky, M., “Some Original Sources for Modern Tales of Thales — The Tale of the Pyramids,” *Convergence*, 2015.
- [19] Euclid, Billingsley, H., Dee, J., Candale, F. D. F., and Day, J., *The elements of geometrie of the most auncient philosopher Evclide of Megara*, Imprinted at London: By Iohn Daye, 1570. URL <https://www.loc.gov/item/03020856/>.
- [20] Archibald, R. C., “The First Translation of Euclid’s Elements into English and its Source,” *The American Mathematical Monthly*, Vol. 57, No. 7P1, 1950, pp. 443–452. <https://doi.org/10.1080/00029890.1950.11990256>.
- [21] Toomer, G. J., “The Chord Table of Hipparchus and the Early History of Greek Trigonometry,” *Centarus*, Vol. 18, No. 1, 1974, pp. 6–28. <https://doi.org/10.1111/j.1600-0498.1974.tb00205.x>.
- [22] Ptolemy active 2nd century, and Toomer, G. J., *Ptolemy’s Almagest, translated and annotated by G.J. Toomer*, Springer-Verlag, New-York, 1984.
- [23] Toomer, G. J., “Hipparchus on the Distances of the Sun and Moon,” *Archive for History of Exact Sciences*, Vol. 14, No. 2, 1974, pp. 126–142.
- [24] Lorch, R., “Greek-Arabic-Latin: The Transmission of Mathematical Texts in the Middle Ages,” *Science in Context*, Vol. 14, No. 1–2, 2002, pp. 313–331. <https://doi.org/10.1017/S0269889701000114>.
- [25] Frisius, G., *Libellus de locorum describendorum ratione*, 1533.
- [26] Pogo, A., “Gemma Frisius, His Method of Determining Differences of Longitude by Transporting Timepieces (1530), and His Treatise on Triangulation (1533),” *Isis*, Vol. 22, No. 2, 1935, pp. 469–506.
- [27] Haasbroek, N. D., *Gemma Frisius, Tycho Brahe and Snellius and Their Triangulations*, Rijkscommissie voor Geodesie, Delft, Netherlands, 1968.
- [28] Snellius, W., *De Terrae ambitus vera quantitate*, 1617. URL <https://mdz-nbn-resolving.de/details:bsb10806698>.
- [29] Breitenberger, E., “Gauss’s geodesy and the axiom of parallels,” *Archive for History of Exact Sciences*, Vol. 31, No. 3, 1984, pp. 273–289. <https://doi.org/10.1007/BF00327704>.
- [30] Gauss, C. F., *Supplementum theoriae combinationis observationum erroribus minimis obnoxiae*, typis Dieterichianis, Göttingen, 1828. <https://doi.org/10.3931/e-rara-2858>.
- [31] McCaw, G. T., “Resection in Survey,” *The Geographical Journal*, Vol. 52, No. 2, 1918, pp. 105–123. <https://doi.org/10.2307/1779558>.
- [32] Bernard, A. J., Nafi, A. M., and Geller, D. K., “Using Triangulation in Optical Orbit Determination,” *AAS/AIAA Astrodynamics Specialist Conference*, 2018.
- [33] Chen, L., Liu, C., Li, Z., and Kang, Z., “A New Triangulation Algorithm for Positioning Space Debris,” *Remote Sensing*, Vol. 13, No. 23, 2021. <https://doi.org/10.3390/rs13234878>.

- [34] Pollefeys, M., Koch, R., Vergauwen, M., and Van Gool, L., “Automated reconstruction of 3D scenes from sequences of images,” *ISPRS Journal of Photogrammetry and Remote Sensing*, Vol. 55, No. 4, 2000, pp. 251–267. [https://doi.org/10.1016/S0924-2716\(00\)00023-X](https://doi.org/10.1016/S0924-2716(00)00023-X).
- [35] Snavely, N., Seitz, S. M., and Szeliski, R., “Modeling the World from Internet Photo Collections,” *International Journal of Computer Vision*, Vol. 80, 2008, pp. 189–210. <https://doi.org/10.1007/s11263-007-0107-3>.
- [36] Poirot, J. L., and McWilliams, G. V., “Navigation by Back Triangulation,” *IEEE Transactions on Aerospace and Electronic Systems*, Vol. 12, No. 2, 1976, pp. 270–274.
- [37] Feissel, M., and Mignard, F., “The adoption of ICRS on 1 January 1998: meaning and consequences,” *Astronomy and Astrophysics*, Vol. 331, 1998, pp. L33–L36.
- [38] Ma, C., Arias, E., Eubanks, T., Fey, A., Gontier, A., Jacobs, C., Sovers, O., Archinal, B., and Charlot, P., “The International Celestial Reference Frame as Realized by Very Long Baseline Interferometry,” *The Astronomical Journal*, Vol. 116, 1998, pp. 516–546. <https://doi.org/10.1086/300408>.
- [39] Fey, A., Gordon, D., and et al., “The Second International Celestial Reference Frame by Very Long Baseline Interferometry,” *The Astronomical Journal*, Vol. 150, 2015. <https://doi.org/10.1088/0004-6256/150/2/58>.
- [40] Kaplan, G. H., “Angles-Only Navigation: Position and Velocity Solution from Absolute Triangulation,” *Navigation: Journal of The Institute of Navigation*, Vol. 58, No. 3, 2011, pp. 187–201. <https://doi.org/10.1007/s11263-008-0152-6>.
- [41] Liebe, C. C., “Star Trackers for Attitude Determination,” *IEEE Aerospace and Electronic Systems Magazine*, Vol. 10, No. 6, 1995, pp. 10–16. <https://doi.org/10.1109/62.387971>.
- [42] Liebe, C. C., “Accuracy Performance of Star Trackers — A Tutorial,” *IEEE Transactions on Aerospace and Electronic Systems*, Vol. 38, No. 2, 2002, pp. 587–599. <https://doi.org/10.1109/TAES.2002.1008988>.
- [43] Christian, J. A., and Crassidis, J. L., “Star Identification and Attitude Determination with Projective Cameras,” *IEEE Access*, Vol. 9, 2021, pp. 25,768–25,794. <https://doi.org/10.1109/ACCESS.2021.3054836>.
- [44] El Hassan, I. M., “Two-Dimensional Resection—A Survey Of Analytical Techniques,” *Australian Surveyor*, Vol. 47, No. 1, 2002, pp. 14–23. <https://doi.org/10.1080/00050356.2002.10558838>.
- [45] Grunert, J. A., “Das Pothenot’sche Problem in erweiterter Gestalt; nebst Bemerkungen über seine Anwendungen in der Geodisic,” *Archiv der Mathematik und Physik*, Vol. 1, 1841, pp. 238–248.
- [46] Haralick, R. M., Lee, C., Ottenberg, K., and Nölle, M., “Review and Analysis of Solutions of the Three Point Perspective Pose Estimation Problem,” *International Journal of Computer Vision*, Vol. 13, No. 3, 1994, pp. 331–356. <https://doi.org/10.1007/BF02028352>.

- [47] Gao, X., Hou, X., Tang, J., and Cheng, H., “Complete solution classification for the perspective-three-point problem,” *IEEE Transactions on Pattern Analysis and Machine Intelligence*, Vol. 25, No. 8, 2003, pp. 930–943. <https://doi.org/10.1109/TPAMI.2003.1217599>.
- [48] Pascual-Escudero, B., Nayak, A., Briot, S., Kermorgant, O., Martinet, P., Safey El Din, M., and Chaumette, F., “Complete Singularity Analysis for the Perspective-Four-Point Problem,” *International Journal of Computer Vision*, Vol. 129, 2021, pp. 1217–1237. <https://doi.org/10.1007/s11263-020-01420-0>.
- [49] Hartley, R., and Zisserman, A., *Multiple View Geometry, 2nd Ed.*, Cambridge University Press, Cambridge, UK, 2003, pp. 70–73, 312–321.
- [50] Quan, L., and Lan, Z., “Linear N-Point Camera Pose Estimation,” *IEEE Transactions on Pattern Analysis and Machine Intelligence*, Vol. 21, No. 8, 1999, pp. 774–780. <https://doi.org/10.1109/34.784291>.
- [51] Ansar, A., and Daniilidis, K., “Linear Pose Estimation from Points or Lines,” *IEEE Transactions on Pattern Analysis and Machine Intelligence*, Vol. 25, No. 5, 2003, pp. 578–589. <https://doi.org/10.1109/TPAMI.2003.1195992>.
- [52] Lepetit, V., Moreno-Noguer, F., and Fua, P., “EPnP: An Accurate $O(n)$ Solution to the PnP Problem,” *International Journal of Computer Vision*, Vol. 81, 2009, pp. 155–166. <https://doi.org/10.1007/s11263-008-0152-6>.
- [53] Crassidis, J. L., Alonso, R., and Junkins, J. L., “Optimal Attitude and Position Determination from Line-of-Sight Measurements,” *The Journal of the Astronautical Sciences*, Vol. 48, 2000, pp. 391–408.
- [54] Besl, P. J., and McKay, N. D., “A method for registration of 3-D shapes,” *IEEE Transactions on Pattern Analysis and Machine Intelligence*, Vol. 14, No. 2, 1992, pp. 239–256. <https://doi.org/10.1109/34.121791>.
- [55] Yang, H., Shi, J., and Carlone, L., “TEASER: Fast and Certifiable Point Cloud Registration,” *IEEE Transactions on Robotics*, Vol. 37, No. 2, 2021, pp. 314–333. <https://doi.org/10.1109/TRO.2020.3033695>.
- [56] Nardone, S. C., Lindgren, A. G., and Gong, K. F., “Fundamental properties and performance of conventional bearings-only target motion analysis,” *IEEE Transactions on Automatic Control*, Vol. 29, No. 9, 1984, pp. 775–787. <https://doi.org/10.1109/TAC.1984.1103664>.
- [57] Harper, R. B., “Pilot Boat Identification, Harbor Radar Systems,” *Navigation*, Vol. 4, No. 5, 1955, pp. 195–201. <https://doi.org/10.1002/j.2161-4296.1955.tb00164.x>.
- [58] Casey, J., *A sequel to the first six books of the Elements of Euclid, containing an easy introduction to modern geometry, with numerous examples*, Hodges, Figgis & co., 1888, pp. 173–175.
- [59] Lindgren, A. G., and Gong, K. F., “Position and Velocity Estimation Via Bearing Observations,” *IEEE Transactions on Aerospace and Electronic Systems*, Vol. 14, No. 4, 1977, pp. 564–577. <https://doi.org/10.1109/TAES.1978.308681>.
- [60] Nardone, S. C., and Aidala, V. J., “Observability Criteria for Bearings-Only Target Motion Analysis,” *IEEE Transactions on Aerospace and Electronic Systems*, Vol. 17, No. 2, 1981, pp. 162–166. <https://doi.org/10.1109/TAES.1981.309141>.

- [61] Clohessy, W. H., and Wiltshire, R. S., "Terminal guidance system for satellite rendezvous," *Journal of the Aerospace Sciences*, Vol. 27, No. 9, 1960, pp. 653–658. <https://doi.org/10.2514/8.8704>.
- [62] Woffinden, D. C., and Geller, D. K., "Navigating the Road to Autonomous Orbital Rendezvous," *Journal of Spacecraft and Rockets*, Vol. 44, No. 4, 2007, pp. 898–909. <https://doi.org/10.2514/1.30734>.
- [63] Semple, J. G., and Kneebone, G. T., *Algebraic Projective Geometry*, Oxford University Press, Oxford, UK, 1952.
- [64] Gallier, J., *Geometric Methods and Applications, 2nd Edition*, Springer-Verlag, New York, 2011.
- [65] Christian, J., Benhacine, L., Hikes, J., and D'Souza, C., "Geometric Calibration of the Orion Optical Navigation Camera using Star Field Images," *The Journal of the Astronautical Sciences*, Vol. 63, No. 4, 2016, pp. 335–353. <https://doi.org/10.1007/s40295-016-0091-3>.
- [66] Bos, B. J., and et al., "In-Flight Calibration and Performance of the OSIRIS-REx Touch And Go Camera System (TAGCAMS)," *Space Science Reviews*, Vol. 71, 2020. <https://doi.org/10.1007/s11214-020-00682-x>.
- [67] Wahba, G., "A Least Square Estimate of Satellite Attitude," *SIAM Review*, Vol. 7, No. 3, 1965, p. 409. <https://doi.org/10.1137/1007077>.
- [68] Farrell, J. L., Stuelpnagel, J. C., Wessner, R. H., Velman, J. R., and Brook, J. E., "A Least Squares Estimate of Satellite Attitude (Grace Wahba)," *SIAM Review*, Vol. 8, No. 3, 1966, pp. 384–386. <https://doi.org/10.1137/1008080>.
- [69] Shuster, M. D., and Oh, S. D., "Three-Axis Attitude Determination from Vector Observations," *Journal of Guidance and Control*, Vol. 4, No. 1, 1981, pp. 70–77. <https://doi.org/10.2514/3.19717>.
- [70] Markley, F. L., "Attitude Determination Using Vector Observations and the Singular Value Decomposition," *The Journal of the Astronautical Sciences*, Vol. 36, No. 3, 1988, pp. 245–258.
- [71] Shuster, M. D., "Maximum Likelihood Estimation of Spacecraft Attitude," *The Journal of the Astronautical Sciences*, Vol. 37, No. 1, 1989, pp. 79–88.
- [72] Mortari, D., and Majji, M., "Multiplicative Measurement Model," *The Journal of the Astronautical Sciences*, Vol. 57, No. 1 & 2, 2009, pp. 47–60. <https://doi.org/10.1007/BF03321493>.
- [73] Kaasalainen, M., and Tanga, P., "Photocentre offset in ultraprecise astrometry: Implications for barycentre determination and asteroid modelling," *Astronomy and Astrophysics*, Vol. 416, No. 1, 2004, pp. 367–373. <https://doi.org/10.1051/0004-6361:20031711>.
- [74] Olds, R. D., and et al., "The Use of Digital Terrain Models for Natural Feature Tracking at Asteroid Bennu," *The Planetary Science Journal*, Vol. 3, 2022. <https://doi.org/10.3847/PSJ/ac5184>.
- [75] Lowe, D. G., "Distinctive Image Features from Scale-Invariant Keypoints," *International Journal of Computer Vision*, Vol. 60, No. 2, 2004, pp. 91–110. <https://doi.org/10.1023/B:VISI.0000029664.99615.94>.

- [76] Cheng, Y., Crassidis, J. L., and Markley, F. L., "Attitude Estimation for Large Field-of-View Sensors," *The Journal of the Astronautical Sciences*, Vol. 54, No. 3 & 4, 2006, pp. 433–448. <https://doi.org/10.1007/BF03256499>.
- [77] Tūsī, .-. , Nasīr al-Dīn Muhammad ibn Muhammad, *Traité du quadrilatère attribué a Nassiruddinel-Toussy, d'après un manuscrit tiré de la bibliothèque de S.A. Edhem Pacha*, Typographie et lithographie Osmaniè, Turkey, 1891.
- [78] Aydin, N., Hammoudi, L., and Bakbouk, G., *Al-Kashi's Miftah al-Hisab, Volume II: Geometry*, Birkhäuser Cham, 2020, p. 31. <https://doi.org/10.1007/978-3-030-61330-3>.
- [79] Abdel-Aziz, Y. I., and Karara, H. M., "Direct Linear Transformation from Comparator Coordinates into Object Space Coordinates in Close-Range Photogrammetry," *Photogrammetric Engineering & Remote Sensing*, Vol. 81, No. 2, 2015, pp. 103–107. <https://doi.org/10.14358/PERS.81.2.103>.
- [80] Christian, J. A., "Autonomous Initial Orbit Determination with Optical Observations of Unknown Planetary Landmarks," *Journal of Spacecraft and Rockets*, Vol. 56, No. 1, 2019, pp. 211–220. <https://doi.org/10.2514/1.A34259>.
- [81] Gennery, D. B., *Calibration and Orientation of Cameras in Computer Vision*, Springer, 1992, Chaps. Least-Squares Camera Calibration Including Lens Distortion and Automatic Editing of Calibration Points, pp. 47–48. https://doi.org/10.1007/978-3-662-04567-1_5.
- [82] K, D., and Li, R., "CAHVOR camera model and its photogrammetric conversion for planetary applications," *Journal of Geophysical Research*, Vol. 109, 2004. <https://doi.org/10.1029/2003JE002199>.
- [83] Plücker, J., "On a new geometry of space," *Philosophical Transactions of the Royal Society*, Vol. 155, 1865. <https://doi.org/10.1098/rstl.1865.0017>.
- [84] Franzese, V., and Topputo, F., "Optimal Beacons Selection for Deep-Space Optical Navigation," *The Journal of the Astronautical Sciences*, Vol. 67, 2020, pp. 1775–1792. <https://doi.org/10.1007/s40295-020-00242-z>.
- [85] Shuster, M. D., "Kalman Filtering of Spacecraft Attitude and the QUEST Model," *The Journal of the Astronautical Sciences*, Vol. 38, No. 3, 1990, pp. 377–393.
- [86] Fisher, R. A., "On the mathematical foundations of theoretical statistics," *Philosophical Transactions of the Royal Society of London. Series A*, Vol. 222, 1922, pp. 309–368. <https://doi.org/10.1098/rsta.1922.0009>.
- [87] Tapley, B., Schutz, B., and Born, G., *Statistical Orbit Determination*, Elsevier Academic Press, Amsterdam, 2004, pp. 172–173, 190–194. <https://doi.org/10.1016/B978-0-12-683630-1.X5019-X>.
- [88] Hartley, R. I., "Chirality," *International Journal of Computer Vision*, Vol. 26, No. 1, 1998, pp. 41–61. <https://doi.org/10.1023/A:1007984508483>.
- [89] Kobylka, K. R., and Christian, J. A., "Methods in Triangulation for Image-Based Terrain Relative Navigation," *AAS/AIAA Space Flight Mechanics Meeting*, 2021.

- [90] Goulb, G. H., and Van Loan, C. F., *Matrix Computations, 4th Ed.*, Johns Hopkins University Press, 2013, pp. 260–268,304–306.
- [91] Aldrich, J., “R. A. Fisher and the Making of Maximum Likelihood 1912–1922,” *Statistical Science*, Vol. 12, No. 3, 1997, pp. 162–176. <https://doi.org/10.1214/ss/1030037906>.
- [92] Gelb, A., *Applied Optimal Estimation*, MIT Press, Cambridge, MA, 1974.
- [93] Cheng, Y., and Miller, J., “Autonomous landmark based spacecraft navigation system,” *AAS/AIAA Astrodynamics Specialist Conference*, 2003.
- [94] Y. Cheng, and Ansar, A., “Landmark Based Position Estimation for Pinpoint Landing on Mars,” *IEEE International Conference on Robotics and Automation*, 2005, pp. 1573–1578. <https://doi.org/10.1109/ROBOT.2005.1570338>.
- [95] Adams, D., Criss, T., and Shankar, U., “Passive Optical Terrain Relative Navigation Using APLNav,” *IEEE Aerospace Conference*, 2008, pp. 1–9. <https://doi.org/10.1109/AERO.2008.4526303>.
- [96] Steffes, S. R., Monterroza, F., Benhacine, L., and Mario, C., “Optical Terrain Relative Navigation Approaches to Lunar Orbit, Descent and Landing,” *AIAA Scitech Forum*, 2019. <https://doi.org/10.2514/6.2019-1178>.
- [97] Acton, C., “Ancillary data services of NASA’s Navigation and Ancillary Information Facility,” *Planetary and Space Sciences*, Vol. 44, No. 1, 1996, pp. 65–70. [https://doi.org/10.1016/0032-0633\(95\)00107-7](https://doi.org/10.1016/0032-0633(95)00107-7).
- [98] Acton, C., Bachman, N., Semenov, B., and Wright, E., “A look towards the future in the handling of space science mission geometry,” *Planetary and Space Sciences*, Vol. 150, 2018, pp. 9–12. <https://doi.org/10.1016/j.pss.2017.02.013>.
- [99] Johnson, A., Aaron, S., Chang, J., Cheng, Y., Montgomery, J., Mohan, S., Schroeder, S., Tweddle, B., Trawny, N., and Zheng, J., “The Lander Vision System for Mars 2020 Entry Descent and Landing,” *AAS Guidance Navigation and Control Conference*, 2017.
- [100] National Academies of Sciences, Engineering, and Medicine, *Origins, Worlds, and Life: A Decadal Strategy for Planetary Science and Astrobiology 2023-2032*, The National Academies Press, 2022, pp. S–7. <https://doi.org/10.17226/26522>.
- [101] Jacobson, R. A., “The Orbits of the Uranian Satellites and Rings, the Gravity Field of the Uranian System, and the Orientation of the Pole of Uranus,” *The Astronomical Journal*, Vol. 148, No. 5, 2014. <https://doi.org/10.1088/0004-6256/148/5/76>.
- [102] Lubey, D. P., Bhaskaran, S., Bradley, N., and Olikara, Z., “Ice Giant Exploration Via Autonomous Optical Navigation,” *AAS/AIAA Astrodynamics Specialist Conference*, 2020.
- [103] Bruzelius, C., “The Construction of Notre-Dame in Paris,” *The Art Bulletin*, Vol. 69, 1987, pp. 540–569. <https://doi.org/10.1080/00043079.1987.10788458>.
- [104] Snavely, N., Seitz, S. M., and Szeliski, R., “Photo tourism: exploring photo collections in 3D,” *ACM SIGGRAPH*, 2006. <https://doi.org/10.1145/1179352.1141964>.

- [105] Naasz, B., and Moreau, M., “Autonomous RPOD Challenges for the Coming Decade,” *AAS Guidance Navigation and Control Conference*, 2015.
- [106] Houbolt, J. C., “Problems and Potentialities of Space Rendezvous,” *Space Flight and Re-Entry Trajectories*, Springer, Vienna, 1962, pp. 406–429. https://doi.org/10.1007/978-3-7091-5470-0_6.
- [107] Young, K. A., and Alexander, J. D., “Apollo Lunar Rendezvous,” *Journal of Spacecraft and Rockets*, Vol. 7, No. 9, 1970, pp. 1083–1086. <https://doi.org/10.2514/3.30106>.
- [108] Goodman, J. L., “History of Space Shuttle Rendezvous and Proximity Operations,” *Journal of Spacecraft and Rockets*, Vol. 43, No. 5, 2006, pp. 944–959. <https://doi.org/10.2514/1.19653>.
- [109] Mattingly, R., HAYati, S., and Udomkesmalee, G., “Technology development plans for the Mars Sample Return mission,” 2005. <https://doi.org/10.1109/AERO.2005.1559389>.
- [110] Reed, B. B., Smith, R. C., Naasz, B., and Pellegrino, J., “The Restore-L Servicing Mission,” *AIAA SPACE 2016 Forum*, 2016. <https://doi.org/10.2514/6.2016-5478>.
- [111] Sullivan, J., and D’Amico, S., “Nonlinear Kalman Filtering for Improved Angles-Only Navigation Using Relative Orbital Elements,” *Journal of Guidance, Control, and Dynamics*, Vol. 40, No. 9, 2017, pp. 2183–2200. <https://doi.org/10.2514/1.G002719>.
- [112] Vallado, D., *Fundamentals of Astrodynamics and Applications, 3rd Ed.*, Microcosm Press, Hawthorne, CA, 2007, pp. 389–417.
- [113] Klein, I., and Geller, D., “Zero Δv Solution to the Angles-Only Range Observability Problem during Orbital Proximity Operations,” *Itzhack Y. Bar-Itzhack Memorial Symposium on Estimation, Navigation, and Spacecraft Control*, 2015, pp. 351–369. https://doi.org/10.1007/978-3-662-44785-7_19.